Graduate School Form 30
Updated 1/15/2015

PURDUE UNIVERSITY
GRADUATE SCHOOL
Thesis/Dissertation Acceptance

This is to certify that the thesis/dissertation prepared

By MD ASHIQUR RAHMAN

Entitled

ELECTROCHEMICAL MODEL BASED FAULT DIAGNOSIS OF LITHIUM ION BATTERY

For the degree of Master of Science in Mechanical Engineering

Is approved by the final examining committee:

Sohel Anwar Chair	
Afshin Izadian	
Yongzhu Fu	

To the best of my knowledge and as understood by the student in the Thesis/Dissertation Agreement, Publication Delay, and Certification Disclaimer (Graduate School Form 32), this thesis/dissertation adheres to the provisions of Purdue University's "Policy of Integrity in Research" and the use of copyright material.

Approved by Major Professor(s): Sohel Anwar

Approved by: Sohel Anwar 7/2/2015

Head of the Departmental Graduate Program Date

ELECTROCHEMICAL MODEL BASED FAULT DIAGNOSIS OF LITHIUM ION BATTERY

A Thesis

Submitted to the Faculty

of

Purdue University

by

Md Ashiqur Rahman

In Partial Fulfillment of the

Requirements for the Degree

of

Master of Science in Mechanical Engineering

August 2015

Purdue University

Indianapolis, Indiana

I am dedicating this research endeavors to my late Dadu, late Dada, Nanu, late Nana, Abba, Amma, Vaia, Vaabi, Ayesha, Dipty, Arash and finally to my precious wife Shamima Irin (Arpa). I love you all. Thank you all for being my inspiration.

ACKNOWLEDGMENTS

First of all I would like to pay my gratitude to almighty God for giving me the strength to complete this work successfully. I am highly grateful to Dr. Sohel Anwar, my graduate advisor and thesis supervisor for allowing me to work with the financial support and his precious thoughts regarding my works. I am grateful to Dr. Afshin Izadian, my research advisor for helping me throughout the graduation period. Also I want to thank Dr. Yongzhu Fu for teaching me the basics of Lithium Ion battery chemistry and helping me with his ideas in research. Thanks to all of my wonderful lab mates, my friends and all the well wishers for supporting and helping me throughout this long journey.

TABLE OF CONTENTS

LIST OF TABLES

LIST OF FIGURES

SYMBOLS

c	Concentration of Li^+
Ds_N	Diffusion coefficient at anode
Ds_P	Diffusion coefficient at cathode
F	Faraday's constant
i_e	Current density of electrolyte
i_0	exchange current density of intercalation reaction
j	Local volumetric current density of intercalation reaction
L	Length of cell of the electrode
R	Universal gas constant
R_p	Particle radius
t	Time
t^+	Transport number
T	Temperature
U	Equilibrium potential
x	Length dimension
α_a, α_c	transfer coefficients at anode and cathode respectively
ε	Volume fraction of respective phases
ϕ	Local potential of any phase
κ	Conductivity of electrolyte phase
σ	Conductivity of electrode phase
θ	State of charge
ρ	Density of active material
η	Overpotential
κ	Intercalation / de-intercalation reaction rate constant

ABBREVIATIONS

PSO	Particle Swarm Optimization
MMAE	Multiple Model Adaptive Estimation
UDDS	Urban Dynamometer Driving Schedule
HEV	Hybrid Electric Vehicle
EV	Electric Vehicle
PHEV	Plug-in Hybrid Electric Vehicle
KF	Kalman Filter
EKF	Extended Kalman Filter
ECM	Equivalent Circuit Method
RUL	Remaining Useful Life
ARNN	Adaptive Recurrent Neural Network
SOH	State of Health
SOC	State of Charge
LO	Luenberger Observer
SVM	Support Vector Machine
NN	Neural Network
FL	Fuzzy Logic
IS	Impedance Spectroscopy
OD	Over Discharged
OC	Over Charged
OCP	Open Circuit Potential
GA	Genetic Algorithm
PDAE	Partial Differential Algebraic Equation

ABSTRACT

Rahman, Md Ashiqur. M.S.M.E., Purdue University, August 2015. Electrochemical Model Based Fault Diagnosis of Lithium Ion Battery. Major Professor: Sohel Anwar.

A gradient free function optimization technique, namely particle swarm optimization (PSO) algorithm, is utilized in parameter identification of the electrochemical model of a Lithium-Ion battery having a $LiCoO_2$ chemistry. Battery electrochemical model parameters are subject to change under severe or abusive operating conditions resulting in, for example, Navy over-discharged battery, 24-hr over-discharged battery and over-charged battery. It is important for a battery management system to have these parameters changes fully captured in a bank of battery models that can be used to monitor battery conditions in real time. In this work, PSO methodology has been used to identify four electrochemical model parameters that exhibit significant variations under severe operating conditions. The identified battery models were validated by comparing the model output voltage with the experimental output voltage for the stated operating conditions. These identified conditions of the battery were then used to monitor condition of the battery that can aid the battery management system (BMS) in improving overall performance. An adaptive estimation technique, namely multiple model adaptive estimation (MMAE) method, was implemented for this purpose. In this estimation algorithm, all the identified models were simulated for a battery current input profile extracted from the hybrid pulse power characterization (HPPC) cycle simulation of a hybrid electric vehicle (HEV). A partial differential algebraic equation (PDAE) observer was utilized to obtain the estimated voltage which was used to generate the residuals. Analysis of these residuals through MMAE provided the probability of matching the current battery operating condition to that of one of the identified models. Simulation results show that, the proposed model based

method offered an accurate and effective fault diagnosis of the battery conditions. This type of fault diagnosis which is based on the models capturing true physics of the battery electrochemistry, can lead to a more accurate and robust battery fault diagnosis and help BMS take appropriate steps to prevent battery operation in any of the stated severe or abusive conditions.

1. INTRODUCTION

1.1 Thesis Overview

Among all the secondary (alternative) energy sources available for electric vehicle (EV), hybrid electric vehicle (HEV) and for the direct energy source for the portable electronic devices such as smartphone and laptops, lithium-ion (Li-ion) battery is most promising. Compared to other alternative options for energy sources, lithium-ion batteries have some unique advantages [1] [2], e.g. these batteries have higher specific energy, have minimum memory effect, provide best energy-to-weight ratio and also have low self-discharge when idle [3]. Based on these stated advantages it is clear that, Li-ion battery is the leading candidate for the upcoming generation of aerospace and automotive applications.

Nowadays, people are relying more and more on PHEV, EV and HEV for the sake of emission and efficiency point of view. Performances of these transportation options are significantly dependent on the secondary energy sources e.g. installed battery module integrated with the vehicle power-train. With the availability of Li-Ion battery in different configurations, their application as a power source is widespread and extensive. Depending on the user driving nature and the road conditions, battery undergoes through different operating conditions as the battery load demand changes. Always the safe operation of the entire battery module is expected, as this is a vital component of the stated vehicle configurations. But in reality, it is impossible to maintain safe and healthy operation conditions of the battery system for different reasons. Battery can be overcharged in time, it can be over-discharged as well as battery aging is another potential situation due to long time cycling of the battery etc. Therefore, sometimes the battery suffers from some situation outside of the safe operating zone. Electrochemistry governs those situations. Parameter changes in

operations which governs those significant situations. An innovative technique for identifying those parameters, particle swarm optimization (PSO) algorithm for the electrochemical model of the battery system is illustrated in this thesis work. Using those identified operating conditions, an adaptive estimation scheme, multiple model adaptive estimation (MMAE) is described for fault diagnosis of Li-Ion battery.

Several critical operating conditions of Li-Ion battery is considered in this thesis work. The battery models dictated by those operating conditions will be implemented in the adaptive estimation based fault diagnosis (MMAE) and also in parameter identification of those different battery model operations using different real time operating cycle of EV, HEV. This proposed thesis work can provide the BMS an effective way of fault diagnosis which will be more reliable and realistic in nature.

1.2 Construction of the Battery

A battery is a device, which converts the stored chemical energy into electrical form of energy by electrochemical reactions. All sorts of the battery consist of cathode, the positive electrode, anode, the negative electrode and the separator between them.

Batteries can be categorized into two major groups, i.e. primary and secondary battery. Primary batteries are mostly designed for discharge application and they are not advised to charge for reuse. That is why these batteries are referred also as disposable battery. In contrary, secondary batteries can be recharged after discharging and it can be done for number of cycles.

Li-Ion battery falls under the second category, which has four major constituents, i.e. cathode, anode, separator and the electrolyte. There are numerous forms of chemistries are available for each of the electrode depending on the application of the battery.

While the lithiated graphite, i.e. LiC_6 is the mostly used material for the anode along with some materials like hard carbon, Si and Ge, there are huge variations available for the cathode material. Instead of using only one active material in the

positive side, battery manufacturers use the blend of active materials. Some of the used active materials for cathode are: $LiCoO_2$, $LiFePO_4$, $LiMn_2O_4$ and $LiNiO_2$ etc.

The electrolyte used in Lithium-ion battery can be of solid and liquid phase. The liquid electrolyte mostly contain the salts of Lithium like, $LiPF_6$, $LiBF_4$ and $LiClO_4$ along with some organic solvents like diethyl carbonate, ethylene carbonate and dimethyl carbonate etc.

The general construction of a Li-Ion battery is provided in Figure 1.1.

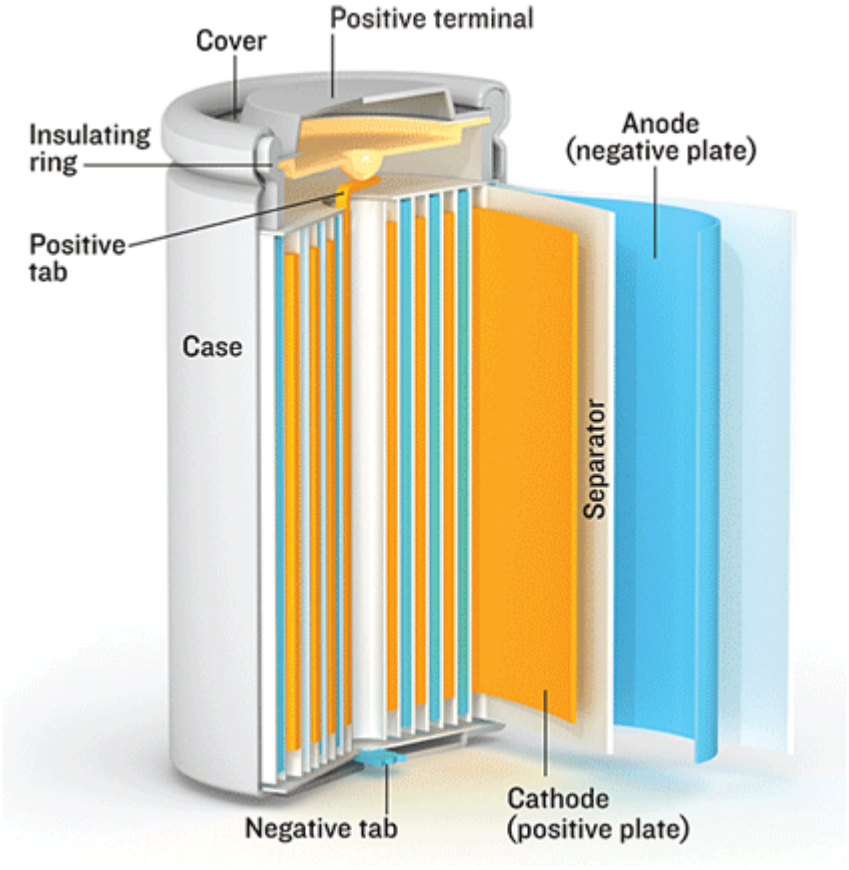

Figure 1.1. General construction of a Li-Ion battery cell [4]

1.3 Li-Ion Battery Chemistry

In both of the electrodes of this battery, there is provision of moving in and out of their interiors. During the insertion (intercalation) of ions, the ion moves into the electrodes and during the extraction / de-intercalation, the ions are moves out of the electrodes. Lithium Ion batteries rely with porous electrodes, which facilitate the electrochemical reactions by providing increased amount of active area between the solid electrodes and the electrolyte [5] [6] [7] [8] [9].

The governing electrochemical reactions of this rechargeable battery is provided in Figure 1.2.

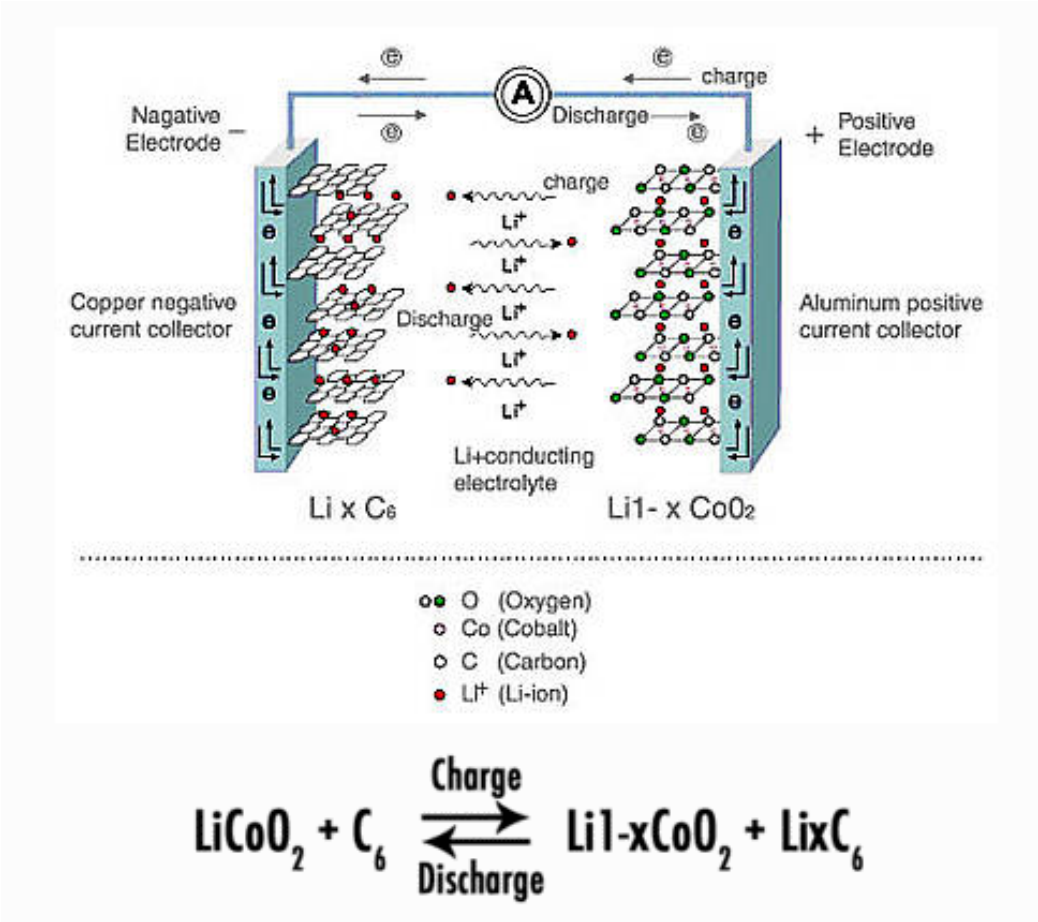

Figure 1.2. Electrochemical reactions of a Li-Ion cell [10]

In this figure,The cathode / positive cell half reaction:

$LiMO_2 \rightleftharpoons Li_{(1-x)}MO_2 + xLi^+ + xe^-$

The anode / negative cell half reaction:

$C + xLi^+ + xe^- \rightleftharpoons Li_xC$

The overall cell reaction:

$LiMO_2 + C \rightleftharpoons Li_{(1-x)}MO_2 + Li_xC$

In the previous reactions, the right directions of the double sided arrow indicates charging process while the left direction of the double sided arrow indicates the discharging process. Moreover, the letter "M" stands for the metallic part of the compound like, Co, Mn etc.

1.4 Contribution of This Thesis Work

An estimation algorithm, multiple model adaptive estimation (MMAE), is developed for the electrochemical model of lithium-ion battery, which provides an accurate technique of condition monitoring. Another major contribution is the development of a gradient free optimization technique, i.e. particle swarm optimization (PSO) algorithm for electrochemical battery model parameter identification. Using the identified parameters, separate models (conditions) are built. These conditions are validated with experimental results obtained by using CADEX battery tester from CADEX Inc.

1.5 Orientation of This Thesis

After providing the literature survey in Chapter 2, electrochemical modeling of Li-ion battery is provided in Chapter 3. PDAE observer equations are provided in Chapter 4. Electrochemical model response validation by comparing with the theoretical response of a Li-ion battery is also presented at Chapter 4. MMAE implementation with UDDS cycle simulated current profile is provided in Chapter 5 of this

thesis. A comprehensive description of parameter identification technique, i.e. PSO is provided in Chapter 6. In Chapter 7, the identified battery model validation is provided by comparing with the experimental voltage responses of different operating conditions. MMAE was again implemented using the identified battery models and for HPPC cycle simulated current profile, which is provided in Chapter 8 and finally conclusion and recommendations are provided in Chapter 9.

2. LITERATURE SURVEY

2.1 Fault Diagnosis

Based on the usage of the battery and type of the operations involved, several methods aiming with fault detection and diagnosis are available. All available techniques can be classified under two major groups: equivalent circuit based model (ECM) [11] [12] [13] and true physics based models. In ECM, the battery is modeled by assuming that the true behavior of the battery is attainable using a combination of voltage source, capacitors, resistors and Warburg impedances. Experimental values are being used as the values of the stated components, in which the insight of the real physics of the battery is ignored. This approach does not deal with the real dynamics of the battery chemistry.

On the other hand, the real physics based model [14] [15] [16] [17] [18], which is given by Doyle, Fuller, and Newman [15] [19], is primarily based on partial differential equations which contains all the required information regarding the true battery chemistry. This electrochemical model is based on the concentrated solution theory [14]. However this electrochemical model is too complex to use in real time application. For this reason model reduction is an option to overcome that issue. The works presented in this thesis work, are based on the reduced order partial differential equation [20].

Works aiming with fault detection and diagnosis have been performed before. Adaptive estimation technique was used in [21], which was based on ECM model. Extended Kalman filter (EKF) was used in this work for the non-linear application. EKF is based on an approximation of Taylor series, which cannot deal with a highly non-linear system. An adaptive recurrent neural network (ARNN) for prediction of remaining useful life (RUL) was used in [22], which is also modeled based on ECM.

Synthesized design of Luenberger observer (LO) was adopted in [23], along with ECM model for fault isolation and estimation. The used observer works well with minimum or no measurement noise in the system. But this methodology will face difficulty from the performance point of view when significant measurement noise is present in the system.

Other major studies related to state of health (SOH) and remaining useful life (RUL) of Li-Ion battery is based on data-driven methods. In [24], the data-driven method is presented for providing diagnosis and prognosis of health of the battery in alternative power-train. For estimation purpose, the authors used a well-known machine learning technique, i.e. support vector machine (SVM). In addition with the similar methodology, in [25], the authors adopted a conditional three-parameter capacity degradation model. In [26], battery parameter identification, estimation and prognosis methodology was presented using several techniques, e.g. neural network (NN), auto regressive moving average (ARMA), fuzzy logic (FL) and impedance spectroscopy (IS) etc. The data-driven method is actually based on the relationship between input and output, the real physics of the battery model is ignored in this approach as in ECM, therefore there may arise some issues with the use of this kind of diagnosis and prognosis method.

Multiple model adaptive estimation (MMAE) is used in this work to identify and detects the faults of Li-Ion battery. This adaptive estimation method requires representation of different fault scenarios, generate the residual signals and then to isolate the faults of different kinds using the algorithm. The generation of residuals and evaluation of them plays a vital role on the performance of the diagnosis [27]. In this work, the used residuals are generated by comparing the simulated outputs of the fault models with the simulated output of the true plant model.

The work presented here aims at detecting several faults, i.e. aging, over-discharge (OD) and over-charge (OC) along with the detection of original model. Among the stated fault scenarios of LI-Ion battery, OD and OC are critical for the health of the battery. While over-charge can lead to overheating and thus vaporization of

active material and hence explosion, over-discharge can short circuit the battery cell [12]. However, these stated faults can be detected quickly according to the described methodology and steps can be taken to solve the issues before the faults can go to their extreme conditions.

Most of the available works on Fault diagnosis are based on equivalent circuit based modeling of the battery, which heavily depends on several assumptions which deny the crucial battery dynamics during application. This work is based on the true physics based complex PDE model of Li-Ion battery, which captures all the dynamics of battery. Moreover, the fault diagnosis include several possible critical operating conditions of the battery, which provides a reliable and comprehensive fault diagnosis. MMAE including the electrochemical model of Lithium-Ion battery is rarely available in literature, which this work is providing as an innovative and trustworthy way of fault diagnosis.

2.2 Parameter Identification

An accurate Identification of the critical parameters of the battery can lead to a better BMS, which eventually can lead to a better condition monitoring of the battery. Particle swarm optimization is a widely used optimization technique developed by Kennedy and Eberhart in 1995 [28] [29] [30].

Parameter identification for Li-Ion battery model was performed before, but almost all of these works are based on genetic algorithm (GA) [31] [32] [33] [34], which is also a population based search technique. A recursive least squares (RLS) algorithm is implemented for Li-Ion battery parameter identification in [35], but the authors adopted the equivalent circuit methodology (ECM) for modeling the battery dynamics. However, in contrast with GA, PSO has some notable advantages. PSO does not involve the mutation and crossover function. In addition to that, PSO is much easier to implement for identification of the desired parameters.

Particle swarm optimization algorithm implementation for the electrochemical model of Li-Ion battery is rarely available. Electrochemical model given by Doyle, Fuller, and Newman is the true physics based model for this battery system, which contains all the required information regarding the true battery chemistry and hence more trustworthy than the other available modeling approach. Therefore, the incorporation of a better parameter search technique with this model can provide a comprehensive insight to the parameters of the battery which are responsible for different operating conditions in real time application.

In this work, identification of the parameters and the validation of the reduced order electrochemical model was performed by comparing the model output voltage and the experimental measured voltage. The stated experimental was carried out on Panasonic NCR18650B 3.7 V Li-Ion battery by a powerful battery tester provided by CADEX Inc. The battery was conditioned for different cases it might operate in, e.g. Navy Over-discharge cycle [35] [36], over-charge etc. along with the normal operating condition of the battery. And the parameters responsible for those cases are identified by PSO algorithm.

Development of this algorithm for electrochemical model of Li-Ion battery is the major contribution as this work is unique. The advantages of PSO encouraged to incorporate this method with the proposed battery model, which will be a tremendous work to be done. As other available techniques are computationally costly, PSO has its advantages here by being computationally cheaper.

3. ELECTROCHEMICAL MODEL OF LI-ION BATTERY

3.1 Intercalation Based Chemistry

Intercalation is defined as the process of moving ions in and out of an interstitial sites in a lattice. Usually found Li-ion cell is based of intercalation, i.e. both electrodes have lattice sites that can store lithium. Discharging and charging of the cell causes the Li^+ to enter into the lattice site of positive electrode and to leave the lattice site of the negative electrode respectively. The geometry of the lithium ion battery being studied, is based on intercalation mechanism of Li-ion.

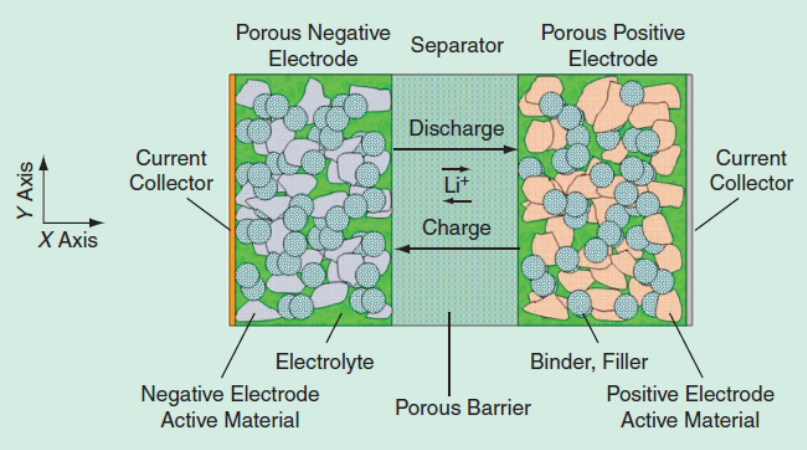

Figure 3.1. Li-Ion battery geometry [37]

The general configuration of a lithium ion battery cell is provided in Figure 3.1. As clearly visible in the figure, it consists of the following four major components: 1. porous negative electrode or anode, 2. porous positive electrode or cathode, 3. separator region and 4. electrolyte.

Anode is connected with the negative terminal of the battery and this is composed of materials which are named as negative electrode active materials. In practice,

for improved performance of lithium ion battery, manufacturers use blend of active materials. But in this battery geometry, for the sake of modeling and simulation time, only one active material was considered in negative end of the battery, which is actually graphite.

Cathode is connected with the positive terminal of the battery. While anode is composed of graphite, the positive end or the cathode properties are different in material selection point of view. Cathode has variable chemistries. Usually, it is a metal oxide or a solution of cation doped oxides such as $LixMn_2O_4$ and Li_xCoO_2.

Separator is the thin and porous medium which separates the above stated two ends of the battery. This region only allows ions to pass through it.

The remaining constituent, electrolyte, allows only ions/charges to pass based on the potential difference in the cell. Electricity cannot pass through the electrolyte. In most cases the electrolyte is liquid medium. But sometime the electrolyte can be a solid or solid polymer too. Whatever the phases of the electrolyte, it is the heart where negative electrode, positive electrode and the separators are immersed in.

In addition to the described major components, electrodes contain some filler agents in both sides. These fillers are non-intercalating in nature but they provide the electrode the physical stability and also improve the electronic conductivity of both of the electrodes. There are current collectors in both sides of the cell.

3.2 Open Circuit Potential

Open circuit potential (OCP) is defined as the potential of positive and negative electrode without any load in the battery circuit. In another word, in case of Li-ion battery, it is the stored free energy of lithium in both of the electrodes. Negative electrode possesses more free energy of lithium. Moreover negative electrode is designed in such a way that, it has the lower potential as compared to positive electrode. Another important term from the electrochemical point of view is "utilization" of the electrodes which refers to the maximum possible lithium concentration

in the electrodes. Thus the open circuit potential can be expressed in terms of the utilization of the electrode materials. Difference between the OCP of positive and negative electrode is the cell potential.

If U^- is the potential of the negative electrode and U^+ is the potential of the positive electrode, then their difference is termed as the complete cell voltage.

3.3 Modeling of Battery Dynamics

There are several modeling approaches available for Li-Ion battery dynamics representation. One of them is empirical approach of modeling which adopts the past data of experiments to predict the future behavior of the battery. This approach of modeling provides a quick evaluation technique of range of vehicle based on battery capacity or energy density. In this modeling approach, there is no consideration of physical principles. Usually logarithmic, polynomial and exponential functions are used in this purpose. These functions are considered only to reduce the computational complexity. As there is no insight on real physics of the battery, this modeling cannot be considered for wide range of applications (for different battery chemistries). Moreover the predication on battery performance based on this modeling approach can be poor from practical application point of view.

Equivalent circuit based method is another approach for modeling Li-Ion battery. This is one of the most used technique for modeling battery dynamics. This modeling approach uses lumped parameters that make them suitable for integration with larger simulation models. A combination of circuit elements such as resistors, capacitors and inductors along with dependent sources are used in this battery model to represent the functional behavior of the electrochemical cells. The model parameters are obtained via experimental data. Although this is one of the most adopted technique for modeling, this cannot be considered as the true model, because this also ignores the real physics of the battery which is significant for providing more accurate prediction of battery performances. On the other hand, the most realistic approach for battery

modeling is the electrochemistry based modeling. In this case all of the parameters are considered during modeling. All of the works presented in this thesis are based on the electrochemical approach.

3.3.1 Electrochemical Modeling Approach

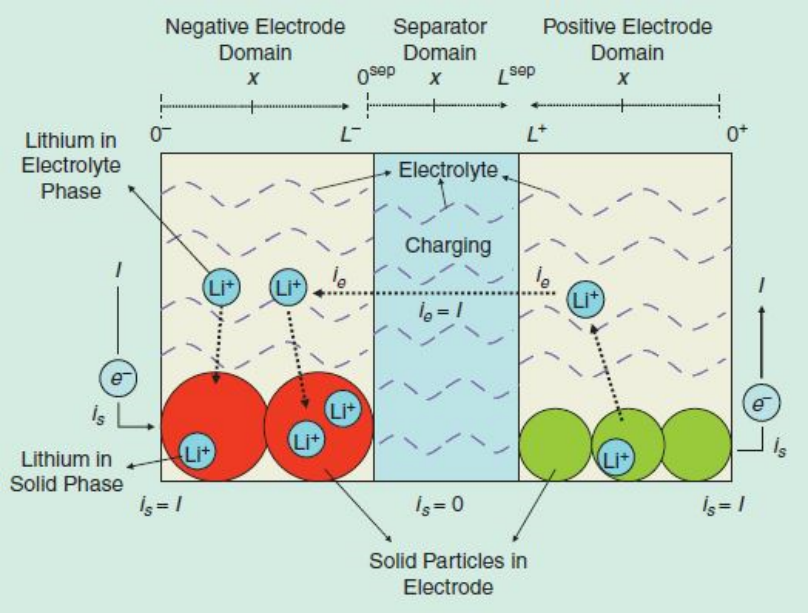

Figure 3.2. Detail of the geometry of Li-Ion battery [37]

Figure 3.2 represents the geometry of the battery cell model considered in electrochemical based modeling. This dynamic modeling considers the dynamics only in the horizontal direction, i.e. X-direction. This model is basically a 1-D spatial model where the dynamics in Y and Z direction is not considered [14] [15] [16] [17] [18] [38]. Another assumption here is that, lithium-ion particles are considered as composed of spherical particles of radius R everywhere along X- axis [37].

As mentioned earlier, there are three domains in the considered geometry, namely, the negative electrode which starts from 0^- to L^-, separator which starts from 0^{sep} to L^{sep} and the positive electrode whose range is from L^+ to 0^+.

Considered state variables for describing the 1-D spatial domains at any instantaneous time t and position x are the current in the solid electrode, $i_s(x,t)$, current in the solid electrolyte, $i_e(x,t)$, potential of the solid electrode, $\Phi_s(x,t)$, potential of the electrolyte phase, $\Phi_e(x,t)$, molar flux of lithium at the surface of the spherical lithium particle, $J_n(x,t)$, concentration of lithium at solid electrode phase, $C_s(x,r,t)$ and concentration at electrolyte phase, $C_e(x,t)$. The superscripts, i.e. $+$, $-$ and *sep* imply that the defined variables are related to the positive electrode, negative electrode and the separator respectively.

3.3.2 Input and Output of the Electrochemical Model

The input to the electrochemical model is the external current and the cell voltage is the output. One significant point which worth mentioning here is that, the current is actually the current density, i.e. the amperage value is divided with the cross-sectional area of the specific electrode of the battery geometry.

3.4 Governing Equations

The overall view of the battery geometry along with the corresponding equations and the boundary and initial conditions can be presented in Figure 3.3.

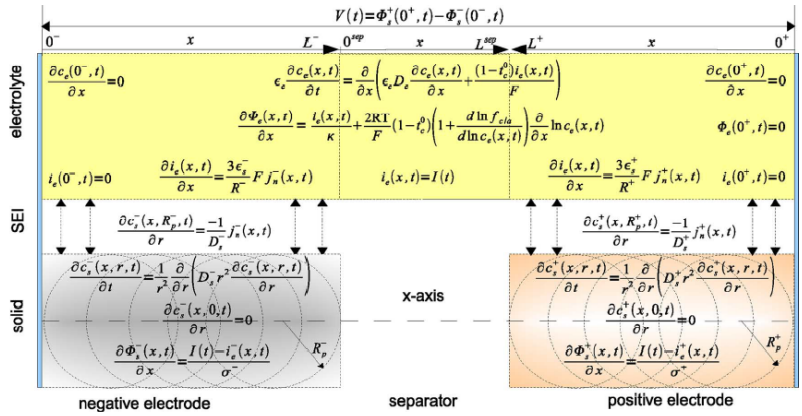

Figure 3.3. Overall view of battery model [20]

The governing equations of the electrochemical model are [19] [20] [37] [39]:

$$\varepsilon_e \frac{\partial c_e(x,t)}{\partial t} = \frac{\partial}{\partial x}(\varepsilon_e D_e \frac{\partial c_e(x,t)}{\partial x}) + \frac{1-t_c^\circ}{F} i_e(x,t) \tag{3.1}$$

$$\frac{\partial c_{s,i}(x,r,t)}{\partial t} = \frac{1}{r^2}\frac{\partial}{\partial r}(D_{s,i} r^2 \frac{\partial c_{s,i}(x,r,t)}{\partial r}) \tag{3.2}$$

$$\frac{\partial \Phi_e(x,t)}{\partial t} = -\frac{i_e(x,t)}{\kappa} + \frac{2RT}{F}(1-t_c^\circ) \times (1 + \frac{dln f_{\frac{c}{a}}}{dln c_e(x,t)}) \frac{\partial ln c_e(x,t)}{\partial x} \tag{3.3}$$

$$\frac{\partial \Phi_s(x,t)}{\partial x} = \frac{i_e(x,t) - I(t)}{\sigma} \tag{3.4}$$

$$\frac{\partial i_e(x,t)}{\partial x} = \sum_{i=1}^{n} \frac{3\varepsilon_{s,i}}{R_{p,i}} F J_{n,i}(x,t) \tag{3.5}$$

$$J_{n,i}(x,t) = \frac{i_{0,i}(x,t)}{F}(e^{\frac{\alpha_a F \eta_i(x,t)}{RT}} - e^{\frac{-\alpha_c F \eta_i(x,t)}{RT}}) \tag{3.6}$$

Here, $i_{0,i}(x,t)$ is the current density of reaction, the expression of which is given by:

$$i_{0,i}(x,t) = r_{eff,i} c_e(x,t)^{\alpha_a} (c_{s,i}^{max} - c_{ss,i}(x,t))^{\alpha_c} c_{ss,i}(x,t)^{\alpha_c} \tag{3.7}$$

And $\eta_i(x,t)$ is the cell over-potential of reaction, the expression of which is given by:

$$\eta_i(x,t) = \Phi_s(x,t) - \Phi_e(x,t) - U(c_{ss,i}(x,t)) - F R_{f,i} J_{n,i}(x,t) \tag{3.8}$$

In the above expressions, $c_{ss,i}(x,t)$ is the i^{th} solid phase concentration, $c_{s,i}^{max}$ is the maximum concentration (concentration at the surface) of the i^{th} active material and $U(c_{ss,i}(x,t))$ is the open circuit potential of the i^{th} active material in the solid electrode phase. Moreover, there are some parameters which varies depending on the temperature distribution, e.g. $R_{f,i}$, $r_{eff,i}$ and $D_{s,i}$. Their dependency on temperature can be expressed by the Arrhenius equations given by [40]:

$$\theta(T) = \theta_{T_0} e^{A_\theta \frac{(T(t) - T_0)}{T_0 T(t)}} \tag{3.9}$$

Here, $T(t)$ is the instantaneous temperature, T_0 is a standard or reference temperature and A_θ is a constant. If the equation of the solid phase concentration at any time t is observed, it is clear that, it depends on a radial variable, which brings complexity while the overall model is under simulation or under trial for solving. To eradicate this solution complexity, this r dependency is solved in [41]. The equations adopted from [41] are provided below:

$$\frac{\partial}{\partial t}\bar{c}^{\pm}_{s,i}(x,t) = -\frac{3}{R^{\pm}_i} J^{\pm}_{n,i}(x,t) \tag{3.10}$$

$$\frac{\partial}{\partial t}\bar{q}^{\pm}_{s,i}(x,t) = -\frac{30}{(R^{\pm}_i)^2}\bar{q}^{\pm}_{s,i}(x,t) - \frac{45}{2(R^{\pm}_i)^2} J^{\pm}_{n,i}(x,t) \tag{3.11}$$

$$c^{\pm}_{ss,i}(x,t) = \bar{c}^{\pm}_{s,i}(x,t) + \frac{8R^{\pm}_i}{35}\bar{q}^{\pm}_{s,i}(x,t) - \frac{R^{\pm}_i}{35D^{\pm}_{s,i}} J^{\pm}_{n,i}(x,t) \tag{3.12}$$

In these equations, + and − sign denotes the positive terminal (cathode) and negative terminal (anode) of the cell. In Addition to these notations, $\bar{c}^{\pm}_{s,i}(x,t)$ is the volume averaged concentration, $\bar{q}^{\pm}_{s,i}(x,t)$ is the averaged concentration flux and $c^{\pm}_{ss,i}(x,t)$ is the concentration at the particle surface.

Among all the parameters involved in the previous equations, some parameters are constant and some are dependent on temperature and the concentration. ε_e, t^0_c, ε_s, α_a, α_c, σ, F, R and $R^{\pm}_i$ are the constant parameters. The constant nature of these parameters is maintained throughout the overall battery geometry. On the other hand, κ, D_e and $f_{\frac{c}{a}}$ are the functions of temperature and the concentration.

Considering the approximation for complexity reduction purpose, the overall equations for the positive side (cathode) of the battery is presented by the followings, where the range of x is L^+ to 0^+.

$$\frac{\partial}{\partial t}\bar{c}^{+}_{s,i}(x,t) = -\frac{3}{R^{+}_i} J^{+}_{n,i}(x,t)$$

$$\frac{\partial}{\partial t}\bar{q}^{+}_{s,i}(x,t) = -\frac{30}{(R^{+}_i)^2}\bar{q}^{+}_{s,i}(x,t) - \frac{45}{2(R^{+}_i)^2} J^{+}_{n,i}(x,t)$$

$$c^{+}_{ss,i}(x,t) = \bar{c}^{+}_{s,i}(x,t) + \frac{8R^{+}_i}{35}\bar{q}^{+}_{s,i}(x,t) - \frac{R^{+}_i}{35D^{+}_{s,i}} J^{+}_{n,i}(x,t)$$

$$\frac{\partial \Phi_e^+(x,t)}{\partial t} = -\frac{i_e^+(x,t)}{\kappa} + \frac{2RT}{F}(1-t_c^\circ) \times (1 + \frac{dlnf_{\frac{c}{a}}}{dlnc_e(x,t)})\frac{\partial lnc_e(x,t)}{\partial x}$$

$$\frac{\partial \Phi_s^+(x,t)}{\partial x} = \frac{i_e^+(x,t) - I(t)}{\sigma^+}$$

$$\frac{\partial i_e^+(x,t)}{\partial x} = \sum_{i=1}^{n} \frac{3\varepsilon_{s,i}^+}{R_, i^+} F J_{n,i}^+(x,t)$$

$$J_{n,i}^+(x,t) = \frac{i_{0,i}^+(x,t)}{F}(e^{\frac{\alpha_a F \eta_i^+(x,t)}{RT}} - e^{\frac{-\alpha_c F \eta_i^+(x,t)}{RT}})$$

Moreover, the equations for negative side (anode) using the same conditions and assumptions are the followings, where the range of x is 0^- to L^-.

$$\frac{\partial}{\partial t}\bar{c}_{s,i}^-(x,t) = -\frac{3}{R_i^-} J_{n,i}^-(x,t)$$

$$\frac{\partial}{\partial t}\bar{q}_{s,i}^-(x,t) = -\frac{30}{(R_i^-)^2}\bar{q}_{s,i}^-(x,t) - \frac{45}{2(R_i^-)^2} J_{n,i}^-(x,t)$$

$$c_{ss,i}^-(x,t) = \bar{c}_{s,i}^-(x,t) + \frac{8R_i^-}{35}\bar{q}_{s,i}^-(x,t) - \frac{R_i^-}{35 D_{s,i}^-} J_{n,i}^-(x,t)$$

$$\frac{\partial \Phi_e^-(x,t)}{\partial t} = -\frac{i_e^-(x,t)}{\kappa} + \frac{2RT}{F}(1-t_c^\circ) \times (1 + \frac{dlnf_{\frac{c}{a}}}{dlnc_e(x,t)})\frac{\partial lnc_e(x,t)}{\partial x}$$

$$\frac{\partial \Phi_s^-(x,t)}{\partial x} = \frac{i_e^-(x,t) - I(t)}{\sigma^-}$$

$$\frac{\partial i_e^-(x,t)}{\partial x} = \sum_{i=1}^{n} \frac{3\varepsilon_{s,i}^-}{R_, i^-} F J_{n,i}^-(x,t)$$

$$J_{n,i}^-(x,t) = \frac{i_{0,i}^-(x,t)}{F}(e^{\frac{\alpha_a F \eta_i^-(x,t)}{RT}} - e^{\frac{-\alpha_c F \eta_i^-(x,t)}{RT}})$$

Output equation of this electrochemical model is, $V(t) = \Phi_s(0^+,t)$ - $\Phi_s(0^-,t)$

3.5 Temperature Equation of the Battery Model

The internal average temperature distribution in this electrochemical model of Li-Ion battery is a lumped one, which is given by:

$$\rho^{avg} c_p \frac{dT(t)}{dt} = h_{cell}(T_{amb} - T(t)) + I(t)V(t) - \sum_{i=1}^{n}[\int_{0^-}^{0^+} \frac{3\varepsilon_{s,i}}{R_{p,i}} F J_{n,i}(x,t)\Delta U_i(x,t)dx] \tag{3.13}$$

Here, h_{cell} is a constant and $T_{amb}(t)$ is the ambient temperature.

In the temperature equation,

$$\Delta U_i(x,t) \triangleq U_i(\bar{c}_{s,i}(x,t) - T(t)\frac{\partial U_i(\bar{c}_{s,i}(x,t))}{\partial T})$$

$\bar{c}_{s,i}(x,t)$ is the Volume averaged concentration of a single particle, which is again defined as :

$$\bar{c}_{s,i}(x,t) \triangleq \frac{3}{R_i^3}\int_0^{R_i} r^2 c_{s,i}(x,r,t)dr$$

3.6 Equations of OCP

There are two empirical equations which are adopted to calculate the individual electrode potentials. For the positive terminal ($LiCoO_2$) of the battery, the following equation is adopted [42]:

$$U_p = \frac{-4.656 + 88.669\theta_p^2 - 401.119\theta_p^4 + 342.909\theta_p^6 - 462.471\theta_p^8 + 433.434\theta_p^{10}}{-1 + 18.933\theta_p^2 - 79.532\theta_p^4 + 37.311\theta_p^6 - 73.083\theta_p^8 + 95.96\theta_p^{10}}$$

Here, $\theta_p = \frac{c_{s,p \ at \ r=R_p}}{c_{s,p,max}}$, a dimensionless number which in turn can be regarded as the State of charge in cathode. The profile for U_p with respect to θ_p is given in Figure 3.4.

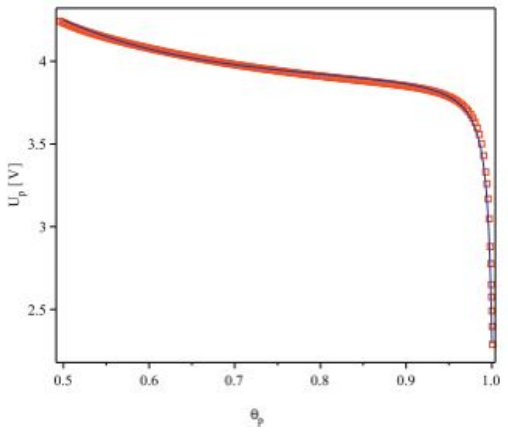

Figure 3.4. U_p profile [43]

For anode (LiC_6), the empirical equation is given by [42]:

$$U_n = 0.7222 + 0.1387\theta_n + 0.029\theta_n^{0.5} - \frac{0.0172}{\theta_n} + \frac{0.0019}{\theta_n^{1.5}} + 0.2808e^{(0.90-15\theta_n)} - 0.7984e^{(0.4465\theta_n - 0.4108)}$$

Here, $\theta_n = \frac{c_{s,n \ at \ r=R_n}}{c_{s,n,max}}$, a dimensionless number which in turn can be regarded as the State of charge in anode. The distribution of U_n with respect to θ_n is provided in Figure 3.5.

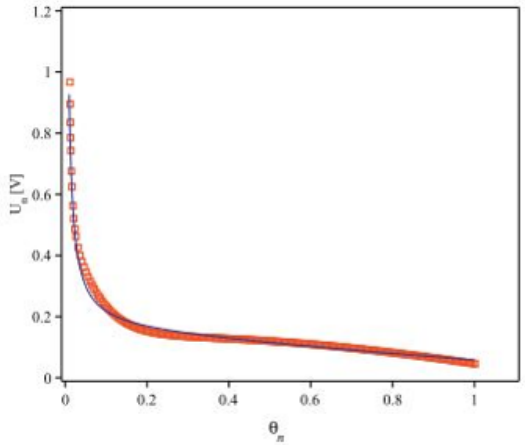

Figure 3.5. U_n profile [43]

In Figure 3.4 and Figure 3.5, the square points refer the original empirical equation plot while the solid line represents the simplified curve fitted plot of the individual potential equations at positive and negative electrode respectively [42].

3.7 Model Simplification

The above described electrochemical model of Li-Ion battery is based on few assumptions. Even after using the assumptions the model is still too complex to solve. For this point of view, a model simplification is performed. The model simplification was done in a manner that, the reduced model will be simple enough to use this in control purpose but at the same time, the reduced model should capture the main dynamic behavior of the battery [20]. Keeping these requirements in mind a key assumption was considered which gives the desired reduced model to work with.

The adopted assumption for the model reduction purpose is a constant electrolyte concentration [20], i.e. $c_e(x,t) = c_e$, where, c_e is a constant which reduces the model significantly.

After using the above assumption based reduction, the model is reduced significantly which is computationally inexpensive. The reduced model is given below [20]: For the cathode terminal, i.e. $x\epsilon[L^+, 0^+]$, the reduced model equations are [20]:

$$\frac{\partial}{\partial t}\bar{c}^+_{s,i}(x,t) = -\frac{3}{R^+_i}J^+_{n,i}(x,t)$$

$$\frac{\partial}{\partial t}\bar{q}^+_{s,i}(x,t) = -\frac{30}{(R^+_i)^2}\bar{q}^+_{s,i}(x,t) - \frac{45}{2(R^+_i)^2}J^+_{n,i}(x,t)$$

$$c^+_{ss,i}(x,t) = \bar{c}^+_{s,i}(x,t) + \frac{8R^+_i}{35}\bar{q}^+_{s,i}(x,t) - \frac{R^+_i}{35D^+_{s,i}}J^+_{n,i}(x,t)$$

$$\frac{\partial \Phi^+_e(x,t)}{\partial t} = -\frac{i^+_e(x,t)}{\kappa^+}$$

$$\frac{\partial \Phi^+_s(x,t)}{\partial x} = \frac{i^+_e(x,t) - I(t)}{\sigma^+}$$

$$\frac{\partial i^+_e(x,t)}{\partial x} = \sum_{i=1}^{n}\frac{3\varepsilon^+_{s,i}}{R_, i^+}FJ^+_{n,i}(x,t)$$

$$J^+_{n,i}(x,t) = \frac{i^+_{0,i}(x,t)}{F}(e^{\frac{\alpha_a F\eta^+_i(x,t)}{RT}} - e^{\frac{-\alpha_c F\eta^+_i(x,t)}{RT}})$$

Following the similar fashion for the anode, i.e. $x\epsilon[0^-, L^-]$, the reduced model equations are [20]:

$$\frac{\partial}{\partial t}\bar{c}^-_{s,i}(x,t) = -\frac{3}{R^-_i}J^-_{n,i}(x,t)$$

$$\frac{\partial}{\partial t}\bar{q}^-_{s,i}(x,t) = -\frac{30}{(R^-_i)^2}\bar{q}^-_{s,i}(x,t) - \frac{45}{2(R^-_i)^2}J^-_{n,i}(x,t)$$

$$c^-_{ss,i}(x,t) = \bar{c}^-_{s,i}(x,t) + \frac{8R^-_i}{35}\bar{q}^-_{s,i}(x,t) - \frac{R^-_i}{35D^-_{s,i}}J^-_{n,i}(x,t)$$

$$\frac{\partial \Phi^-_e(x,t)}{\partial t} = -\frac{i^-_e(x,t)}{\kappa^-}$$

$$\frac{\partial \Phi^-_s(x,t)}{\partial x} = \frac{i^-_e(x,t) - I(t)}{\sigma^-}$$

$$\frac{\partial i^-_e(x,t)}{\partial x} = \sum_{i=1}^{n}\frac{3\varepsilon^-_{s,i}}{R_, i^-}FJ^-_{n,i}(x,t)$$

$$J_{n,i}^{-}(x,t) = \frac{i_{0,i}^{-}(x,t)}{F}(e^{\frac{\alpha_a F \eta_i^{-}(x,t)}{RT}} - e^{\frac{-\alpha_c F \eta_i^{-}(x,t)}{RT}})$$

The temperature model equation for the reduced model remains same as the previous one which is given below by indicating the regional notations in the equation:

$$\rho^{avg} c_p \frac{dT(t)}{dt} = h_{cell}(T_{amb} - T(t)) + I(t)V(t) - \sum_{i=1}^{n}[\int_{0^-}^{L^-} \frac{3\varepsilon_{s,i}}{R_{p,i}} F J_{n,i}(x,t)\Delta U_i(x,t)dx]$$

$$-\sum_{i=1}^{n}[\int_{L^+}^{0^+} \frac{3\varepsilon_{s,i}}{R_{p,i}} F J_{n,i}(x,t)\Delta U_i(x,t)dx]$$

The output equation remains same as the previous one, which is:

$$V(t) = \Phi_s(0^+,t) - \Phi_s(0^-,t)$$

3.8 Initial and Boundary Conditions of the Model

The initial conditions for the described PDE equation based system are given as:

$$\bar{c}_{s,i}^{\pm}(x,0) = \bar{c}_{s,i,0}^{\pm}(x)$$

$$\bar{q}_{s,i}^{\pm}(x,0) = \bar{q}_{s,i,0}^{\pm}(x)$$

$$T(0) = T_0$$

The boundary conditions are as followings:

$$\Phi_e^{+}(0^+,t) = 0$$

$$\Phi_e^{-}(L^-,t) = \Phi_e^{+}(L^+,t) - \frac{I(t)L^{sep}}{\kappa^{sep}}$$

$$i_e^{\pm}(0^{\pm},t) = 0$$

$$i_e^{\pm}(L^{\pm},t) = \pm I(t)$$

3.9 Verification of Model Response

The reduced order model was first validated using the standard current data. The model ran for $1C$, $2C$ and $0.5C$ rate and the responses was compared with the theoretical responses.

First the model ran in $1C$ rate, i.e. $30A/m^2$ and the response is provided in Figure 3.6.

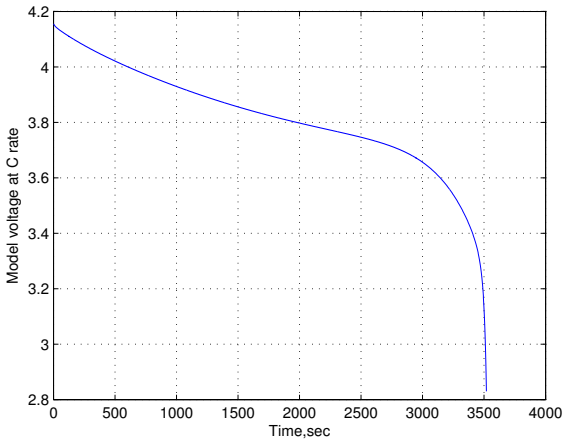

Figure 3.6. Reduced order model response for 1C rate

From the above plot, it is clear that, the battery is discharged at almost 1hr (nearly at 3600s), which is in accord with the theoretical response of the Li-Ion battery.

For further assurance, the model ran in $2C$ rate, where the battery should be discharged at 30 minutes. Here, the battery ran under $60A/m^2$ and the battery model response to this input current is provided in Figure 3.7.

In $2C$ rate, the whole battery is discharged at nearly 30 minutes, which is again in accord with the theoretical response.

Furthermore, the model ran in slower discharge rate, in $0.5C$ rate, where theoretically, the whole battery should be discharged at 2hrs. In this case, the battery model ran under $15A/m^2$ and the response was recorded which is provided in Figure 3.8.

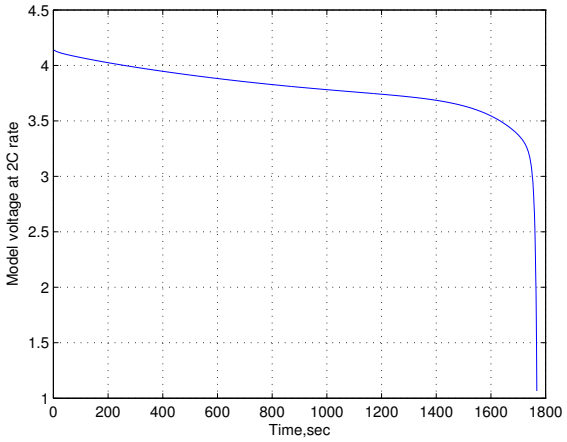

Figure 3.7. Reduced order model response for 2C rate

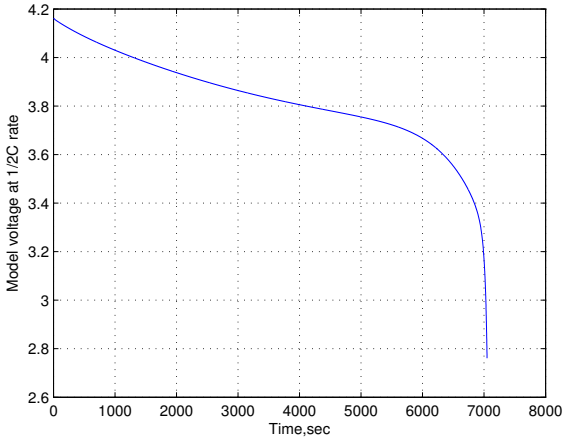

Figure 3.8. Reduced order model response for 0.5C rate

This response also keeps consistency with the theory of battery discharge. After getting these kind of responses from the model, a decision was taken, which is, this reduced electrochemical model can be used for any kind of input current profile for the estimation and control purpose.

4. PDAE OBSERVER EQUATIONS

As the main objective of this thesis work is to have a fault diagnosis, residual is an important factor here. The residuals of the measured signal (voltage, current or SOC) can be obtained by comparing the simulated model response with the response from another source. This reference source is the observer. That means, to have the faults diagnosed, an observer is crucial. For this reduced electrochemical model of the battery, a partial differential algebraic equation (PDAE) based observer was used. During the design of the observer. In this adopted model of observer, the difference between the model predicted voltage and the calculated voltage is injected via multiplication of a linear corrective term, i.e. gain, in the volume averaged concentration equation as well as the average internal temperature equation in the reduced order model equations [20].

The PDAE observer equations are adopted from [20] which are as followings:

For the cathode terminal, i.e. $x\epsilon[L^+, 0^+]$:

$$\frac{\partial}{\partial t}\hat{\bar{c}}^+_{s,i}(x,t) = -\frac{3}{R^+_i}\hat{J}^+_{n,i}(x,t) + \gamma^+_i(V(t) - \hat{V}(t))$$

$$\frac{\partial}{\partial t}\hat{\bar{q}}^+_{s,i}(x,t) = -\frac{30}{(R^+_i)^2}\hat{\bar{q}}^+_{s,i}(x,t) - \frac{45}{2(R^+_i)^2}\hat{J}^+_{n,i}(x,t)$$

$$\hat{c}^+_{ss,i}(x,t) = \hat{\bar{c}}^+_{s,i}(x,t) + \frac{8R^+_i}{35}\hat{\bar{q}}^+_{s,i}(x,t) - \frac{R^+_i}{35D^+_{s,i}}\hat{J}^+_{n,i}(x,t)$$

$$\frac{\partial\hat{\Phi}^+_e(x,t)}{\partial t} = -\frac{\hat{i}^+_e(x,t)}{\kappa^+}$$

$$\frac{\partial\hat{\Phi}^+_s(x,t)}{\partial x} = \frac{\hat{i}^+_e(x,t) - I(t)}{\sigma^+}$$

$$\frac{\partial\hat{i}^+_e(x,t)}{\partial x} = \sum_{i=1}^{n}\frac{3\varepsilon^+_{s,i}}{R,i^+}F\hat{J}^+_{n,i}(x,t)$$

$$\hat{J}^+_{n,i}(x,t) = \frac{\hat{i}^+_{0,i}(x,t)}{F}(e^{\frac{\alpha_a F\hat{\eta}^+_i(x,t)}{RT}} - e^{\frac{-\alpha_c F\hat{\eta}^+_i(x,t)}{RT}})$$

Similarly for the anode, i.e. $x\epsilon[0^-, L^-]$, the observer equations are as the followings:

$$\frac{\partial}{\partial t}\hat{\bar{c}}^-_{s,i}(x,t) = -\frac{3}{R^-_i}\hat{J}^-_{n,i}(x,t) + \gamma^-_i(V(t) - \hat{V}(t))$$

$$\frac{\partial}{\partial t}\hat{\bar{q}}^-_{s,i}(x,t) = -\frac{30}{(R^-_i)^2}\hat{\bar{q}}^-_{s,i}(x,t) - \frac{45}{2(R^-_i)^2}\hat{J}^-_{n,i}(x,t)$$

$$\hat{c}^-_{ss,i}(x,t) = \hat{\bar{c}}^-_{s,i}(x,t) + \frac{8R^-_i}{35}\hat{\bar{q}}^-_{s,i}(x,t) - \frac{R^-_i}{35D^-_{s,i}}\hat{J}^-_{n,i}(x,t)$$

$$\frac{\partial\hat{\Phi}^-_e(x,t)}{\partial t} = -\frac{\hat{i}^-_e(x,t)}{\kappa^-}$$

$$\frac{\partial\hat{\Phi}^-_s(x,t)}{\partial x} = \frac{\hat{i}^-_e(x,t) - I(t)}{\sigma^-}$$

$$\frac{\partial\hat{i}^-_e(x,t)}{\partial x} = \sum_{i=1}^{n}\frac{3\varepsilon^-_{s,i}}{R_,i^-}F\hat{J}^-_{n,i}(x,t)$$

$$\hat{J}^-_{n,i}(x,t) = \frac{\hat{i}^-_{0,i}(x,t)}{F}(e^{\frac{\alpha_a F\hat{\eta}^-_i(x,t)}{RT}} - e^{\frac{-\alpha_c F\hat{\eta}^-_i(x,t)}{RT}})$$

The observer equation for the internal average temperature is given [20] below:

$$\rho^{avg}c_p\frac{d\hat{T}(t)}{dt} = h_{cell}(T_{amb} - \hat{T}(t)) + I(t)\hat{V}(t) - \sum_{i=1}^{n}[\int_{0^-}^{L^-}\frac{3\varepsilon_{s,i}}{R_{p,i}}FJ_{n,i}(x,t)\Delta U_i(x,t)dx]$$

$$-\sum_{i=1}^{n}[\int_{L^+}^{0^+}\frac{3\varepsilon_{s,i}}{R_{p,i}}FJ_{n,i}(x,t)\Delta U_i(x,t)dx] + \gamma^{\pm}_T(V(t) - \hat{V}(t))$$

The output equation of the observer is:

$$\hat{V}(t) = \hat{\Phi}_s(0^+,t) - \hat{\Phi}_s(0^-,t)$$

In the above observer equations, the hat sign indicates the observed variables and the observer gain was denoted by γ. When the value of γ changes, depending on this the corresponding gain in particular electrode side also changes. The gain value for the particular electrodes are calculated using the mass conservation principles in each of the electrodes [20]. The observer gain values are expressed as [20]:

$$\begin{bmatrix}\gamma^-_i\\ \gamma^+_i\end{bmatrix} = \gamma \times \begin{bmatrix}\frac{1}{n^-\varepsilon^-_{s,i}L^-}\\ \frac{1}{n^+\varepsilon^+_{s,i}L^+}\end{bmatrix} \tag{4.1}$$

Depending on the γ value, the observer gain for the individual electrode changes following the equation provided for the observer. This deterministic γ value is determined by trial and error method. One important point to be noted here is that, although the observer gain for the temperature equation is provided in this thesis work, the observer gain for temperature is considered as zero, because during this electrochemical modeling, temperature was assumed to be constant at room temperature, i.e. 298.15K.

4.1 Initial Conditions of the Observer

The initial condition for the observer are given as:

$$\hat{c}^{\pm}_{s,i}(x,0) = \hat{c}^{\pm}_{s,i,0}(x)$$

$$\hat{q}^{\pm}_{s,i}(x,0) = \hat{q}^{\pm}_{s,i,0}(x)$$

$$\hat{T}(0) = \hat{T}_0$$

4.2 Tuning of Observer Gain

As mentioned earlier, the observer gain value was determined by trial and error method keeping the aim to achieve the minimum error value between the model output voltage and the observer output voltage. This γ value was tuned to get an optimum value which gives the minimum difference between the stated two variables.

After several trials, the approximate of the desired value of γ was obtained. For example for $1C$ rate of the battery, for $\gamma = 1 \times 10^{-3}$, the voltage plot is as Figure 4.1.

In naked eye, there is no difference seen. But, if this plot is observed carefully, it is evident that, there are significant amount of error exists between the voltage profiles.

The zoomed portion for time between 3300 to 3350 sec, is provided in Figure 4.2.

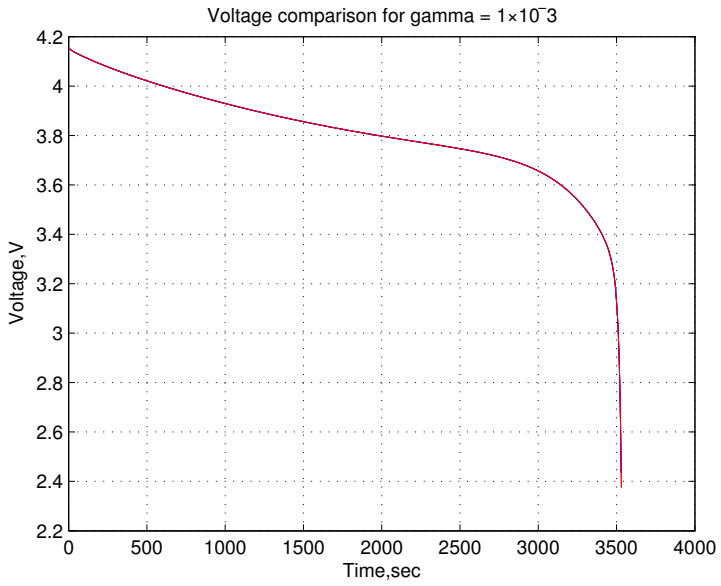

Figure 4.1. Model and observer voltage for $\gamma = 1 \times 10^{-3}$

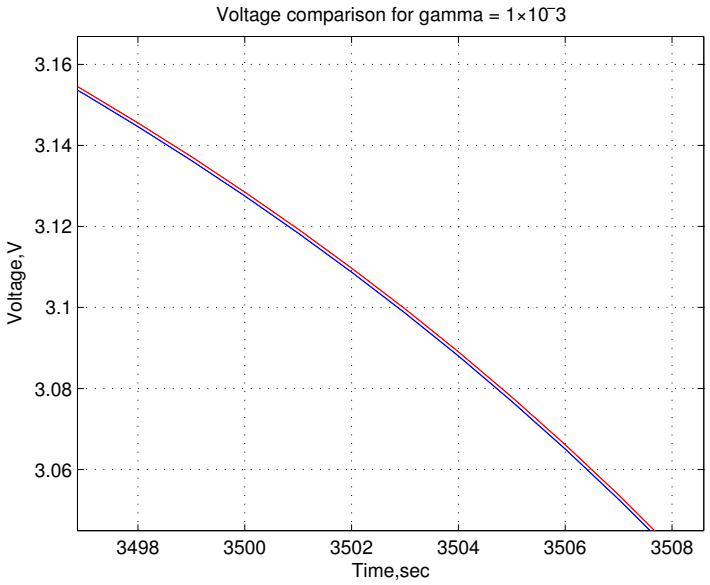

Figure 4.2. Zoomed view of the Model and observer voltage response for $\gamma = 1 \times 10^{-3}$

The similar profiles were evaluated for the gain value, $\gamma = 53 \times 10^{-3}$, which is provided in Figure 4.3.

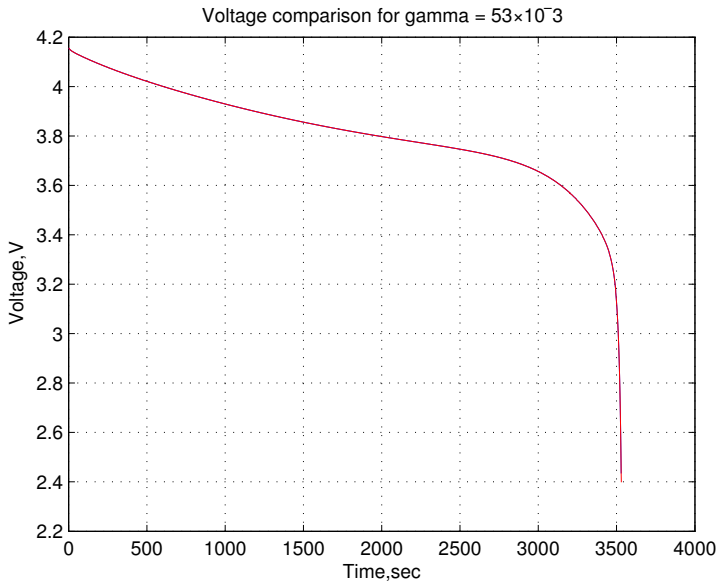

Figure 4.3. Model and observer voltage for $\gamma = 53 \times 10^{-3}$

A zoomed view of Figure 4.3 is provided in Figure 4.4, as the previous zoomed view for a better look at the differences of the voltage responses for changing value of γ.

In this comparison, a negligible amount of error is present, which is the optimum for the error value. For reference of this error value, the mean error value between these two profiles are provided in Table 4.1, for both of the γ values. Here, mean error is defined as the average difference of the voltage responses from the model and the observer, i.e. mean error = (model voltage - observer voltage)/number of sample data.

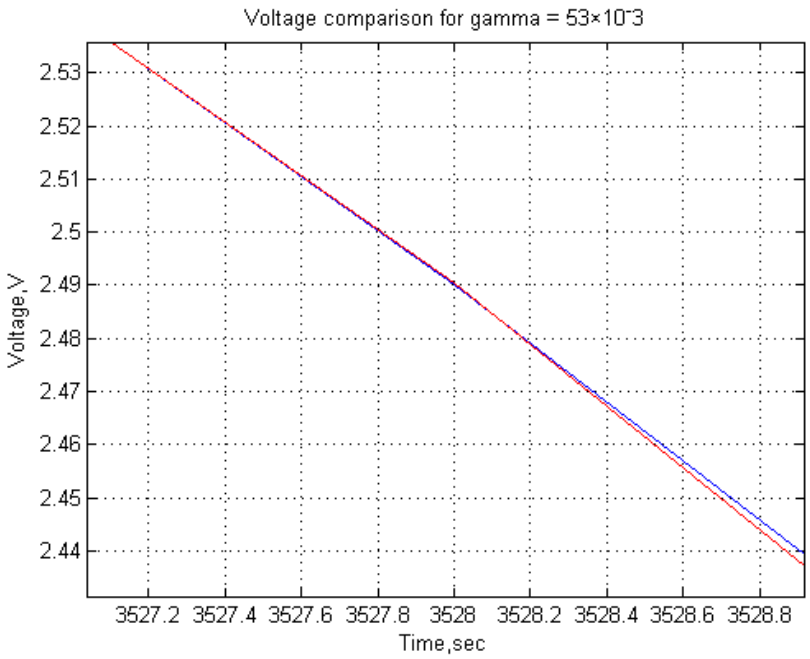

Figure 4.4. Zoomed view of the Model and observer voltage response for $\gamma = 53 \times 10^{-3}$

Table 4.1. Tuned γ value and associated mean error value

Reference γ value	Associated mean error value
1×10^{-3}	7.0148×10^{-5}
53×10^{-3}	9.3306×10^{-6}

If the value of γ is taken beyond the stated maximum referred value in Table 4.1, there is an increase in mean error value. Therefore, the estimation and diagnosis works are performed based on this gain value, i.e. $\gamma = 53 \times 10^{-3}$.

5. MULTIPLE MODEL ADAPTIVE ESTIMATION

This adaptive estimation scheme is a unique type of observer based condition monitoring / fault diagnosis technique [44] [45] [46] [47] [48]. This incorporates observer bank of n observer, among which only one of the corresponding models represents the normal or the Healthy condition of the battery plant model being monitored and the remaining $(n-1)$ observers represent the faulty conditions or the unhealthy scenarios [21] [49] [50]. MMAE [50] [51] [52] [53] [54] provides an excellent scope of fault diagnosis, i.e. the decision can be made based on multiple possible scenarios instead of based on only one model. The major distinguishing feature of MMAE is that, this provides a probabilistic approach of condition monitoring. Figure 5.1 represents a skeleton of MMAE algorithm.

The conditional probability evaluator adopts the information of the residuals to assign the probability of exactness weighting to each of all of the observer output.The summation of all of the output probability vale from the conditional probability evaluator scheme is one, i.e.

$$p_1 + p_2 + p_3 + ... + p_n = 1$$

The expressions of the above probability values for n^{th} model at time sample k is given by [49] [52] [55]:

$$p_{n,k} = \frac{f_{z(k)|a,z(k-1)}(z_k|a_n, z_{k-1})p_n(k-1)}{\sum_{j=1}^{n} f_{z(k)|a,z(k-1)}(z_k|a_j, z_{k-1})p_j(k-1)}$$

where, $f_{z(k)|a,z(k-1)}(z_k|a_n, z_{k-1})p_n(k-1)$ is the conditional probability density function of the n^{th} model considering the history of the measurement.

The conditional probability function is given by [55]:

$$f_{z(k)|a,z(k-1)}(z_k|a_n, z_{k-1}) = \beta_n \exp(\circ)$$

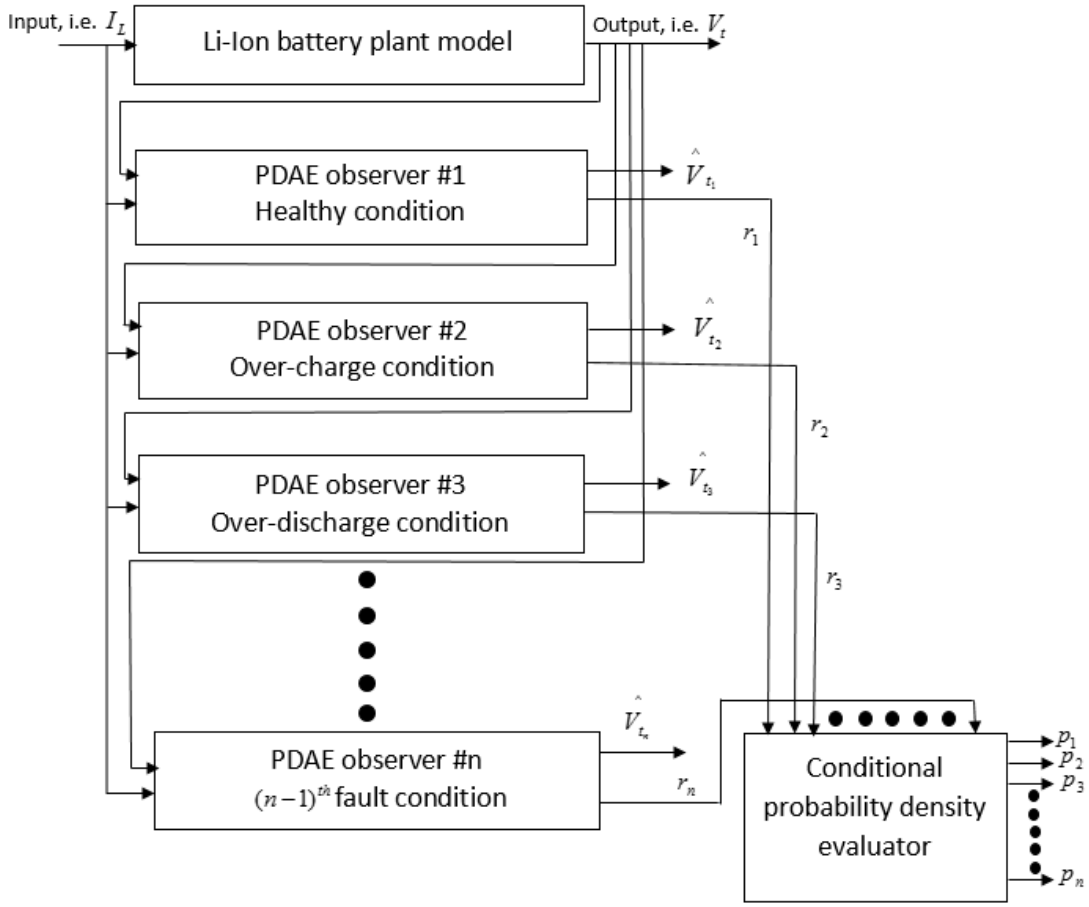

Figure 5.1. MMAE algorithm skeleton

where,

$$\beta_n = \frac{1}{(2\pi)^{l/2}|\psi_n(k)|^{1/2}}$$

l is the measurement dimension and in this work l is equal to 1 (because, only the cell voltage is being measured) and

$$(\circ) = \frac{1}{2} r_{n,k}^T \psi_{n,k}^{-1} r_{n,k}$$

Where, $r_{(n,k)}$ is the residual signal for the n^{th} model at time sample k. $\psi_{n,k}$ is the covariance of the residual signal evaluated at each sample and is given by [51] [52] [54]:

$$\psi_{n,k} = C_{n,k} P_{n,k|k} C_{n,k}^T + R$$

Where, $C_{n,k}$ is the output vector for n^{th} system at any time sample k. P and R are the process and measurement noise covariance matrices respectively.

5.1 MMAE Implementation for UDDS Current Profile

In this work, the MMAE algorithm implemented for UDDS cycle current profile. UDDS stands for Urban Dynamometer Driving Schedule [56], which is authorized by the United States environmental protection agency (EPA) for light duty vehicles. The velocity (speed) profile of a hybrid electric vehicle under the standard of UDDS is provided in Figure 5.2.

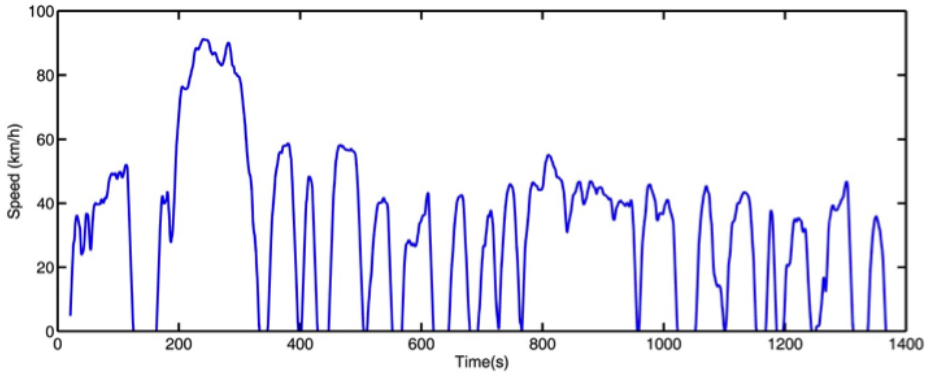

Figure 5.2. Speed profile of UDDS [57]

A Hybrid electric vehicle (HEV) model was simulated having the objective to get an optimum fuel efficiency and better energy management algorithm of the vehicle. For the simulation purpose, AUTONOMIE [58], a vehicle simulator developed by Argonne National Laboratory was adopted.

For fault diagnosis purpose, a small portion of the UDDS cycle simulated current profile of the battery is adopted, which is provided in Figure 5.3.

This current profile was later used in the adaptive estimation purpose for different possible operating conditions of the Li-Ion battery.

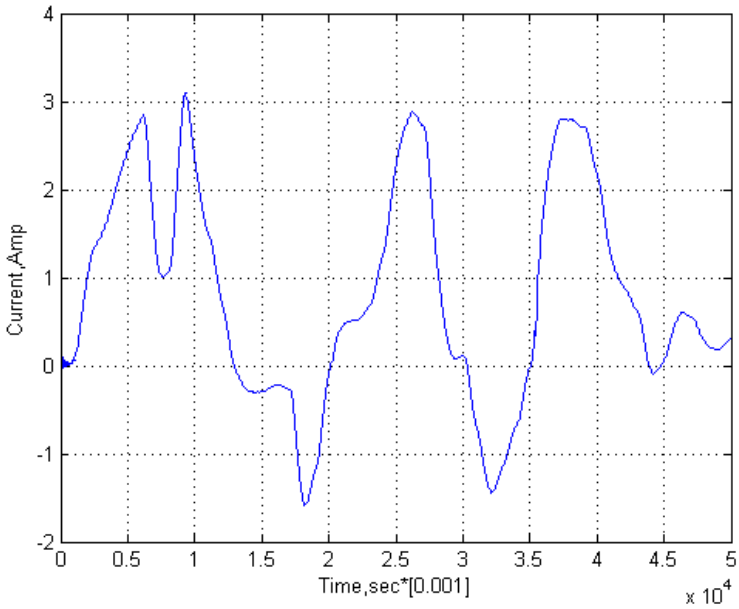

Figure 5.3. A portion of battery load current from a HEV simulation for UDDS cycle

The general parameters for the battery geometry is provided in Table 5.1, which are assumed to be common to all of the possible battery conditions.

Four possible conditions of the battery were considered to work with, i.e. Healthy or normal condition, degraded or aged condition, over-charged condition and over-discharged condition. There are some condition specific parameters which governs those particular conditions. Those model specific parameters for the Li-Ion battery are the diffusion coefficient in cathode and anode and the diffusional conductivity or intercalation / de-intercalation reaction rate constant in cathode and anode. These values are listed in Table 5.2.

Table 5.1. General parameters of electrochemical model [42]

Symbol	Unit	Positive electrode	Separator	Negative separator
σ_i	S/m	100		100
$\varepsilon_{f,i}$		0.025		0.0326
ε_i		0.385	0.724	0.485
$c_{s,i,max}$	mol/m^3	51554		30555
$c_{s,i0}$	mol/m^3	0.4955×51554		0.8551×30555
c_0	mol/m^3		1000	
R_p	m	2×10^{-6}		2×10^{-6}
L_i	m	80×10^{-6}	25×10^{-6}	88×10^{-6}
R_{SEI}	Ωm^2	0.0	0.0	0.0
F	C/mol		96487	
R	$J/molK$		8.314	
T	JK		298.15	

Table 5.2. Model specific parameters [59]

Parameter	Healthy	Aged	OD	OC
D_n	$3.9 \times 10^{-}14$	$4.875 \times 10^{-}15$	$7.8 \times 10^{-}15$	$6.5 \times 10^{-}15$
D_p	$1.0 \times 10^{-}14$	$1.5 \times 10^{-}14$	$5.0 \times 10^{-}15$	$5.0 \times 10^{-}15$
k_n	$5.0307 \times 10^{-}11$	$6.2884 \times 10^{-}12$	$1.0061 \times 10^{-}11$	$8.38 \times 10^{-}12$
k_p	$2.334 \times 10^{-}11$	$2.33 \times 10^{-}11$	$1.17 \times 10^{-}11$	$1.17 \times 10^{-}11$

5.2 Model and PDAE Observer Responses to the UDDS Current Profile

The reduced order model was simulated with the input current profile from UDDS cycle simulation on a HEV. For four different models as stated earlier, their responses were investigated. After simulating the electrochemical model of the battery, the battery voltage was observed using the stated PDAE observer. Here, both the model and observer voltage responses are provided. The response of the reduced order model and the PDAE observer for the Healthy condition of the battery is provided in Figure 5.4.

Figure 5.4. Healthy battery model and observer voltage responses

Similarly, the reduced order model was simulated and observed for the degraded situation of the battery and the voltage responses are provided in Figure 5.5.

Figure 5.5. Aged battery model and observer voltage responses

In addition to previous two, voltage comparison of the model and the observer for the over-charged battery is provided in Figure 5.6.

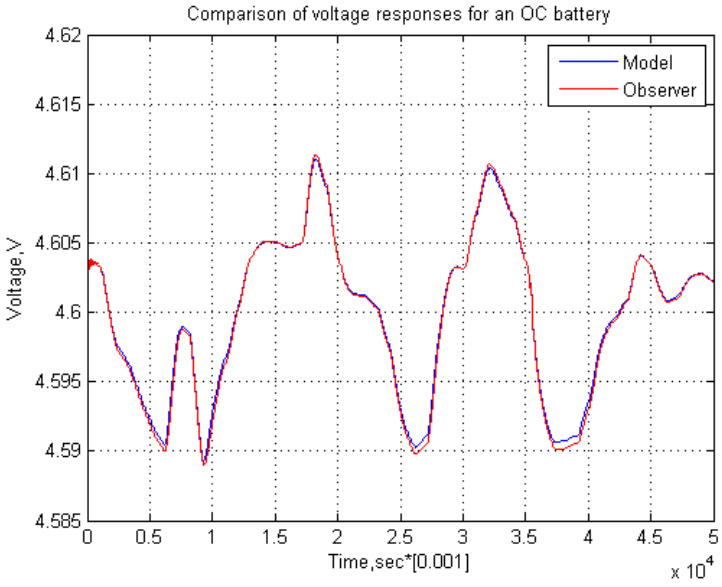

Figure 5.6. OC battery model and observer voltage responses

Finally, the model output voltage and the observer output voltage responses for the remaining model, i.e. the over-discharged model is investigated as Figure 5.7.

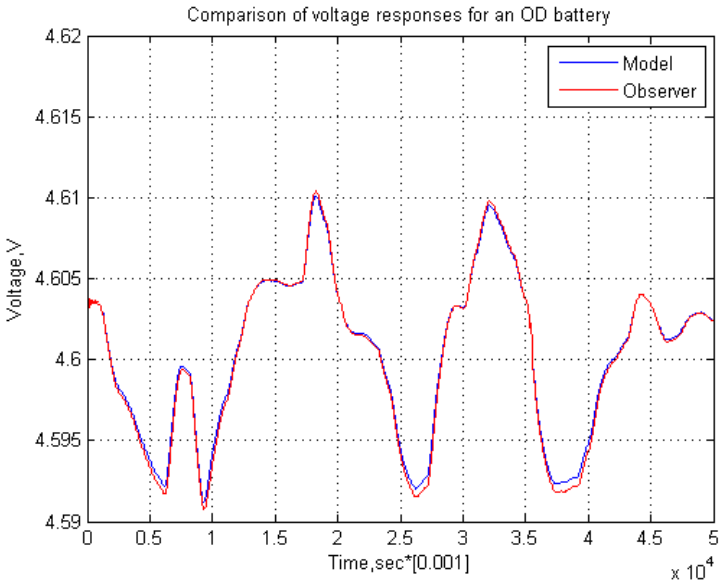

Figure 5.7. OD battery model and observer voltage responses

5.3 Voltage Response Difference Between the Model and Observer

After evaluating the reduced order model response and the response of the observer, the difference between the voltage outputs are calculated. The voltage response differences or the residuals are defined as, Voltage residual = Individual model voltage response - the individual battery observer voltage response. The mean value of the differences or residuals is almost zero.

For the Healthy battery condition, the difference between the responses is nearly zero and the difference profile is provided in Figure 5.8.

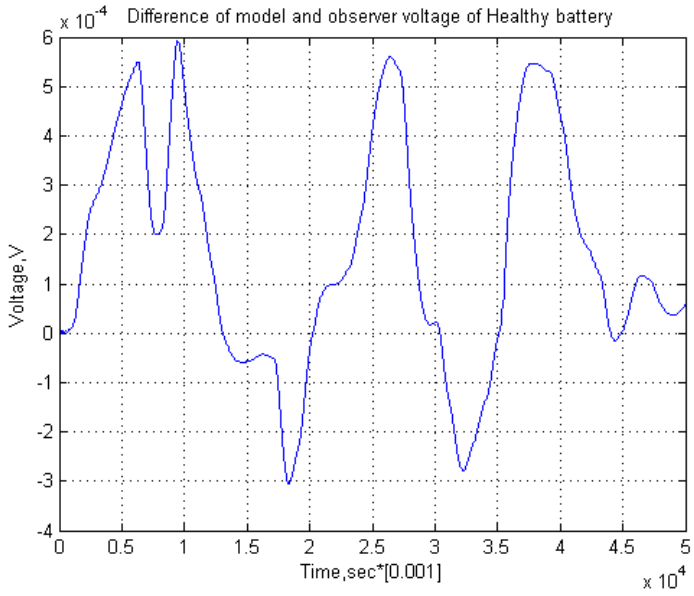

Figure 5.8. Model and observer response difference of Healthy battery

Similarly, the voltage difference between the model and the observer model for aged battery is provided in Figure 5.9, which is also nearly of zero valued.

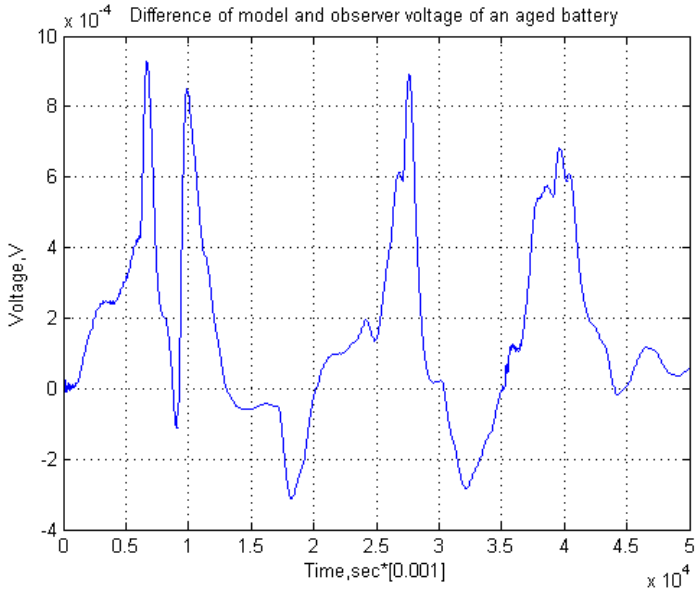

Figure 5.9. Model and observer response difference of an aged battery

For the OC battery, the voltage difference profile is as provided in Figure 5.10.

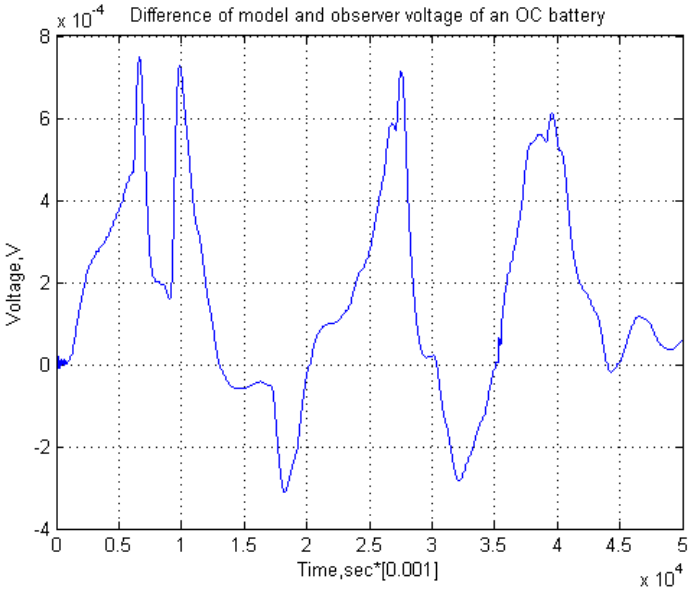

Figure 5.10. Model and observer response difference of over-charged battery

And the voltage difference profile for OD battery is given in Figure 5.11.

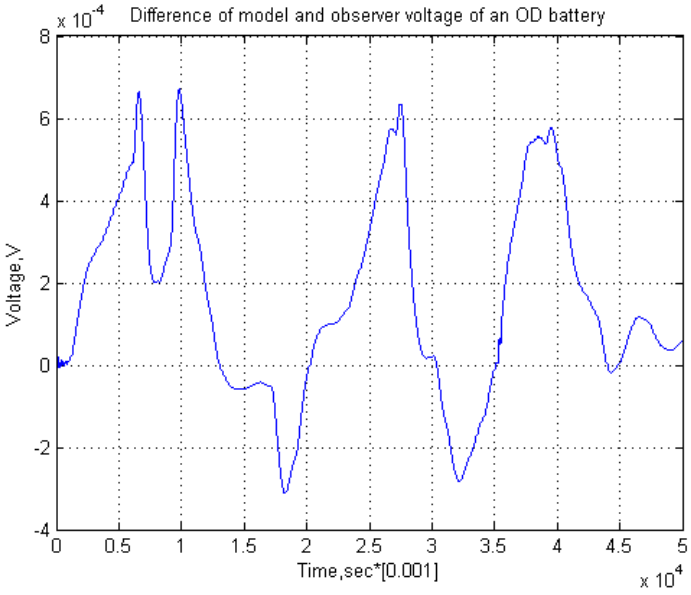

Figure 5.11. Model and observer response difference of over-discharged battery

5.4 Plant Model Build-up for Estimation Purpose

As described in the MMAE section of this thesis, the probability will be generated based on the residuals of different models. For this purpose, a reference plant model is required with which all of the possible scenarios will be compared and consequently the voltage residuals will be generated. The plant model voltage profile is constructed by the following way:

The total length of data samples is divided into the possible scenarios. Then those segmented time periods are assigned the voltage value from the considered scenarios one after another and they are added together to build up the plant model voltage.

For example, 50K data samples were considered among which very first 10K and very last 5K samples are assigned as Healthy battery condition. After first 10K samples, next 15K samples are assigned for the aged battery condition. Next 10K samples are allocated for over-discharged battery and the remaining next 10K samples are provided for the over-charged battery condition.

By following the previously stated way of voltage data allocation, the built plant model voltage profile is as the Figure 5.12.

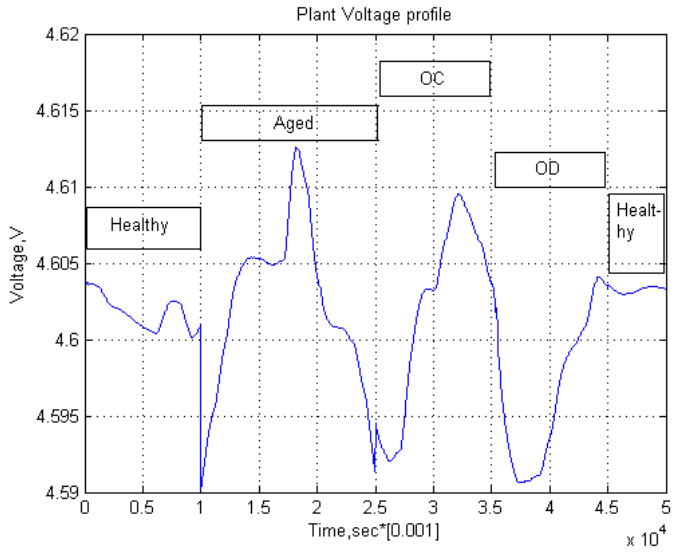

Figure 5.12. Built plant model voltage profile

To generate the residuals for different models, the observed model voltage response of the respective condition is deducted from the reference voltage profile, i.e. the plant model voltage profile. After following the procedure, the obtained residual profile for Healthy battery condition is provided in Figure 5.13.

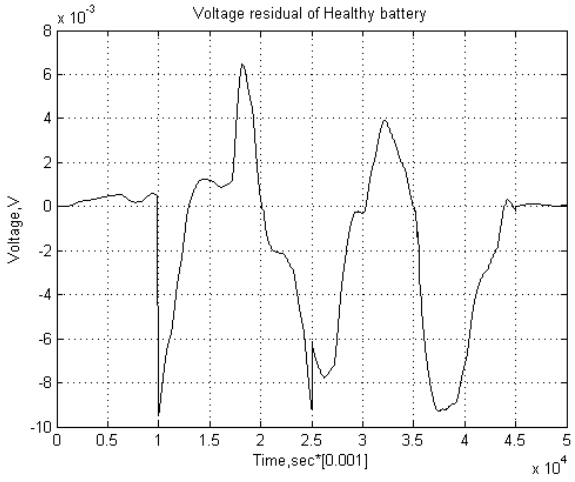

Figure 5.13. Healthy model residual

Similarly, the residual voltage profile for the aged battery condition is provided in Figure 5.14.

Figure 5.14. Aged model residual

Residual voltage for the OD battery condition is given in Figure 5.15.

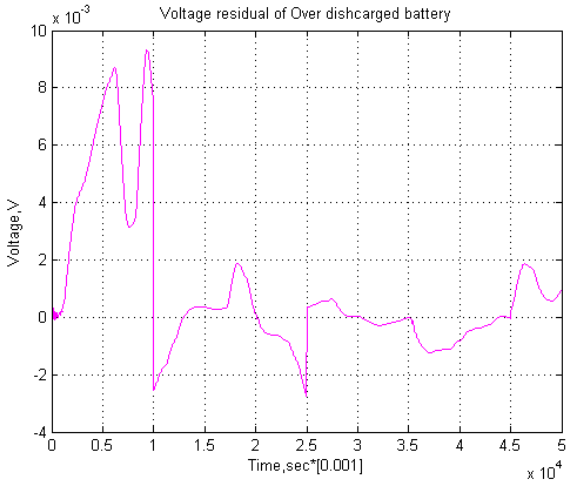

Figure 5.15. OD model residual

And the voltage residual profile for OC battery model is given in Figure 5.16.

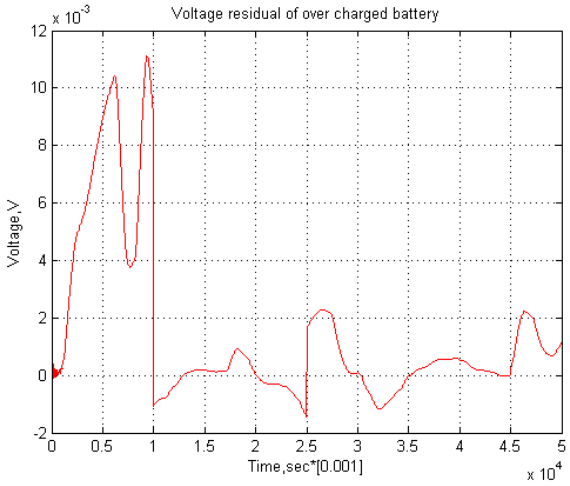

Figure 5.16. OC model residual

5.5 Fault Diagnosis

To have the state-space model of the corresponding battery condition, the system identification toolbox provided by MATLAB was used. The time domain data of the input current and the respective model output voltages were used to generate the state space models. While generating the state space models the discrete time analysis was performed and the sample time was taken as 0.001s.

After having the discrete state space model of the respective battery models, the state covariance matrices, i.e. P was evaluated using the Kalman-gain generation loop. To do this, for each model, the P matrices was initialized with an identity matrix of order two, i.e.

$$P_1 = P_2 = P_3 = P_4 = \begin{bmatrix} 1 & 0 \\ 0 & 1 \end{bmatrix}$$

Here, P_1 denotes the state covariance matrix for Healthy battery, P_2 denotes the state covariance matrix for aged battery, P_3 denotes the state covariance matrix for OD battery and P_4 denotes the state covariance matrix for OC battery.

After evaluating the Kalman-gain generation loop, the updated P matrices are provided below:

$$P_1 = \begin{bmatrix} 6.85738472847 \times 10^{-13} & -3.7634736427549454 \times 10^{-10} \\ -4.74545734342 \times 10^{-10} & 1.9233546034343435 \times 10^{-11} \end{bmatrix}$$

$$P_2 = \begin{bmatrix} 3.272637236726353 \times 10^{-15} & -9.23323083485 \times 10^{-12} \\ -7.81213343535646 \times 10^{-12} & 8.924838573761 \times 10^{-10} \end{bmatrix}$$

$$P_3 = \begin{bmatrix} 7.93545768743434 \times 10^{-13} & -2.354576861212 \times 10^{-10} \\ -2.3435687873232 \times 10^{-10} & 1.5788096454232 \times 10^{-11} \end{bmatrix}$$

$$P_4 = \begin{bmatrix} 6.34455668900676 \times 10^{-13} & -3.3445576670 \times 10^{-10} \\ -2.2446687542323 \times 10^{-10} & 5.93435687889 \times 10^{-10} \end{bmatrix}$$

These updated state covariance matrices were used in simulating the conditional probability densities for all of the models. The probability distribution was evaluated for different values of R, the measurement noise covariance matrix.

If the residuals are observed, which are obtained after comparing the individual battery condition observer voltage response with the plant model voltage response, it is clear that, the maximum amount of residual, i.e. noise present is order of 10^{-4}. So, the measurement covariance can not exceed the system noise present among all four of the battery conditions. Therefore, the conditional probabilities were evaluated at different values of R, which are lower than the actual system noise or the residual voltage signal.

Using the above described reasoning, for the four stated conditions of the battery, for $R = 1 \times 10^{-5}$, evaluated probabilities are provided in Figure 5.17.

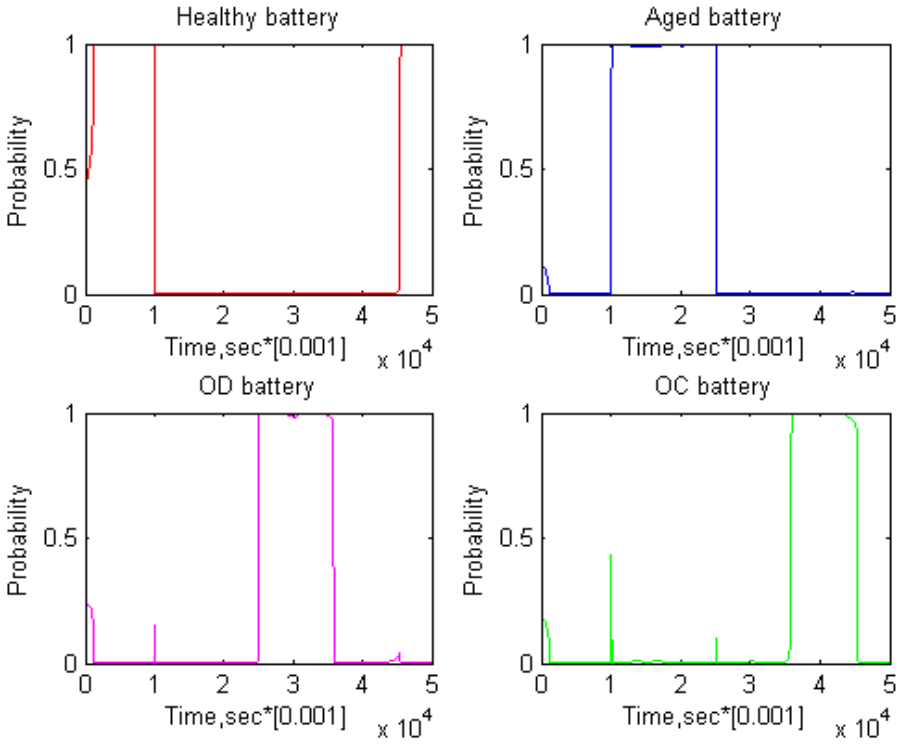

Figure 5.17. Probability distribution for $R = 1 \times 10^{-5}$

If the above plot of probabilities are analyzed, this can be said that, the prediction is too poor. Then the value of R was changed and the probability distribution was observed.

For $R = 1 \times 10^{-6}$, evaluated probabilities are provided in Figure 5.18.

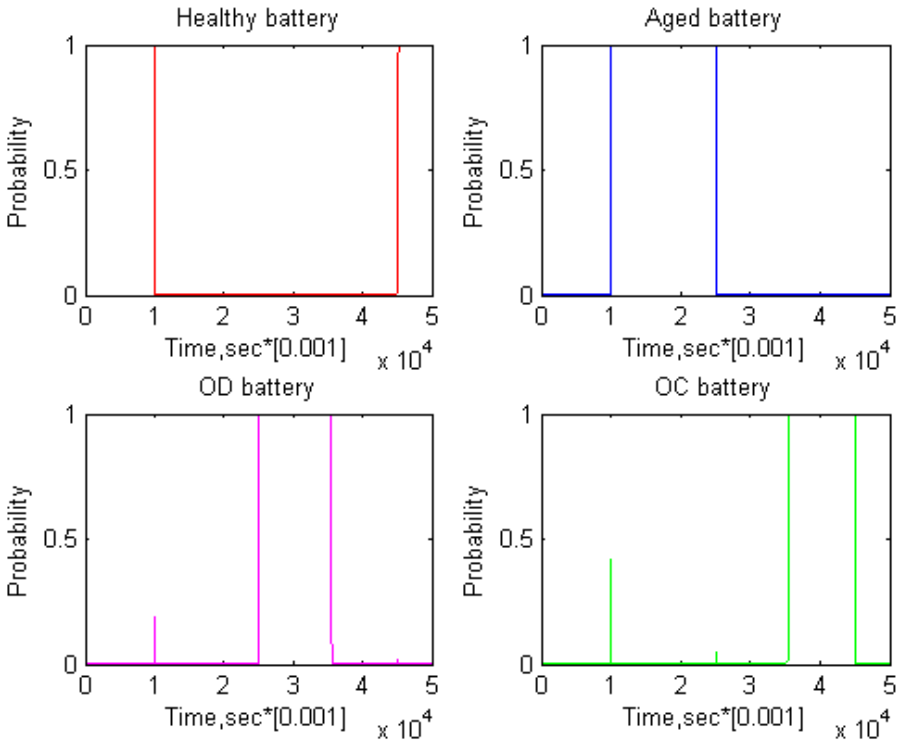

Figure 5.18. Probability distribution for $R = 1 \times 10^{-6}$

This prediction is better than the previous one, but not the desired one. Then again, the R value was further changed and for $R = 1 \times 10^{-7}$, evaluated probabilities are provided in Figure 5.19.

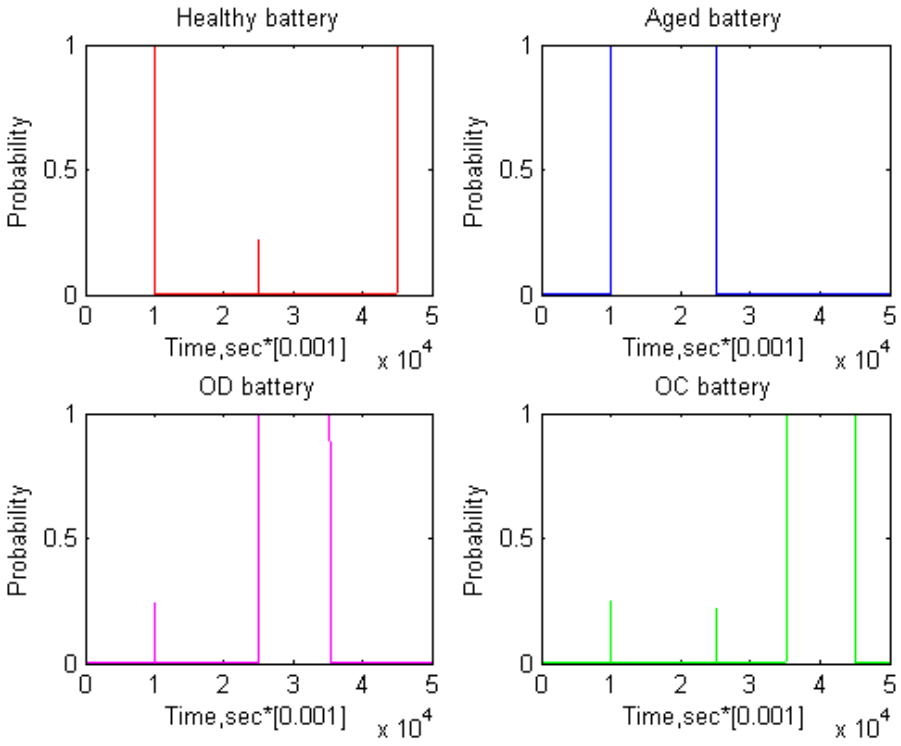

Figure 5.19. Probability distribution for $R = 1 \times 10^{-7}$

This prediction is exactly as the desired one for the fault diagnosis using the MMAE algorithm.

6. PARAMETER IDENTIFICATION

6.1 Particle Swarm Optimization

For HEV, the onboard battery management system (BMS) is responsible for managing the rechargeable battery system by monitoring its state of operation, protecting the battery from unsafe operating zone and reporting the diagnostic data to the operator while managing the battery operation. An accurate monitoring is possible if the significant battery parameters can be reliably identified which consequently can lead to a better BMS. With this objective, identification of the crucial battery parameters is developed in this thesis work. An accurate identification of the critical model parameters of the battery can lead to a better battery management system through better condition monitoring and fault diagnosis of the battery. PSO is an optimization technique.This is developed by Kennedy and Eberhart in 1995 using the inspiration from flocking behavior of birds or the schooling of fish [60]. In another word, this technique is a population based optimization technique [60].

This technique has some accord with other heuristic search techniques, i.e. genetic algorithm (GA) [28]. Like GA, PSO is also initialized with some population of random candidates [28] [61] [62] [63] [64] [65] [66] [67] and then it looks for the global minimum for the defined objective function by updating the generations from iteration to iterations. But there are clear differences between GA and PSO. There is no such term like mutation and crossover as these are the part of GA [60]. Rather in PSO, like the bird swarm, the particles or the potential candidate solutions move randomly through the problem space and look for the global optimum value [68].

In PSO, each of the particles keeps the record of the particular best location (coordinate in the problem space) which gives the best value of the fitness function with respect to that particular particle. This position / location value is denoted

by particle best value or *pbest* [66]. After gathering the informations of *pbest*, the algorithm uses these values to find the global optimal solution which is denoted by *gbest* [66].

In each iterations of PSO, particle velocity is updated which is associated with some random numbers. And according to the velocity update, particle position is also updated [68]. This updated position and the velocity values are used to find the optimal solution.

In past several years, PSO has been successfully applied in many research and application areas. It is demonstrated that PSO gets better results in a faster, cheaper way compared with other methods [60].

PSO technique is widely used in research and application areas. There are some significant advantages of PSO while comparing with some similar techniques available. PSO can give the optimal solution in a quick time and with less computational expenses. Another advantage of PSO is that, it has a few parameters to work with or to update. The equations with which the velocity and the positions of the particles are updated, are given by [66]:

$$v_i^{k+1} = wv_i^k + c_1 r_i^k (p_i^k - x_i^k) + c_2 s_i^k (g_i^k - x_i^k) \tag{6.1}$$

$$x_i^{k+1} = x_i^k + v_i^{k+1} \tag{6.2}$$

r and s are random numbers.

In this algorithm, w is referred as the inertia constant and the recommended value for this constant is slightly less than 1, usually from 0.7 to 0.8. c_1 and c_2 are the constants, which determine how much the particles are directed towards the good position. One of them is termed as cognitive component and the other is termed as social component. The significance of these two constants is that, they determine how much the particle best position and the global best position value affect the particles movement. Recommended value for these two constant is approximately 2. For each of the target parameters, this thesis work was carried out with 3 particles.

A schematic of PSO algorithm is provided in Figure 6.1.

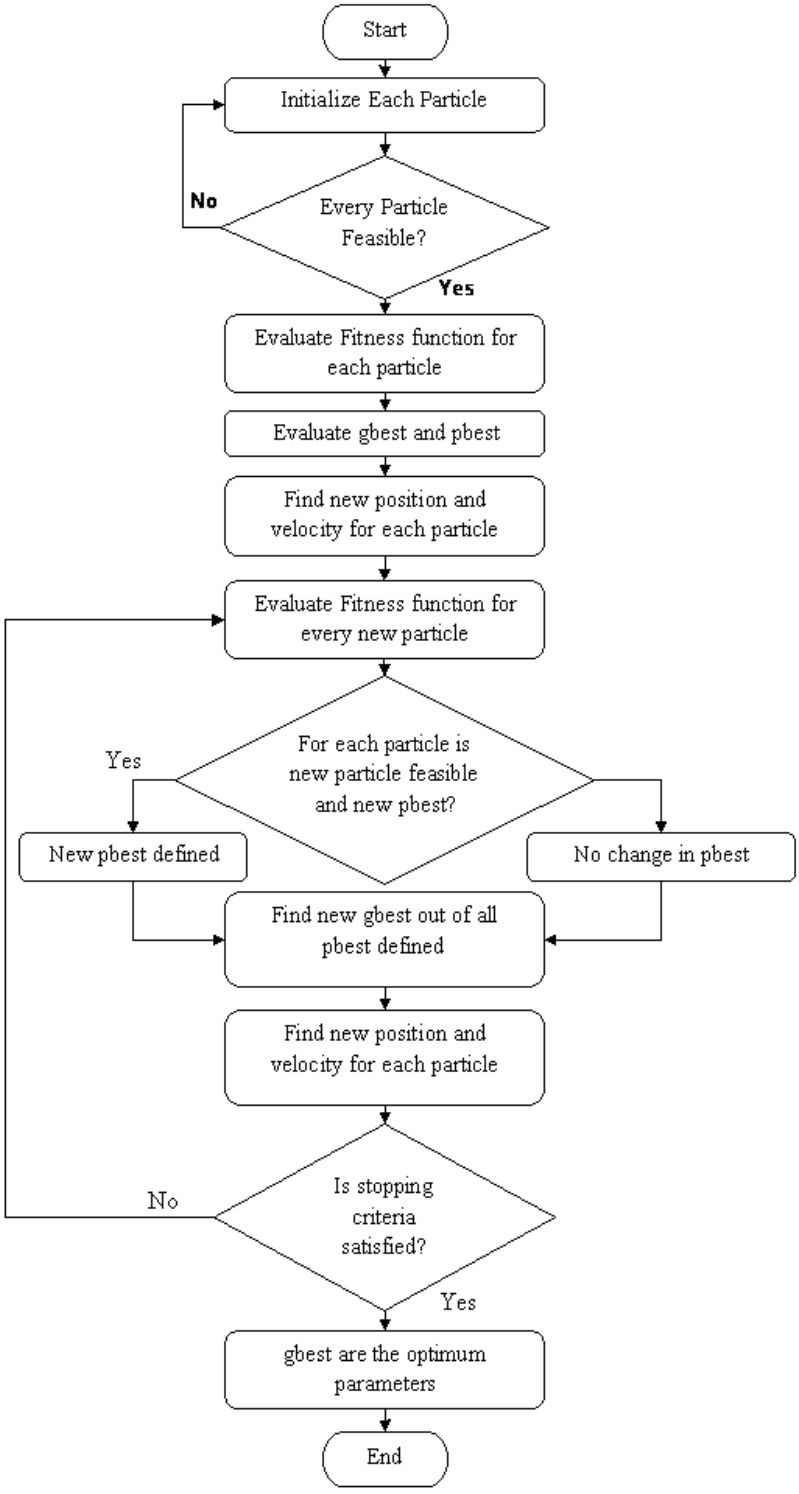

Figure 6.1. PSO algorithm flow chart [69]

6.2 Experimental Parameter Identification

6.2.1 Experimental Setup

For parameter identification purpose, the battery was tested at different operating conditions with different rates of discharging and charging. These experiments were carried out with a powerful battery tester from CADEX Inc. (Model CADEX C8000). Out of four channels of this tester, the battery was connected with one of the those with the alligator clips provided by the battery tester manufacturer. Experimental results were monitored using a software named Battery Lab Analyzer provided by CADEX Inc. A clear view of the experimental during a battery testing is provided in Figure 6.2.

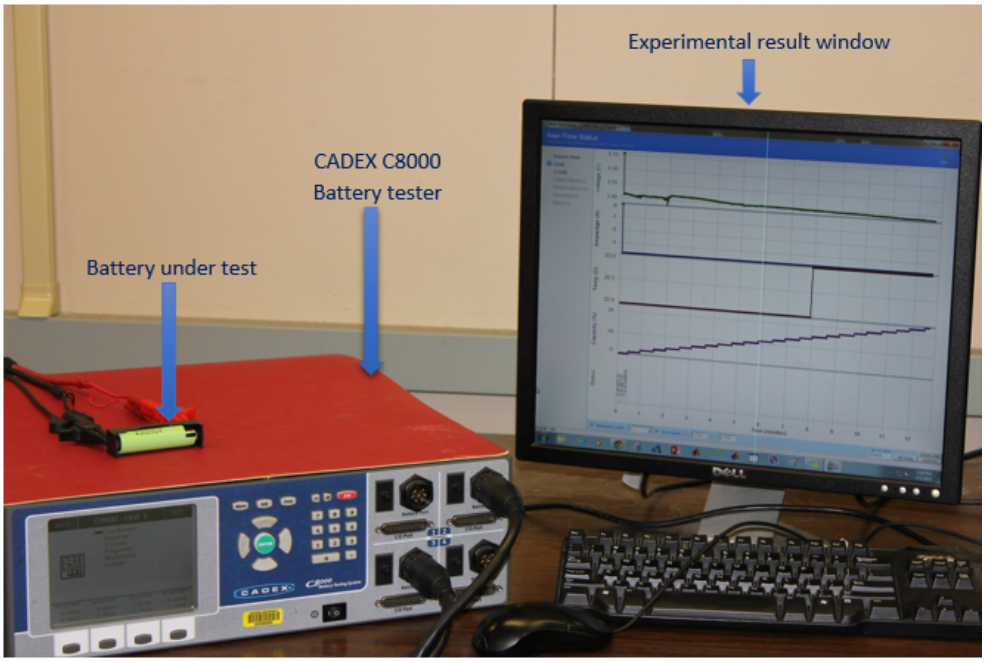

Figure 6.2. Experimental setup for battery testing

Although the electrochemical model of Li-Ion battery is a reduced one owing to the issue of complexity in case of solution, this model still depends on a significant number of parameters which are vital for system identification procedure. Among all of these insinuated parameters, some are dependent on the geometry of the battery,

which in turn can be regarded as the physical parameters and some other parameters are dependent on the chemistry of the battery. In battery modeling, value of the some parameters are adopted from the literature and some other values are collected from the battery providers.

In the parameter identification works, four parameters were considered to be identified, which are significant and can lead to different conditions of battery due to their variation. The mentioned four parameters to identify in this work are solid phase diffusion coefficient at positive electrode (cathode), Ds_P, solid phase diffusion coefficient at the negative electrode (anode), Ds_N, intercalation/de-intercalation reaction rate constant at cathode, k_P and intercalation/de-intercalation reaction rate constant at anode, k_N.

The target parameters were identified for the following operating conditions of the battery:

1. Nominal (1C) discharge and nominal (1C) charge of the battery, which is designated as Healthy battery.

2. 25% over-discharge (1.25C) followed by nominal (1C) charge of the battery, which is denoted as Navy over-discharged battery.

3. 20% over-discharge (1.2C) followed by nominal (1C) charge of the battery, which is denoted as 24-hr over-discharged battery.

4. Nominal (1C) discharge followed by 25% over-charge (1.25C) of the battery, which is denoted as over-charged battery.

The initialized value of the parameters to identify were taken from some well guessed values based on published literatures [32] [59] and provided in Table 6.1.

Table 6.1. Initialized value of the parameters to be identified using PSO

Name of the parameter	Initial value
Ds_P	1×10^{-15}
k_P	2×10^{-16}
Ds_N	3×10^{-14}
k_N	5×10^{-16}

All of these values were adopted while initializing the particle swarm optimization (PSO) algorithm. The objective function/fitness function for this parameter optimization technique is the following [32]:

$$\int_{t_0}^{t_f} (V_{m,i} - V_e)^2 dt \tag{6.3}$$

Where, $t_0 = 0$ and $t_f = n \times \Delta t$ (n denotes the number of iterations and Δt is the value of time step during integration, which was taken as 1 sec), $V_{m,i}$ is the model predicated voltage for i^{th} sample data, corresponding to an input current signal, V_e is measured experimental voltage corresponding to the same input current signal. The integral of the objective function was carried out for different time scales which differ in case of all of the battery operating conditions. In simple term, the integration time scale was the length of the relevant current signal during parameter identification algorithm, which in turn is equal to the total number of iterations in each case.

There was a preset limit of the fitness function under which the fitness function can be regarded as the optimal one and the corresponding parameter values are the optimized value for that particular condition of the battery. The limit was set as 0.5V in this parameter identification works. The optimization algorithm runs until the fitness function is optimized.

6.2.2 Parameter Identification Based on Healthy Battery Operation

By the word *Healthy* as a battery condition, it is meant that, the battery is discharged at $1C$ rate and also the charging region was also for $1C$ rate. The battery was cycled for twenty (20) times. Here also, the initial values of the parameters are taken as provided in Table 6.1. Healthy battery parameters were identified for both discharging and charging operation of the battery.

Parameter Identification for the Discharge Region

As mentioned earlier, the capacity of the battery under test is $3.4Ah$. Hence, the discharge operation of the battery was conducted at 3.4A current and the parameter was identified using this current as the input to the battery model. The input current for the discharge operation is provided in Figure 6.3.

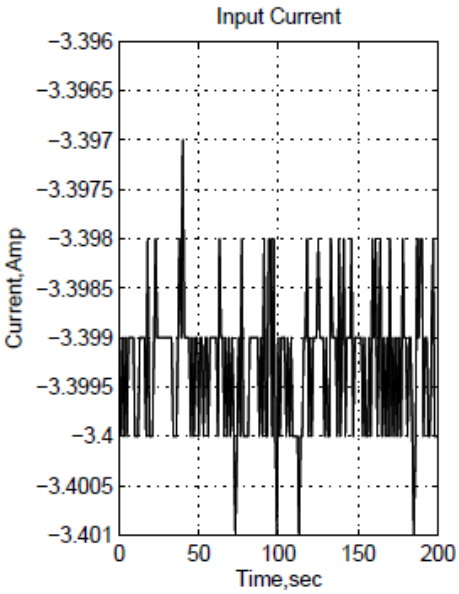

Figure 6.3. Input current during discharging of Healthy battery

The particle trajectories for all of the target parameters were observed throughout the iterations, which are provided next.

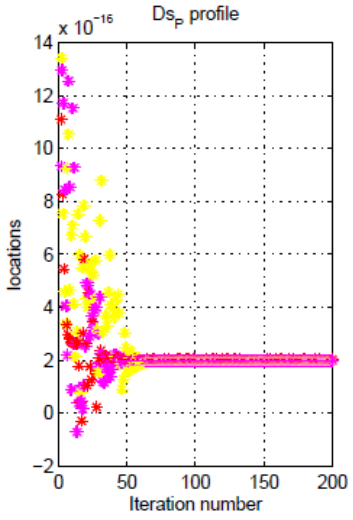

Figure 6.4. Ds_P update history for Healthy battery discharge

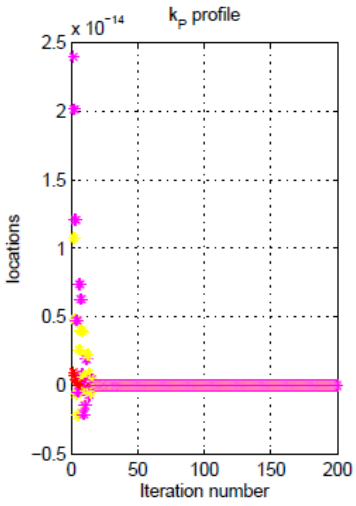

Figure 6.5. k_P update history for Healthy battery discharge

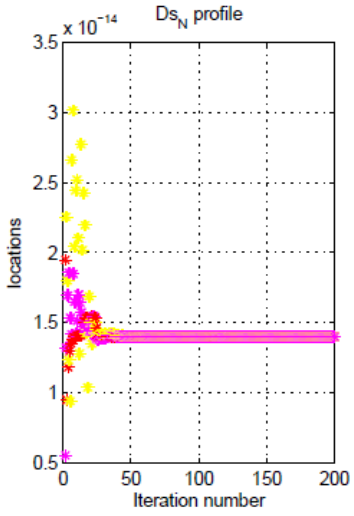

Figure 6.6. Ds_N update history for Healthy battery discharge

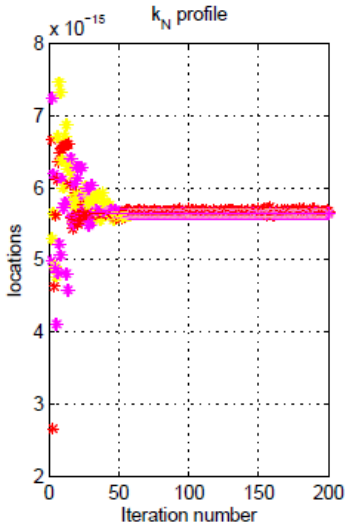

Figure 6.7. k_N update history for Healthy battery discharge

The obtained fitness function profile is provided in Figure 6.8.

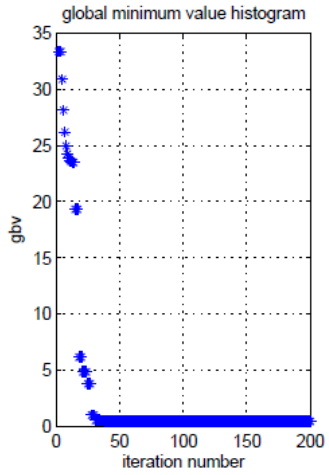

Figure 6.8. Fitness function trajectory for discharging of Healthy battery

The identified items for this type of battery operation is provided in Table 6.2.

Table 6.2. Identified parameters for discharging of Healthy battery

Name of the parameter	Identified value by PSO
Ds_P	4.0264×10^{-16}
k_P	6.0555×10^{-14}
Ds_N	4.3196×10^{-14}
k_N	3.5484×10^{-15}
Optimized fitness	0.4633

Parameter Identification for the Charge Region

The charging operation was carried out also at $3.4A$ as the battery is defined as Healthy. The input current for the identification process is provided in Figure 6.9.

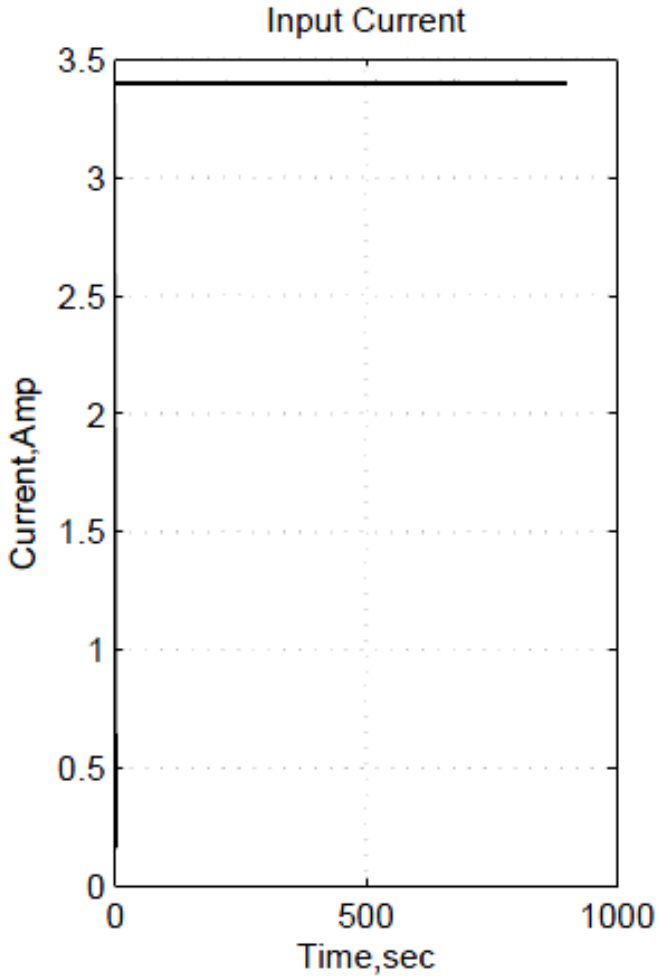

Figure 6.9. Input current during charging of Healthy battery

Using this input current and the defined, particle swarm optimization algorithm was adopted to optimize the objective function by defining four parameters to identify. The trajectories of the particle parameters are monitored to check the convergence of those and the particles trajectories are provided here.

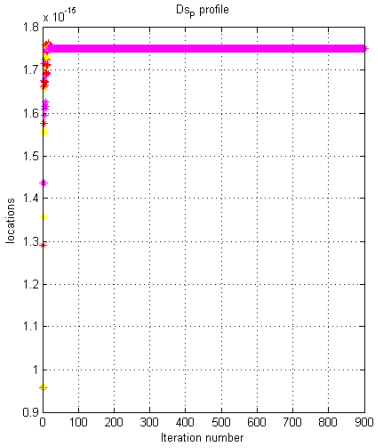

Figure 6.10. Ds_P update history for Healthy battery charge

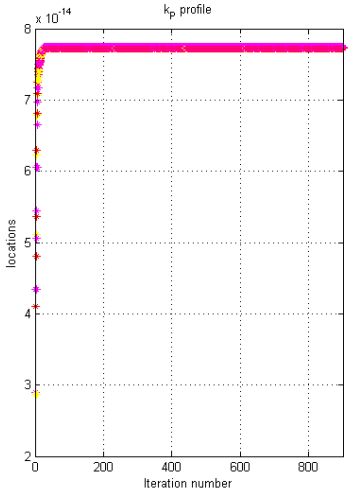

Figure 6.11. k_P update history for Healthy battery charge

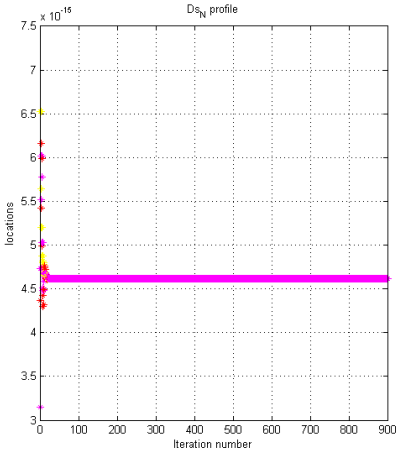

Figure 6.12. Ds_N update history for Healthy battery charge

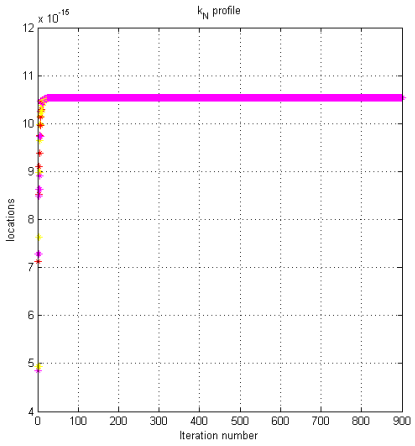

Figure 6.13. k_N update history for Healthy battery charge

The fitness function was monitored from iteration to iteration and provided in Figure 6.14.

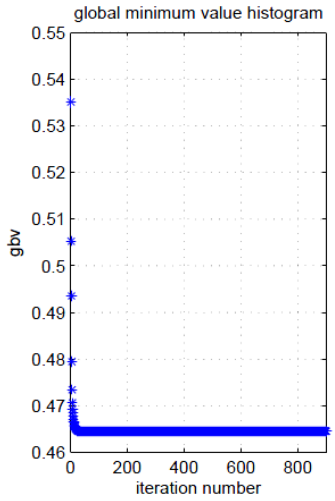

Figure 6.14. Fitness function trajectory for charging of Healthy battery

The identified value of the parameters and the optimized value of the fitness function is provided in Table 6.3.

Table 6.3. Identified parameters for charging of Healthy battery

Name of the parameter	Identified value by PSO
Ds_P	1.7507×10^{-15}
k_P	7.7358×10^{-14}
Ds_N	4.6174×10^{-15}
k_N	1.0532×10^{-14}
Optimized fitness	0.46458

6.2.3 Parameter Identification Based on Navy Over-Discharge Battery Operation

The 2^{nd} condition of the battery, which was identified using particle swarm optimization (PSO) algorithm, is Navy over-discharged battery. As mentioned in the earlier section, in case of Navy over-discharged [36] [35] battery, the battery was discharged at a rate of $1.25C$, i.e. 25% over-discharge (approximately $4.25A$ current discharge) and the charge period was run at normal condition, i.e. $1C$ rate ($3.4A$ charge). This pattern of battery operations ran for twenty (20) cycles.

Parameter Identification for the Discharge Region

The parameters were identified for both the discharge and the charge region of the battery experiment. For the discharge region of the Navy over-discharged battery, as mentioned earlier, the current was $4.25A$ throughout and the parameters were continuously observed while the optimum value of the defined fitness function is reached. The input current for this region of operation of the battery is provided in Figure 6.15.

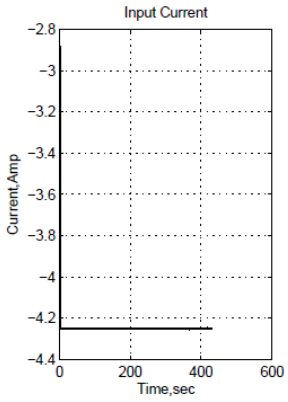

Figure 6.15. Input current during discharge of Navy OD battery

The particle update histories are observed from iteration to iteration while they yield the optimum value of the fitness function. The particles's trajectory for all of the parameters are provided next.

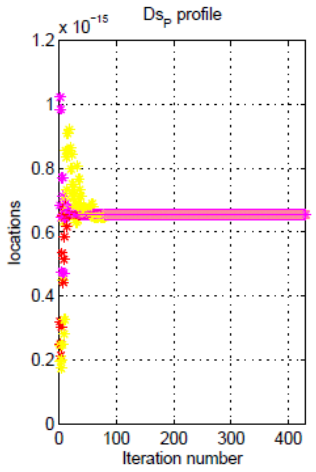

Figure 6.16. Ds_P update history for Navy OD battery discharge

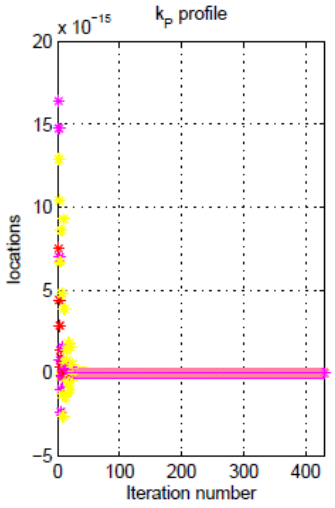

Figure 6.17. k_P update history for Navy OD battery discharge

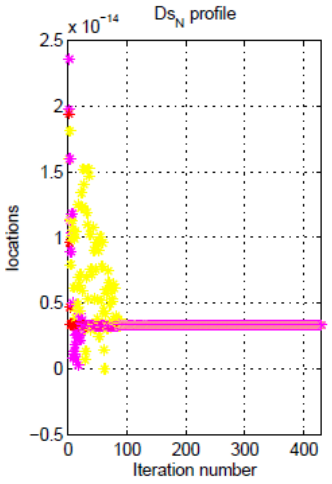

Figure 6.18. Ds_N update history for Navy OD battery discharge

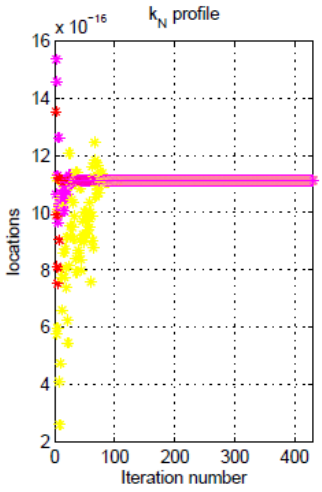

Figure 6.19. k_N update history for Navy OD battery discharge

If the particles position update trend is observed, it is clear that, all the particles are converged into a single location starting from their individual locations which are different form each other. At the same time, the fitness function is reached into a converged value and the update history of the fitness function is provided in Figure 6.20.

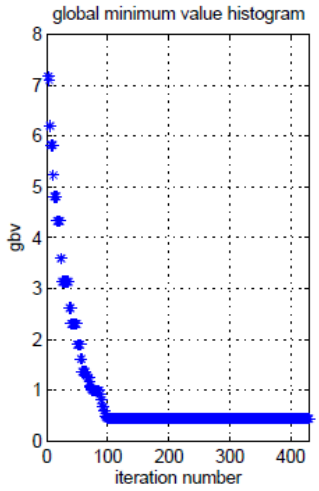

Figure 6.20. Fitness function trajectory for discharging of Navy-OD battery

The identified parameter values along with the optimized fitness function value is provided in Table 6.4.

Table 6.4. Identified parameters for discharging of Navy-OD battery

Name of the parameter	Identified value by PSO
Ds_P	6.5481×10^{-16}
k_P	7.3194×10^{-13}
Ds_N	3.35×10^{-15}
k_N	1.1129×10^{-15}
Optimized fitness	0.4444

Parameter Identification for the Charge Region

Following the similar way, the parameters were identified using PSO algorithm for the charging region of Navy OD battery operation. For the charging operation of the battery, the experimental current, which was taken as the input for parameter identification, is provided in Figure 6.21.

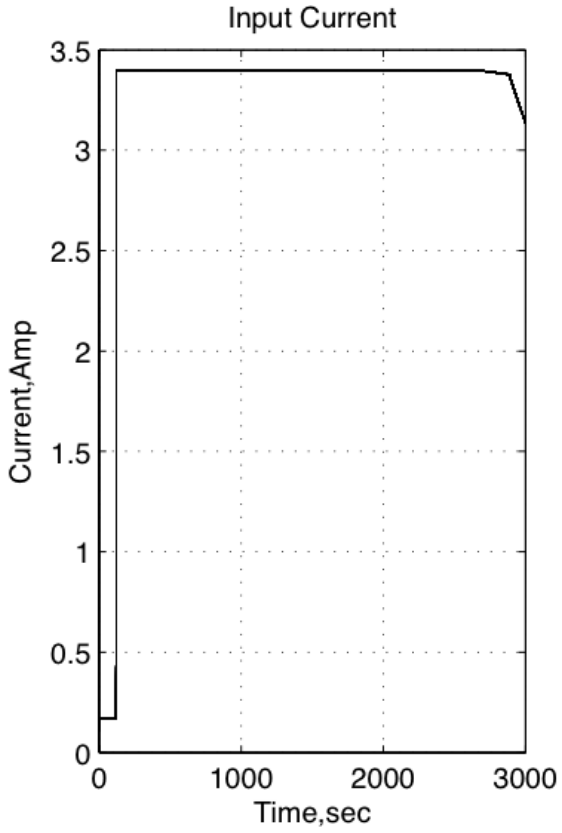

Figure 6.21. Input current during charging of Navy OD battery

The parameters changing by every iterations and at the end of the iterations all the parameters converged to a single location which is the vital point for PSO. The trajectories of all of the particles were tracked with iterations and the parameter particle convergence histories are provided next.

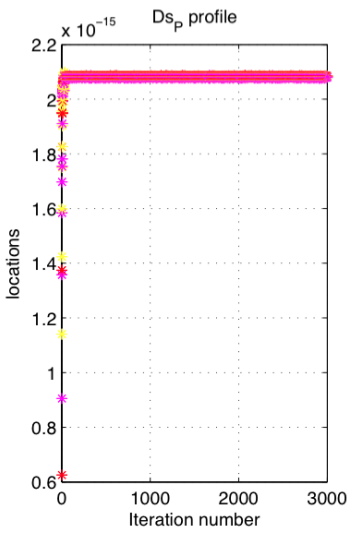

Figure 6.22. Ds_P update history for Navy OD battery charge

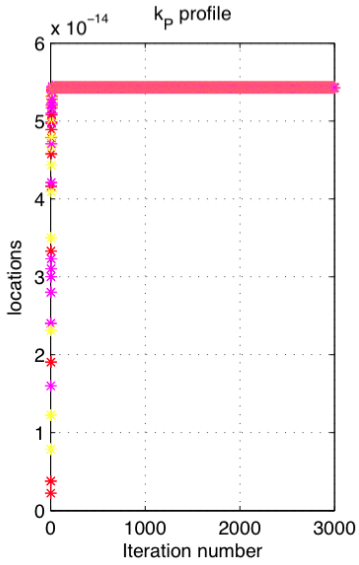

Figure 6.23. k_P update history for Navy OD battery charge

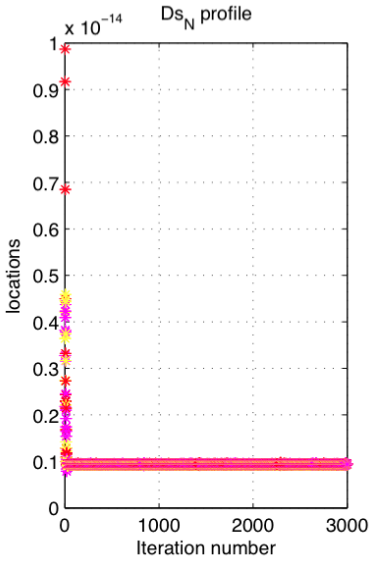

Figure 6.24. Ds_N update history for Navy OD battery charge

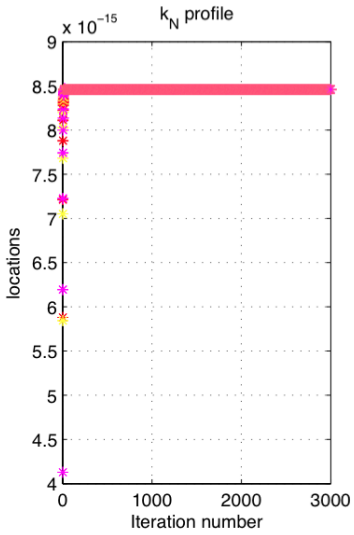

Figure 6.25. k_N update history for Navy OD battery charge

After analyzing all the parameter particles trajectory, the convergence is confirmed for the charging operation of the battery. Obtained update history of the fitness function is provided in Figure 6.26.

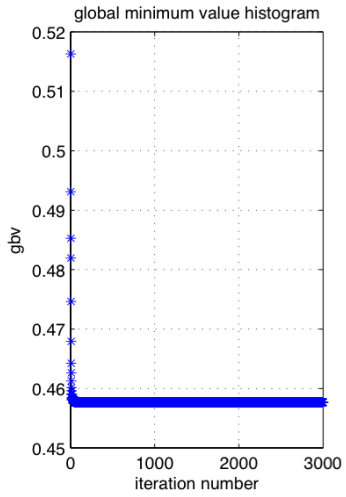

Figure 6.26. Fitness function trajectory for charging of Navy-OD battery

For the charge operation of the battery, the identified values of the parameters and also the value of the optimized fitness function is provided in Table 6.5.

Table 6.5. Identified parameters for charging of Navy-OD battery

Name of the parameter	Identified value by PSO
Ds_P	2.0828×10^{-15}
k_P	5.4301×10^{-14}
Ds_N	9.3458×10^{-16}
k_N	8.4599×10^{-15}
Optimized fitness	0.4577

6.2.4 Parameter Identification Based on 24-hr Over Discharge Battery Operation

The 3^{rd} model that was identified using experimental and model voltages is "24-hr over discharged battery condition". This condition of the battery is constructed as a cycle of discharge and charge for multiple number of cycles. In this condition, the battery ran in 20% over-discharge, i.e. $1.2C$ discharge followed by nominal charge regime, i.e. $1C$ charge and this cycle was repeated for 20 times and the voltage and current data was recorded. Likewise the previous one, the initial values of the parameters to be identified are taken as mentioned in Table 6.1.

Parameter Identification for the Discharge Region

Likewise the previous condition, this battery condition was also identified for both discharge and charge operation of the battery. The discharge operation was carried out for a constant current of $4.08A$. This current profile is provided in Figure 6.27.

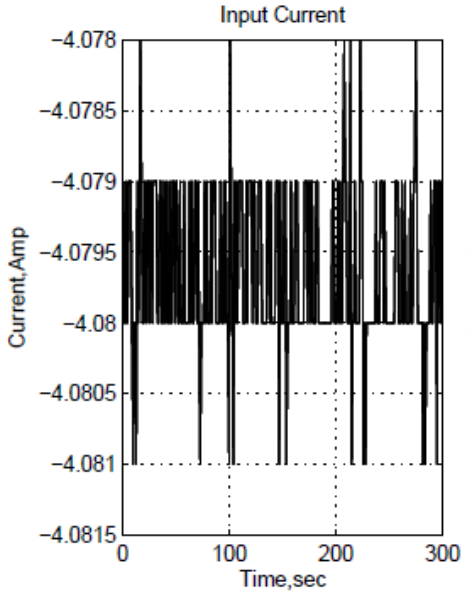

Figure 6.27. Input current during discharging of 24-hr OD battery

For this input current, the particles of the parameters were observed and the converging history of the particles are provided next.

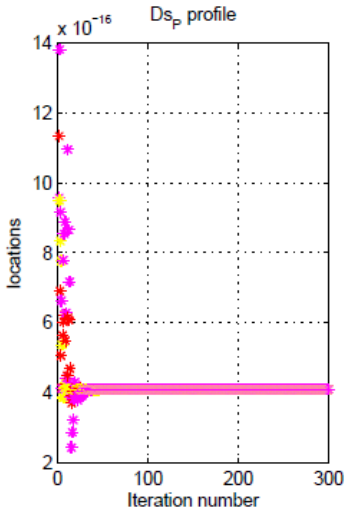

Figure 6.28. Ds_P update history for 24-hr OD battery discharge

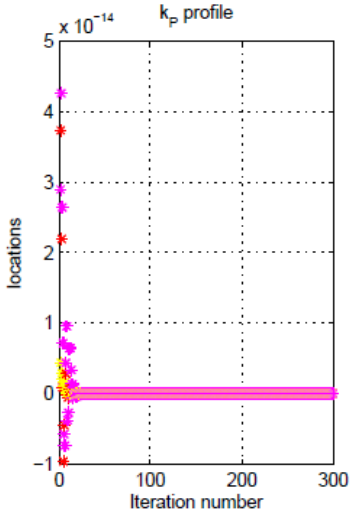

Figure 6.29. k_P update history for 24-hr OD battery discharge

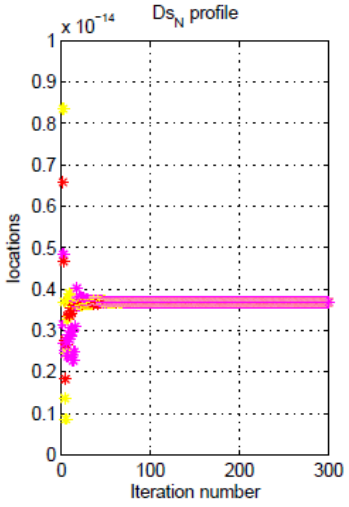

Figure 6.30. Ds_N update history for 24-hr OD battery discharge

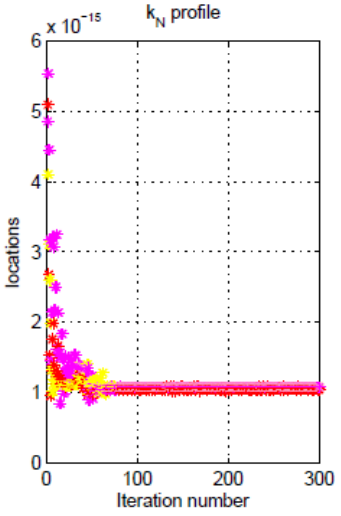

Figure 6.31. k_N update history for 24-hr OD battery discharge

The fitness function profile was also observed and this is provided in Figure 6.32.

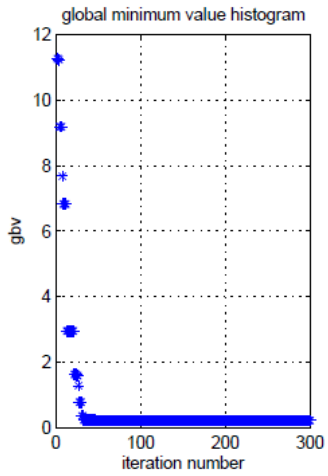

Figure 6.32. Fitness function trajectory for discharging of 24-hr OD battery

The identified values of the parameters and the optimized value of the fitness function is provided in Table 6.6.

Table 6.6. Identified parameters for discharging of 24-hr OD battery

Name of the parameter	Identified value by PSO
Ds_P	4.0995×10^{-16}
k_P	2.1611×10^{-13}
Ds_N	3.6899×10^{-15}
k_N	1.0775×10^{-15}
Optimized fitness	0.18081

Parameter Identification for the Charge Region

For the mentioned operating condition of the battery, the input current measured from the CADEX battery tester is given in Figure 6.33.

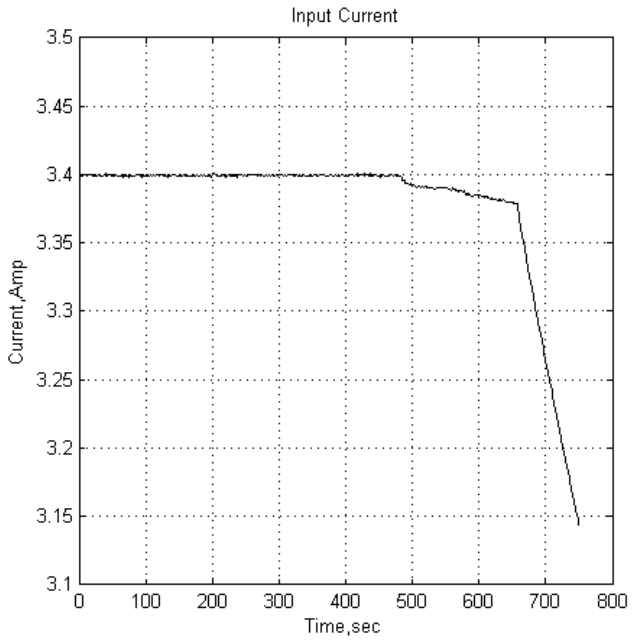

Figure 6.33. Input current during charging of 24-hr OD battery

For the Identification procedure, for all of the four parameters, three (3) particles were selected in PSO algorithm and the locations of the particles are provided next.

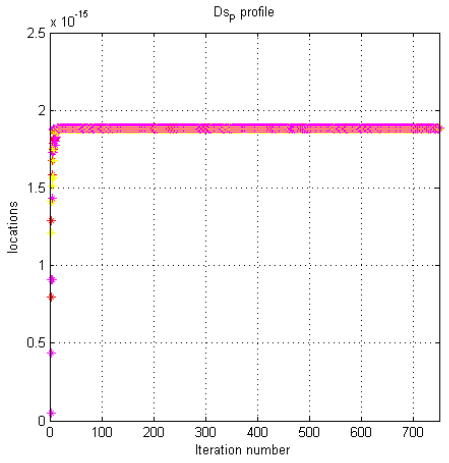

Figure 6.34. Ds_P update history for 24-hr OD battery charge

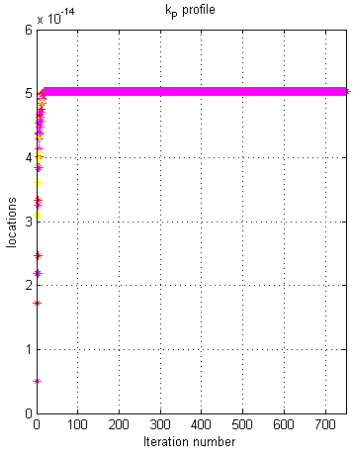

Figure 6.35. k_P update history for 24-hr OD battery discharge

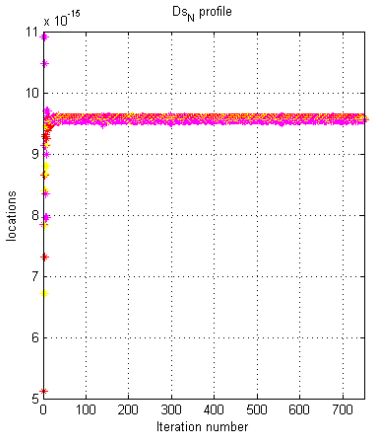

Figure 6.36. Ds_N update history for 24-hr OD battery charge

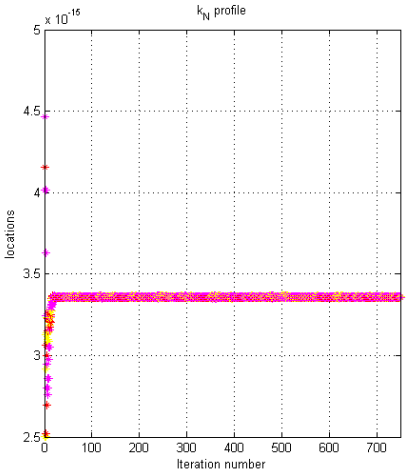

Figure 6.37. k_N update history for 24-hr OD battery charge

While the parameters are changing their locations and converged to a particular value by following the PSO algorithm, the fitness function is optimized and provided in Figure 6.38.

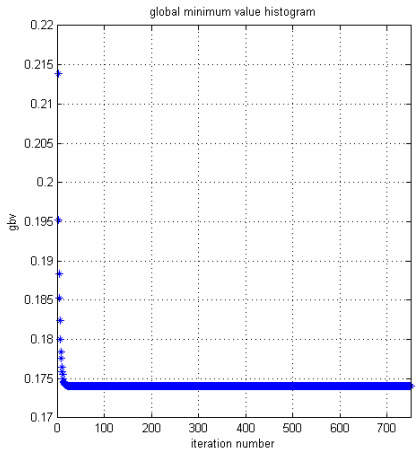

Figure 6.38. Fitness function trajectory for charging of 24-hr OD battery

With the time being, the identified value of the target parameters along with the optimized value of the fitness function is obtained as provided in Table 6.7.

Table 6.7. Identified parameters for charging of 24-hr OD battery

Name of the parameter	Identified value by PSO
Ds_P	1.8848×10^{-15}
k_P	5.0345×10^{-14}
Ds_N	9.5869×10^{-15}
k_N	3.3563×10^{-15}
Optimized fitness	0.17409

6.2.5 Parameter Identification Based on an Over-Charged Battery Operation

The final model of the battery used for parameter identification purpose, is an Over-charged battery. The battery was tested with a nominal ($1C$) discharge region followed by 25% over-charge ($1.25C - charge$) region. The same initial parameter values were adopted for the identification procedure. This battery parameters were identified for both discharge and charge operation as for the previous conditions.

Parameter Identification for the Discharge Region

As this battery is an over-charged one, the discharge operation was carried out at $1C$ rate, i.e. $3.4A$, while the charge was at 25% over, i.e. $1.25C$. The discharge operation of the battery is carried out for a constant current of $3.4A$. This discharge current profile is provided in Figure 6.39.

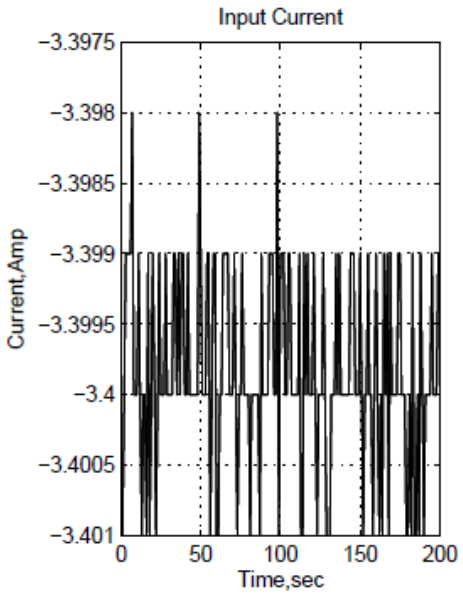

Figure 6.39. Input current during discharging of an OC battery

The trajectories of the parameter particles, which are converged to a single location are provided next.

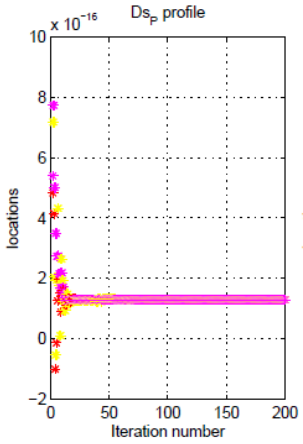

Figure 6.40. Ds_P update history for OC battery discharge

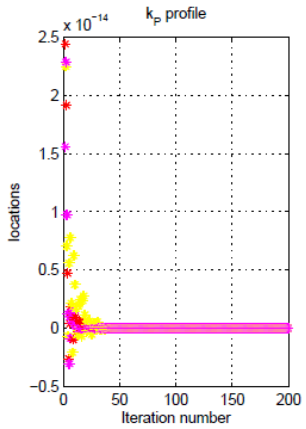

Figure 6.41. k_P update history for OC battery discharge

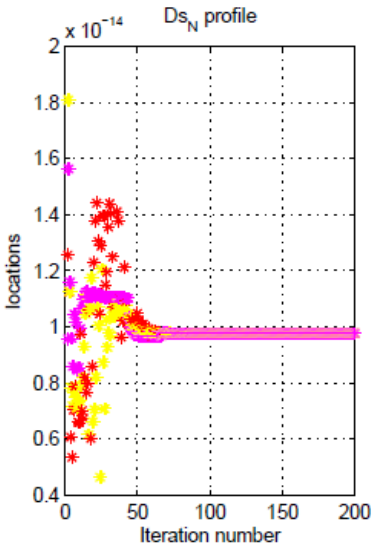

Figure 6.42. Ds_N update history for OC battery discharge

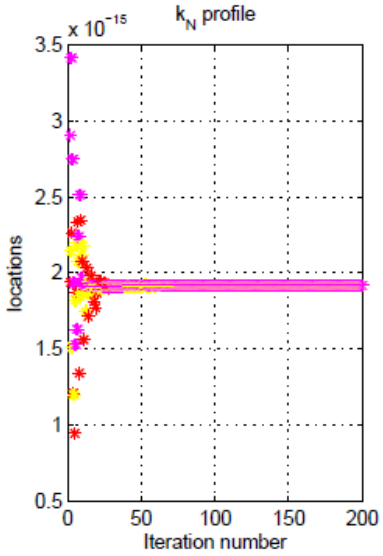

Figure 6.43. k_N update history for OC battery discharge

The fitness function was observed and the profile is provided in Figure 6.44.

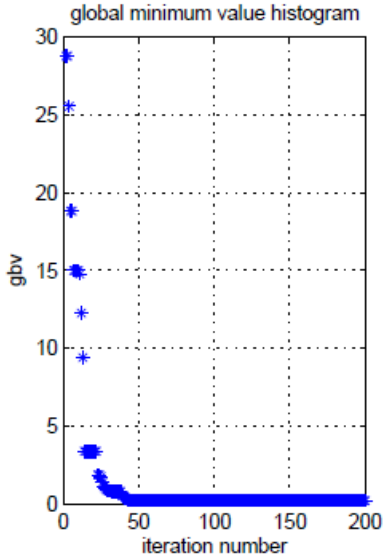

Figure 6.44. Fitness function trajectory for discharging of an OC battery

The identified items are provided in Table 6.8.

Table 6.8. Identified parameters for discharging of an OC battery

Name of the parameter	Identified value by PSO
Ds_P	1.2884×10^{-16}
k_P	3.3685×10^{-13}
Ds_N	9.7622×10^{-15}
k_N	1.9175×10^{-15}
Optimized fitness	0.23166

Parameter Identification for the Charge Region

The battery was operated at $4.25A$ current. This input current runs through the battery in this identification step is given in Figure 6.45.

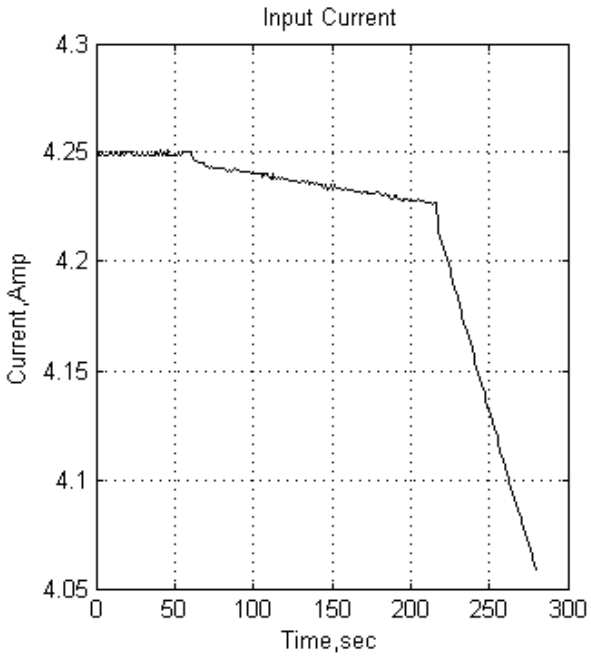

Figure 6.45. Input current during charging of an OC battery

The updated location history of the particles of the target parameters are provided next.

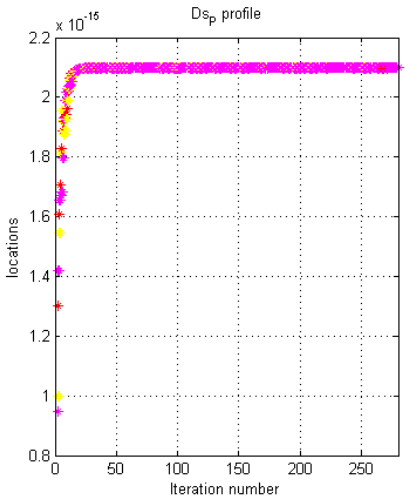

Figure 6.46. Ds_P update history for OC battery charge

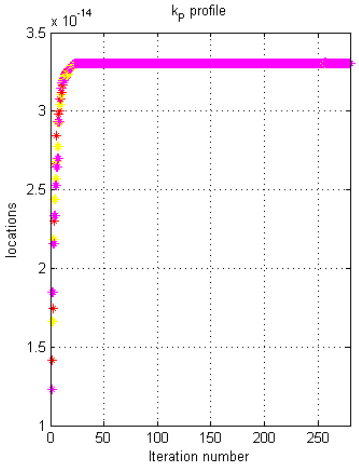

Figure 6.47. k_P update history for OC battery charge

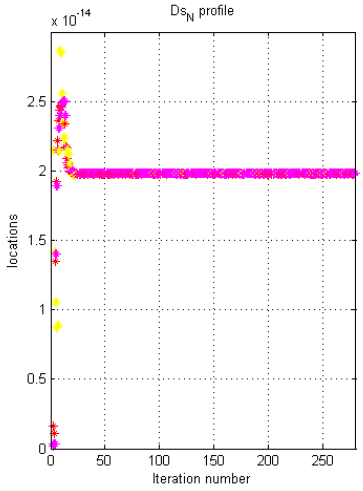

Figure 6.48. Ds_N update history for OC battery charge

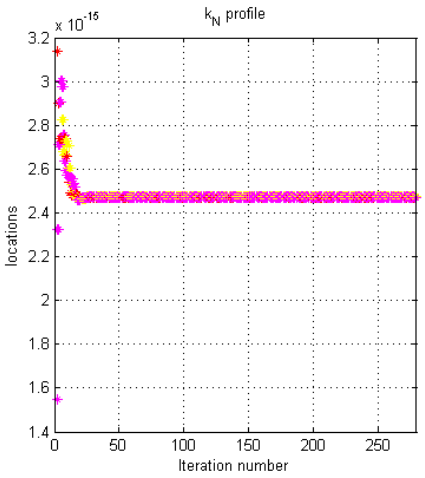

Figure 6.49. k_N update history for OC battery charge

The histogram of the fitness function is provided in Figure 6.50.

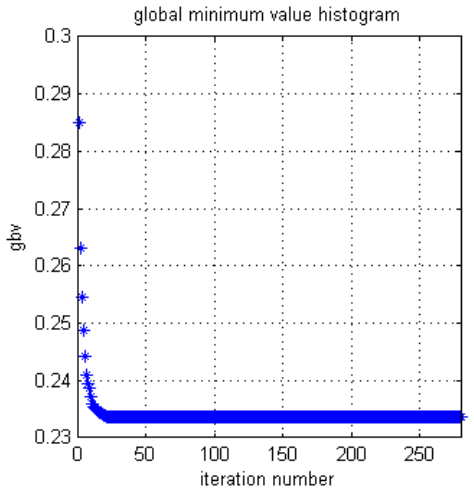

Figure 6.50. Fitness function trajectory for charging of an OC battery

Finally, the identified value of the parameters and the optimized value of the fitness function is provided in Table 6.9.

Table 6.9. Identified parameters for charging of an OC battery

Name of the parameter	Identified value by PSO
Ds_P	2.0986×10^{-15}
k_P	3.3064×10^{-14}
Ds_N	1.9827×10^{-14}
k_N	2.4734×10^{-15}
Optimized fitness	0.23364

6.2.6 Analysis of the Identified Models

In case of Healthy battery identified parameters for discharging and charging region, if the obtained values are analyzed, it is clear that, parameter values are different in case of two operating conditions. Value of Ds_P increases when the operating condition switches from discharge to charge. Similar pattern of changes in values is noticed in case of k_P and k_N. But, the value of Ds_N decreases when the operating condition changes from discharge to charge. Despite this discrepancies in parameter values, the fitness function value keeps consistency in both cases of battery operation with a negligible variation in optimized values, 0.27% (0.4633 to 0.46458) changes in optimized value of the fitness function.

Meanwhile in case of Navy over-discharged battery operation, when the operating condition switches from discharge to charge, there are noticeable changes in parameter values. While there is an increase in values of Ds_P and k_N, when the operating condition changes from discharge to charge, there is decrease in the value of k_P and Ds_N. Objective function changes about 3% (0.4444 to 0.4577), from discharge to charge region of operation of the battery.

In case of another over-discharged battery, i.e. 24-hr OD battery, there is an increase in value of Ds_P, Ds_N and k_N while there is a decrease in the value of k_P, when the operating condition switches from discharge to charge mode. There is around 3.7% (0.18081 to 0.17409) change in the value of fitness function when the operating condition changes from discharge to charge during the experiments.

Moreover, in case of over-charged battery, when the operating condition switches from discharge to charge, there is an increase in the value of Ds_P, Ds_N and k_N, while there is a clear decrease in the value of k_P. And in this case, there is a 0.85% (0.23166 to 0.23364) change in fitness function during the switching of operating conditions.

Now, if a single parameter is compared with changing different operating conditions keeping the operating mode same, the analysis will be more interesting. For example, for Ds_P in discharge region is compared like the following:

From Healthy battery condition Ds_P value, it increases while the operating mode changes form Healthy to 24-hr OD and then to Navy OD, but there is a decrease in Ds_P value when the operating mode shifts to over-charged condition.

In case of Ds_P for charging scenarios, the identified value changes among the operating conditions like: Healthy $\rightarrow$ 24-hr OD $\rightarrow$ over-charged $\rightarrow$ Navy OD.

In case of k_P for discharging scenarios, the identified value changes among the operating conditions like: Healthy $\rightarrow$ 24-hr OD $\rightarrow$ over-charged $\rightarrow$ Navy OD.

Similarly, in case of k_P for charging scenarios, the identified value changes among the operating conditions like: over-charged $\leftarrow$ 24-hr OD $\leftarrow$ Navy OD $\leftarrow$ Healthy.

Moreover, in case of Ds_N for discharging scenarios, the identified value changes among the operating conditions like: Navy OD $\leftarrow$ 24-hr OD $\leftarrow$ over-charged $\leftarrow$ Healthy.

Similarly, in case of Ds_N for charging scenarios, the identified value changes among the operating conditions like: Navy OD $\leftarrow$ Healthy $\rightarrow$ 24-hr OD $\rightarrow$ over-charged.

In addition to those, in case of k_N for discharging scenarios, the identified value changes among the operating conditions like: 24-hr OD $\leftarrow$ Navy OD $\leftarrow$ over-charged$\leftarrow$ Healthy.

Finally, in case of k_N for charging scenarios, the identified value changes among the operating conditions like: over-charged $\leftarrow$ 24-hr OD $\leftarrow$ Navy OD $\leftarrow$ Healthy.

For the easiness of understanding, Healthy battery model was taken as the reference while comparing the identified parameter values for both of the operating modes. Right arrow and left arrow indicates the pattern of changing direction. Right arrow indicates an increase in parameter value while the left arrow indicates a decrease in parameter value.

Moreover, for every single cycle of discharge and charge for all four battery operating conditions, parameters were identified using PSO, which are provided in Appendix of this thesis work.

7. ELECTROCHEMICAL MODEL VALIDATION

To validate the reduced order electrochemical model of the Li-Ion battery, experimental voltage response was compared with the model predicted voltage response, which is governed by the identified electrochemical battery parameters by PSO algorithm. In this section, the voltage comparison for different operating conditions of the battery is provided. To validate the electrochemical model for identified parameters for Healthy battery, the previously mentioned conditioned battery was taken under test again and was cycled only once and the discharge ($1C$) and charge ($1C$) current data was used as the input to the battery model to compare with the relevant experimental voltage response. As both discharge and charge of the Healthy battery is significant equally, the model validation was performed for both of the states of operation. The experimental discharge current which was used as an input to the battery electrochemical model, is provided in Figure 7.1.

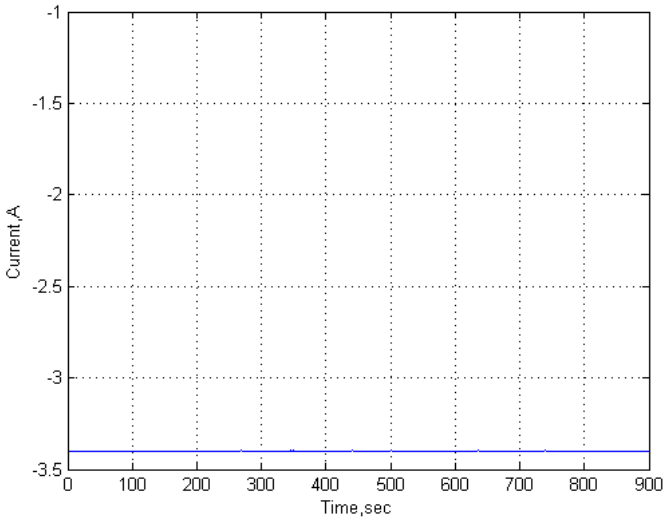

Figure 7.1. Input current to Healthy battery discharge model

For discharge at constant 3.4A current, the model voltage response and the experimental voltage is compared and provided in Figure 7.2. If the discharge voltage

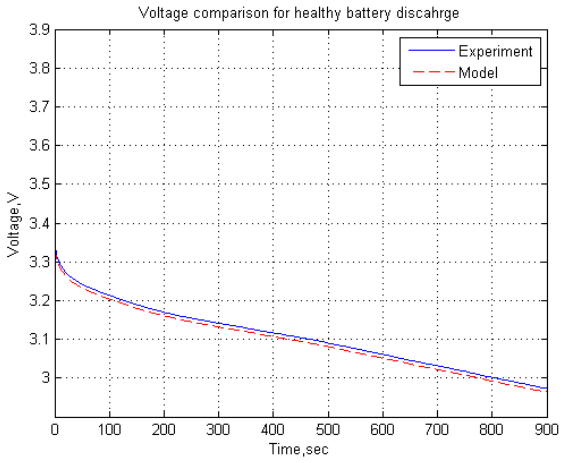

Figure 7.2. Voltage comparison for Healthy battery discharge operation

pattern is observed, it is clear that, the battery did not start to discharge from it's rated voltage, i.e. 3.7 V, rather from near 3.3 V. The reason behind this discrepancy can be correlated to the SOC variation during battery discharge, which is provided in Figure 7.3 for reference.

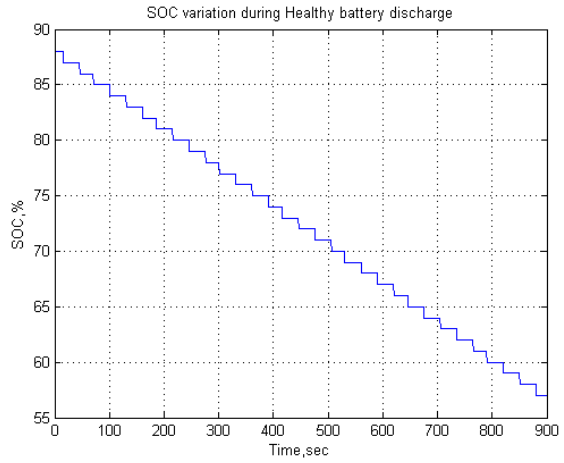

Figure 7.3. SOC variation during Healthy battery discharge

From the SOC plot, it is clearly seen that, the battery did not start discharging from 100% capacity, rather form 87%. For this reason, the battery voltage was lower while the discharge starts. The reason behind lower SOC at initial phase of discharge is the long time cycling (20 times) of the battery during experiments.

As stated earlier, the Healthy battery model was also validated for charging operation. The experimental charging current, which was later used as an input to the battery model, is provided in Figure 7.4.

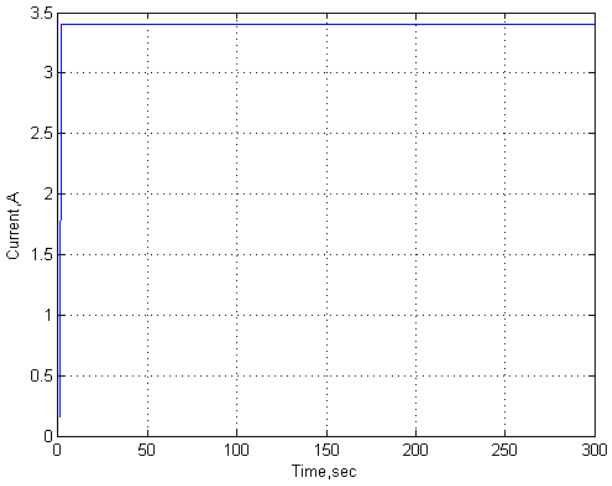

Figure 7.4. Input current to Healthy battery charge model

For the charge input current to the battery model, the compared voltage responses between the model and the experiment is provided in Figure 7.5.

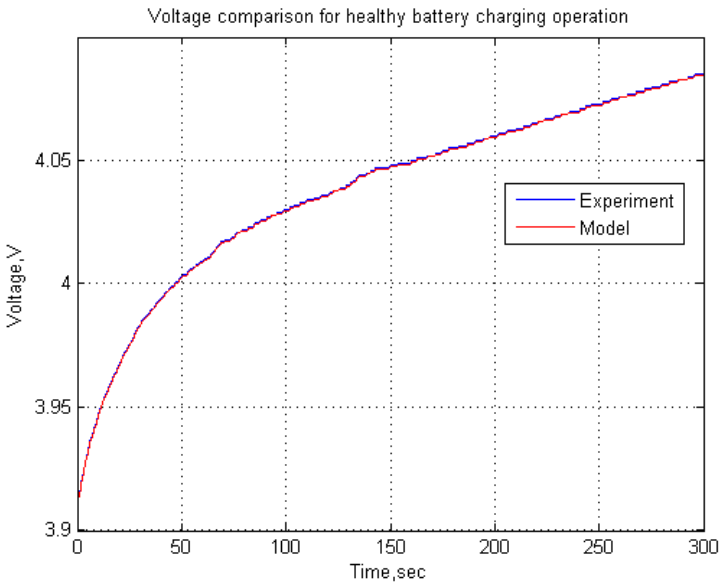

Figure 7.5. Voltage comparison for Healthy battery discharge operation

From the provided comparison of voltages for both discharge and charge operation of the battery, it is clear that, the identified battery parameters by PSO, provides an accurate validation of the considered reduced electrochemical model of Li-Ion battery.

To validate the Navy over-discharged battery electrochemical model using the PSO identified parameters, the conditioned battery was again considered for test in similar manner but at different rate of over-discharge. For parameter identification purpose, the battery was 25% over-discharged ($1.25C$ discharge). But for model validation purpose, the battery was 15% over-discharged ($1.15C$ discharge) while the charge of the battery was carried out at normal rate ($1C$) and this cycle was performed for once.

As the discharge operation of this battery is more crucial as compared to the charge operation, the model validation was carried out for the discharge operation. The input current to the discharge operation of the Navy OD battery, is provided in Figure 7.6.

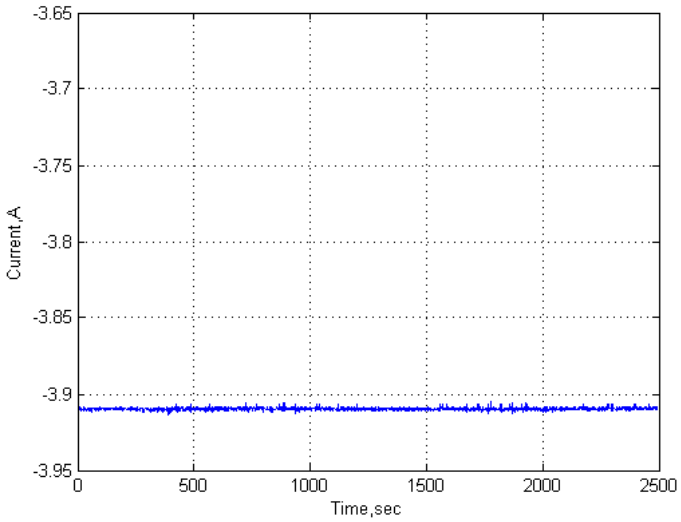

Figure 7.6. Input current to Navy OD battery discharge model

The voltage comparison for model validation purpose of this battery operation, is provided in Figure 7.7.

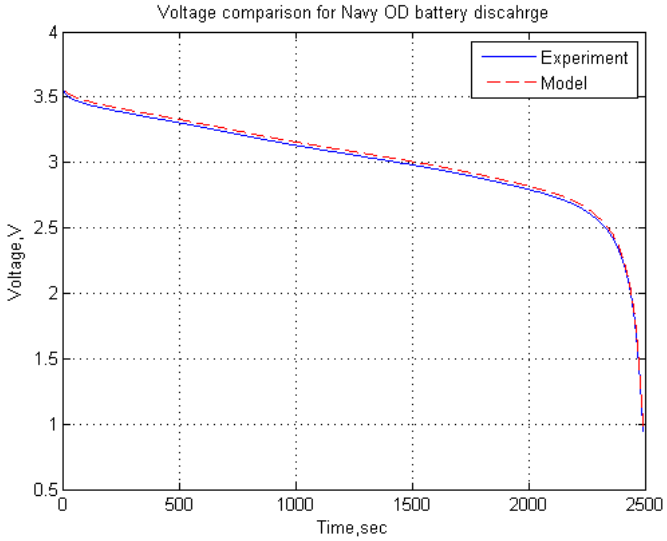

Figure 7.7. Voltage comparison for Navy OD battery discharge operation

From the voltage comparison plot provided for the discharge operation of the Navy OD battery, it can be said that, the PSO identified battery parameters are providing a well accurate battery model.

Although, the electrochemical battery model is accurate one, if the discharge pattern is observed closely, it is clear that, here also like the Healthy battery discharge operation, the voltage didn't start discharging from it's rated voltage rather from 3.5V. The reason for this can be explained from Figure 7.8.

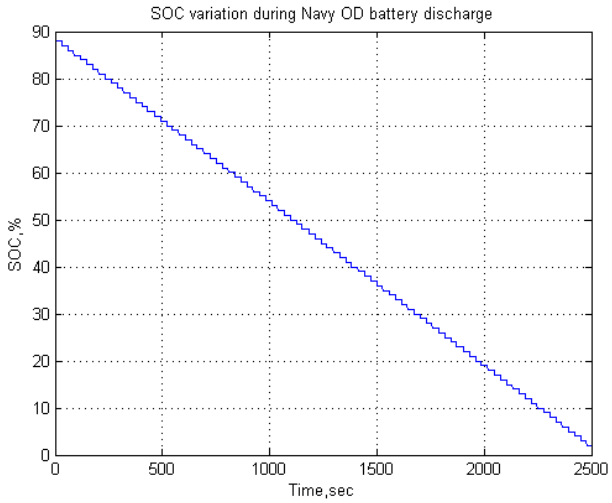

Figure 7.8. SOC variation during Navy OD battery discharge

The initial SOC of this battery was near 90%, which is not as the expected starting point of discharge and the reason behind is also the long time cycling of the battery (20 times).

For 24-hr over discharged battery model validation, previously conditioned battery at $1.2C$ discharge (20% over-discharged), was taken under test for one cycle at different rate of over-discharge. For validation purpose, the battery was 10% over-discharged ($1.1C$), while the charging operation was maintained at nominal rate ($1C$).

Here also, as the discharge operation of this battery is more crucial as compared to the charge operation, the model validation was carried out for the discharge operation.

The input current to the discharge operation of the 24-hr OD battery, is provided in Figure 7.9.

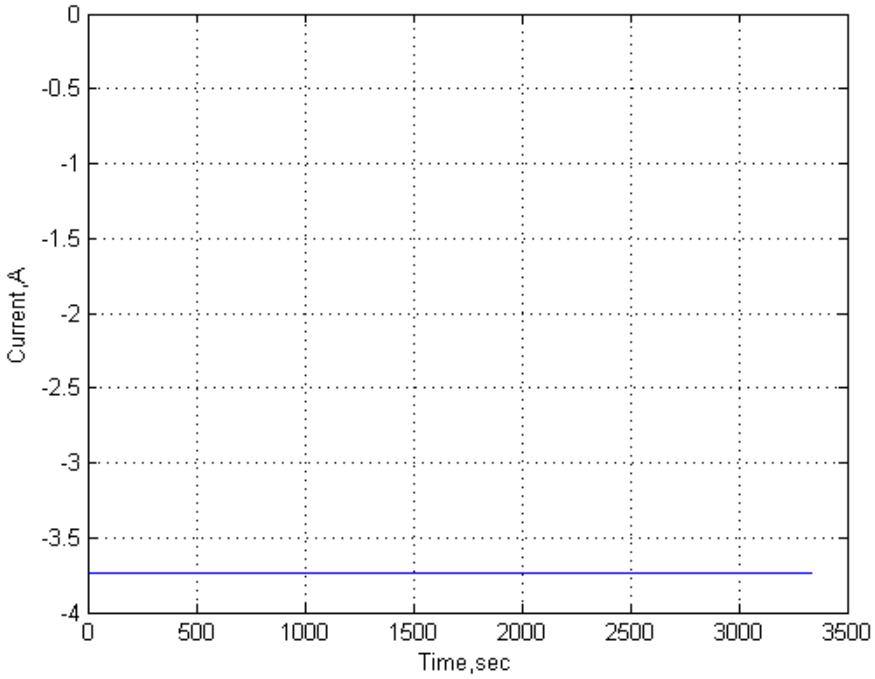

Figure 7.9. Input current to 24-hr OD battery discharge model

For this current input, the battery model parameters were identified again. Using those parameters, the built electrochemical model of this 24-hr OD battery, was simulated for this current signal and the voltage responses were compared with the relevant voltage response of the experiment. The voltage comparison of this battery operating condition, is provided in Figure 7.10.

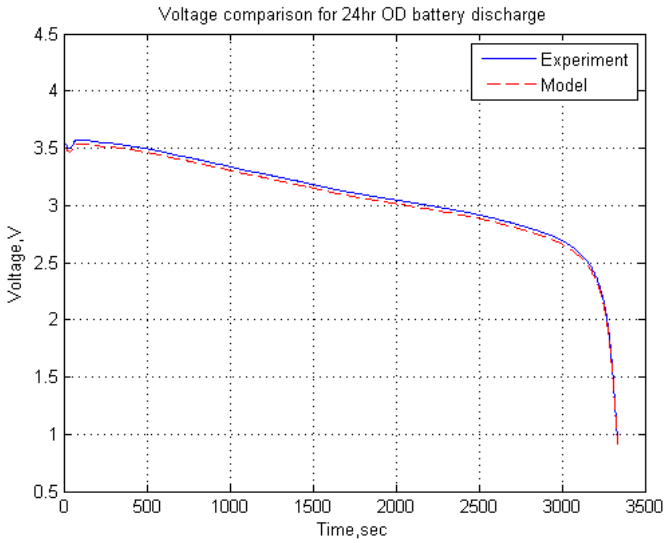

Figure 7.10. Voltage comparison for 24-hr OD battery discharge operation

From this voltage comparison provided, this is clear that, the PSO identified parameters of the electrochemical model of 24-hr over discharged battery is well accurate.

The discrepancy of the starting voltage of discharge with the rated voltage can be explained form Figure 7.11.

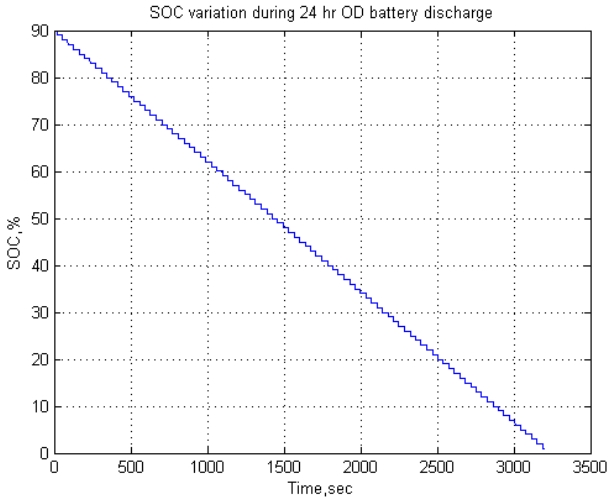

Figure 7.11. SOC variation during 24-hr OD battery discharge

Here also, the SOC at battery initial phase of discharge is near 90% and this is also because of long time cycling of the battery (20 times). That's why, the battery starts to discharge from 3.5 V instead of 3.7 V, which is it's rated voltage.

Moreover, for model validation of the over-charged battery, the previously conditioned battery at 25% over-charge ($1.25C$) operation, was taken under test for one cycle at 15% over-charge ($1.15C$), while the discharge operation was carried out at $1C$ rate as previously.

As, charging operation of this battery is crucial, the model was validated only for the charging operation of the battery. The input current to the battery model for charging operation of this over-charged battery, is provided in Figure 7.12.

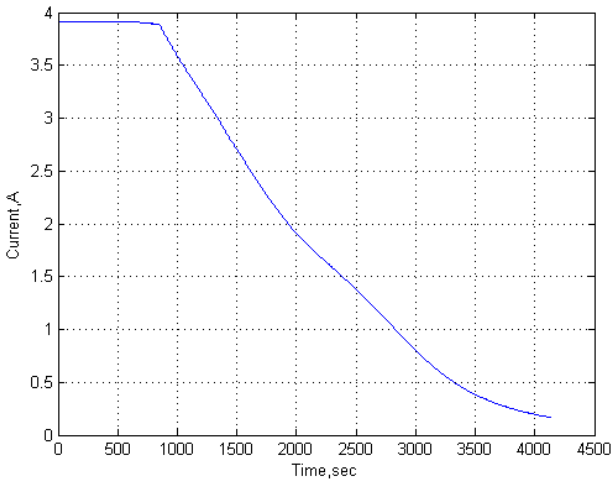

Figure 7.12. Input current to OC battery charge model

The compared voltage responses for this input current, is provided in Figure 7.13.

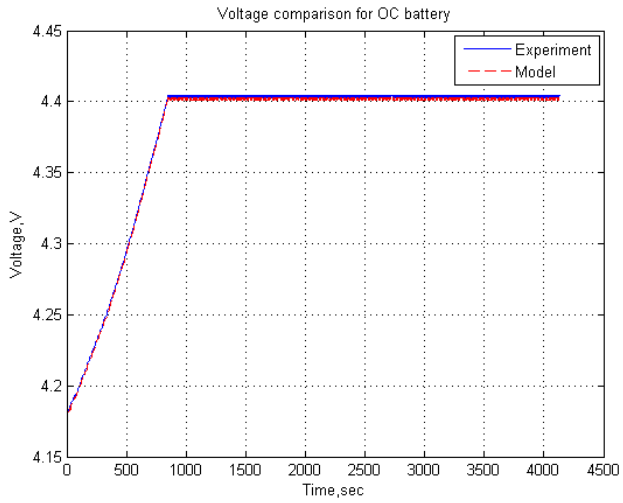

Figure 7.13. Voltage comparison for OC battery charge operation

From the voltage comparison of the over-charged battery model, it is clear that, the battery model of the over-charged battery using the PSO identified parameters is a precise one.

If all of the voltage comparisons are analyzed provided in this section, it can be said that, the battery electrochemical model is a validated one. This validation provided the way to proceed with the adaptive estimation approach of fault diagnosis, which is provided in a later section of this thesis works.

7.1 Temperature Variation During Experiments

In the reduced electrochemical model of Li-Ion battery, the temperature was assumed to be constant at room temperature, namely 298.15K. To check the validity of the assumption on temperature variation, the temperature during the experiments was measured. The temperature was measured during every cycle of operation and are providing the temperature profile all operating conditions of the battery. For Healthy battery operation, i.e. both discharge and charge, the temperature variation during experiments is provided in Figure 7.14.

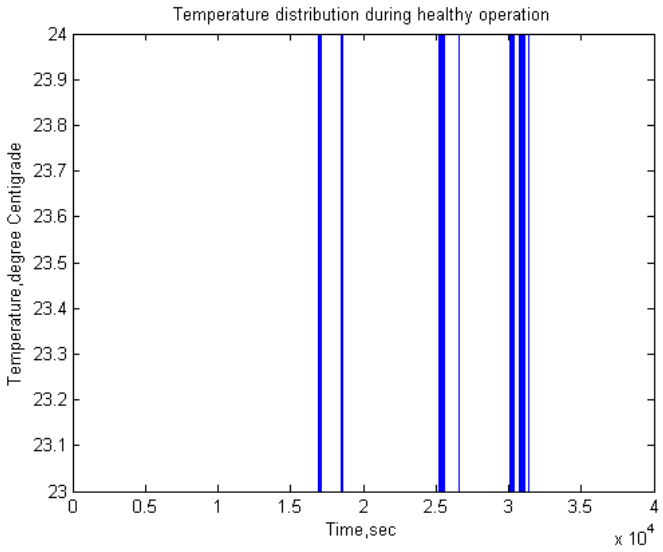

Figure 7.14. Temperature variation for Healthy battery operation

Temperature variation during Navy OD battery operation ($1.25C$ discharge) is provided in Figure 7.15.

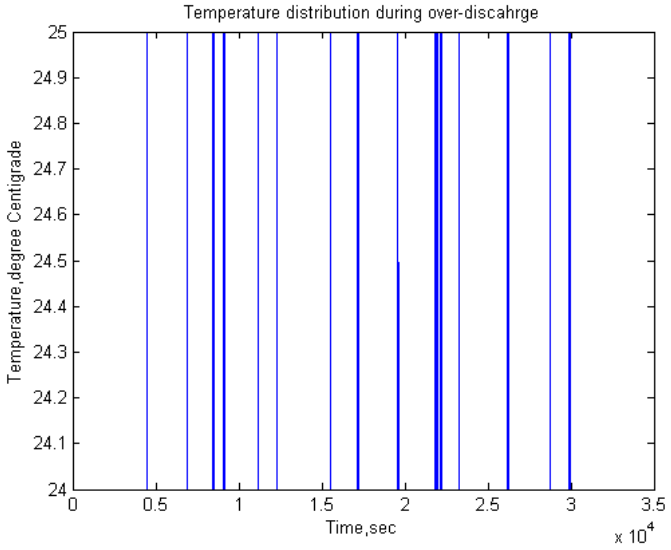

Figure 7.15. Temperature variation for Navy OD battery operation

For 24-hr OD battery, the temperature variation is provided in Figure 7.16.

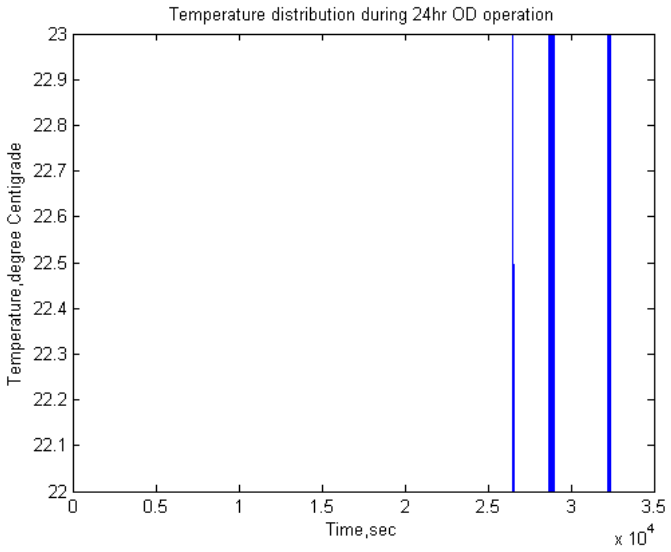

Figure 7.16. Temperature variation for 24-hr OD battery operation

Temperature variation was also observed for the over-charge operation of the battery (25% over), which is provided in Figure 7.17.

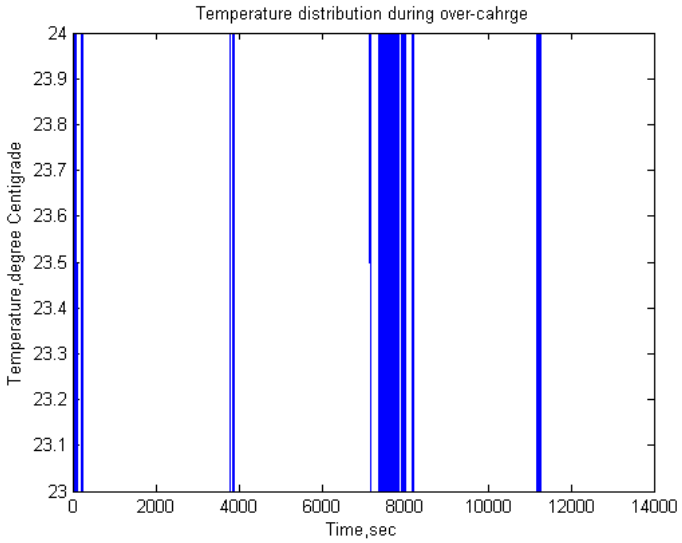

Figure 7.17. Temperature variation for OC battery charge operation

Provided temperature profiles are for four critical operations of the battery. For the Navy OD battery, temperature changes is limited within $24°C$ to $25°C$, only one degree centigrade variation during the overall operation time of the battery. On the other hand, for the OC battery, temperature changes from $23°C$ to $24°C$, here also only one degree centigrade variation during the overall operation period of the battery. Moreover for Healthy operation and also for 24-hr OD battery operation, the temperature variation is also only one degree Centigrade, which is consistent with other two operating situations stated earlier. From these observations, it can said that, the assumption adopted for temperature variation in the electrochemical model, is a reasonable one.

8. FAULT DIAGNOSIS USING THE IDENTIFIED MODELS

Having the identified battery models, adaptive estimation algorithm was implemented to have a more realistic fault diagnosis scheme. Four operating conditions of the battery will be used in fault diagnosis, i.e. Healthy battery, Navy over discharged battery, 24-hr over discharged battery and over-charged battery. For fault diagnosis purpose, the identified battery models were simulated for an input current for hybrid pulse power characterization (HPPC) cycle vehicle operation. Hybrid pulse power characterization is vital in HEV, EV or PHEV, because of its' applicability in determining the dynamic power capability over the usable charge and voltage range of the concerned vehicle or the device, where both discharge and regenerative pulses are considered in the test profile current signal [70]. Therefore, fault diagnosis based on the battery current output form a HPPC cycle simulation of a HEV can be an important step in fault diagnosis of Li-Ion battery. This adaptive estimation following the similar techniques described in one of the previous chapters of this thesis.

8.1 Battery Model Selection

As described earlier, all of the battery models were identified for both discharge and charge operation at different rates. Different battery models were defined with the identified significant parameters using the particle swarm optimization (PSO) algorithm. For the adaptive estimation purpose, for Healthy battery, the model for charging operation was selected, because charging operation is significant for a Healthy battery. For Navy over-discharged battery, as the discharge is dominant here (as the battery is over-discharged), the battery model for discharge operation of the battery was selected. For the similar kind of reason, for 24-hr over discharged battery, the battery model for discharge operation is selected and for over-charged battery,

the model was selected for charging operation as the charge is dominant here. All of these defined models were selected for fault diagnosis with MMAE approach.

8.2 Identified Battery Model and PDAE Observer Responses

Same procedure was followed here as the previously described fault diagnosis technique except the input current profile. The reduced order electrochemical model was used and also the PDAE based observer was used in estimation works. The current profile with which the faults are identified is provided in Figure 8.1 [59].

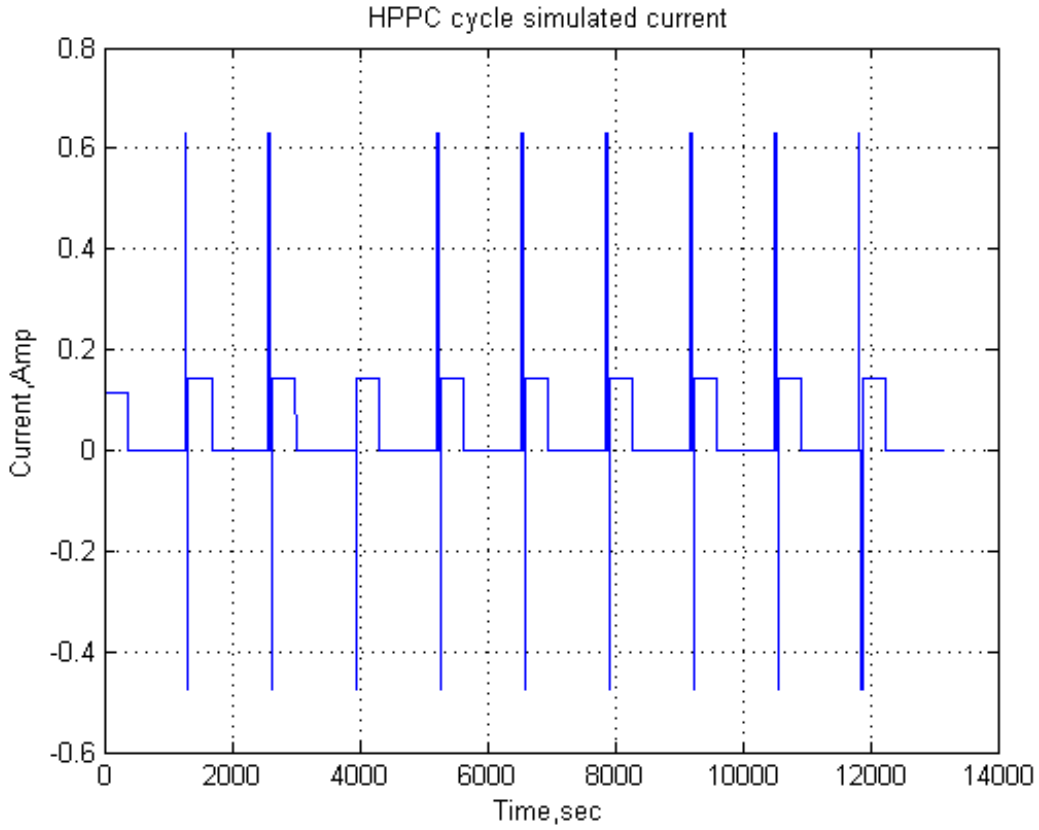

Figure 8.1. HPPC cycle simulated current

For this current input, all the models were simulated and observed. The identified Healthy battery model and the PDAE observer response for this current input is provided in Figure 8.2.

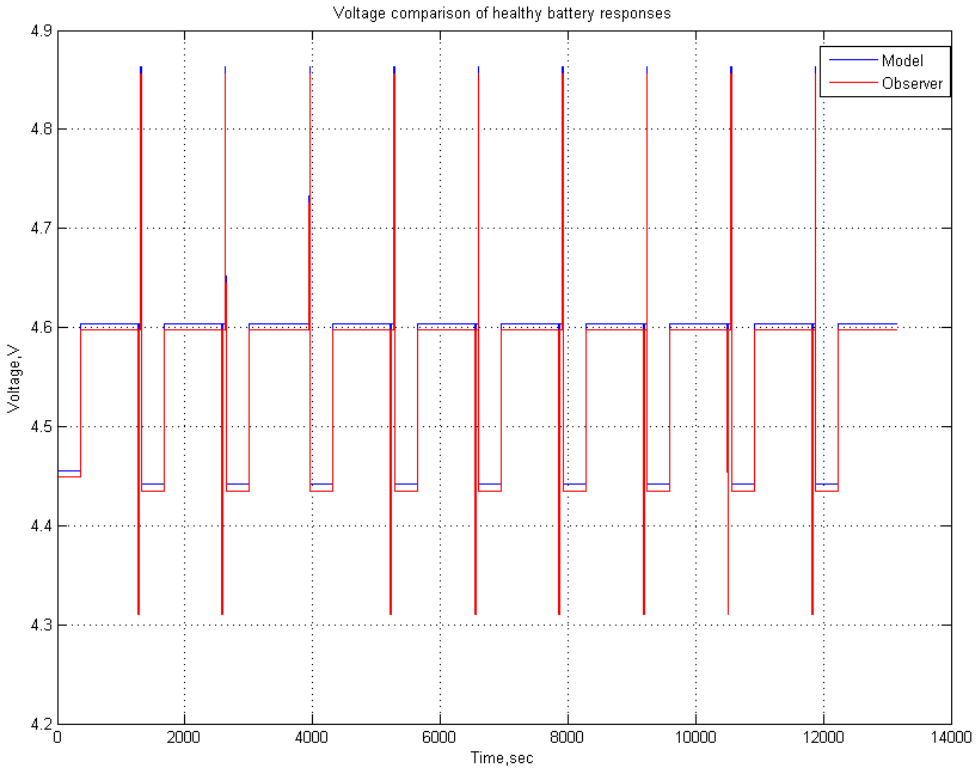

Figure 8.2. Identified Healthy battery model and observer response for HPPC cycle simulated current

Similarly, for the identified battery model for Navy over-discharge is simulated and observed and the responses are provided in Figure 8.3.

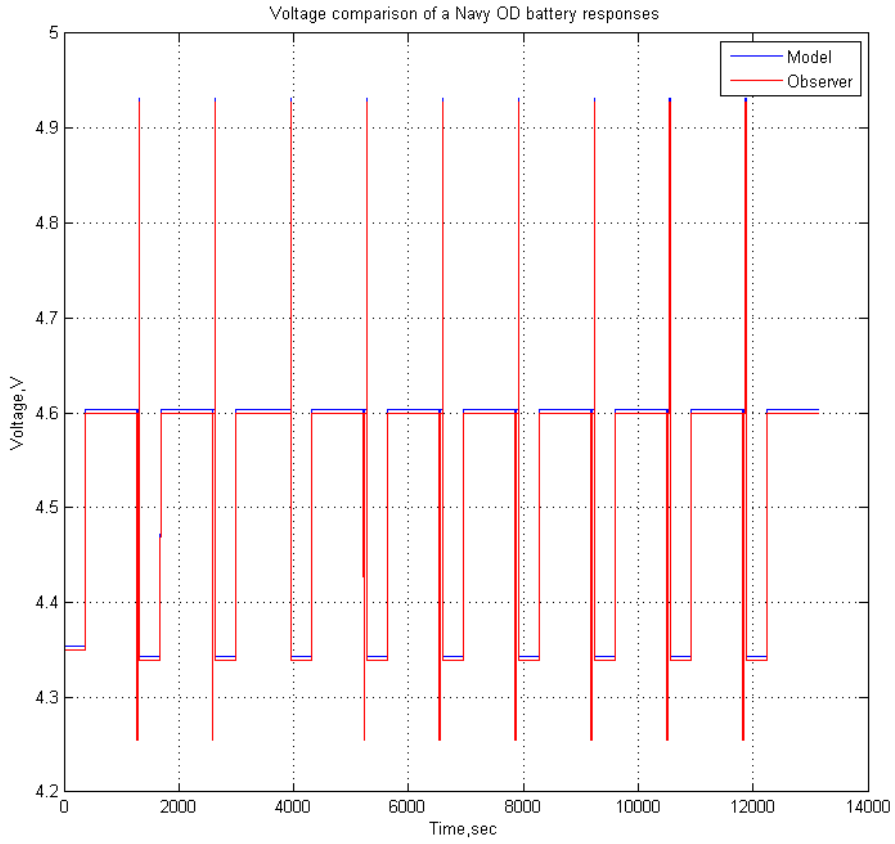

Figure 8.3. Identified Navy OD battery model and observer response for HPPC cycle simulated current

Identified battery model response along with the PDAE observer response for 24-hr overdischarged battery is provided in Figure 8.4.

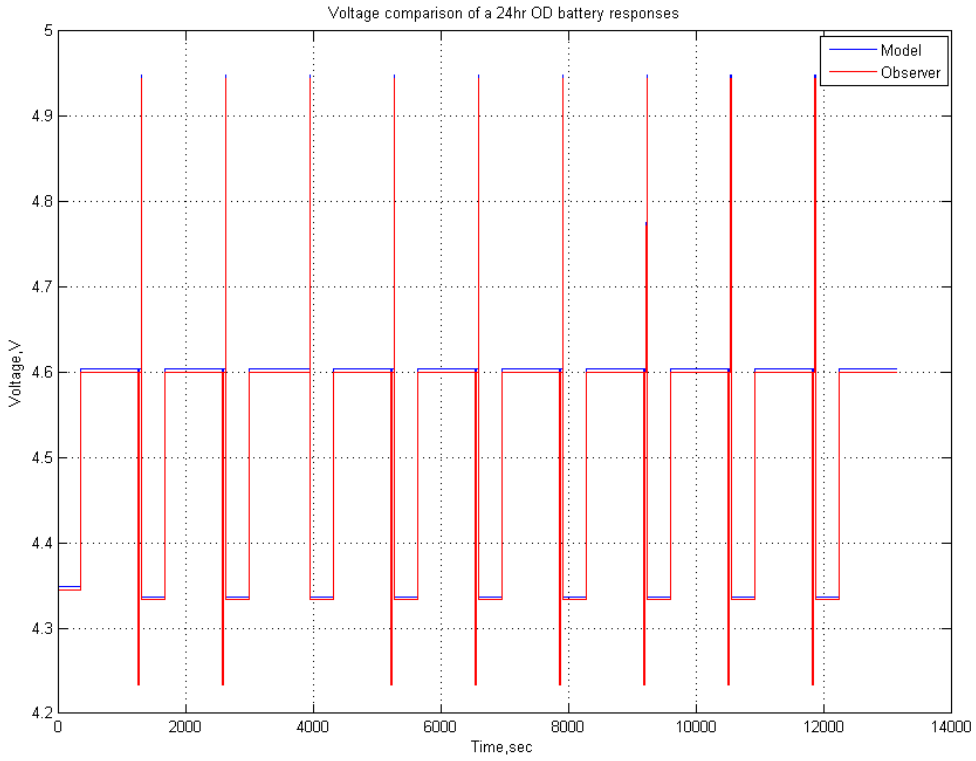

Figure 8.4. Identified 24-hr OD battery model and observer response for HPPC cycle simulated current

And the response of the 25% over-charged battery for HPPC current input is provided in Figure 8.5.

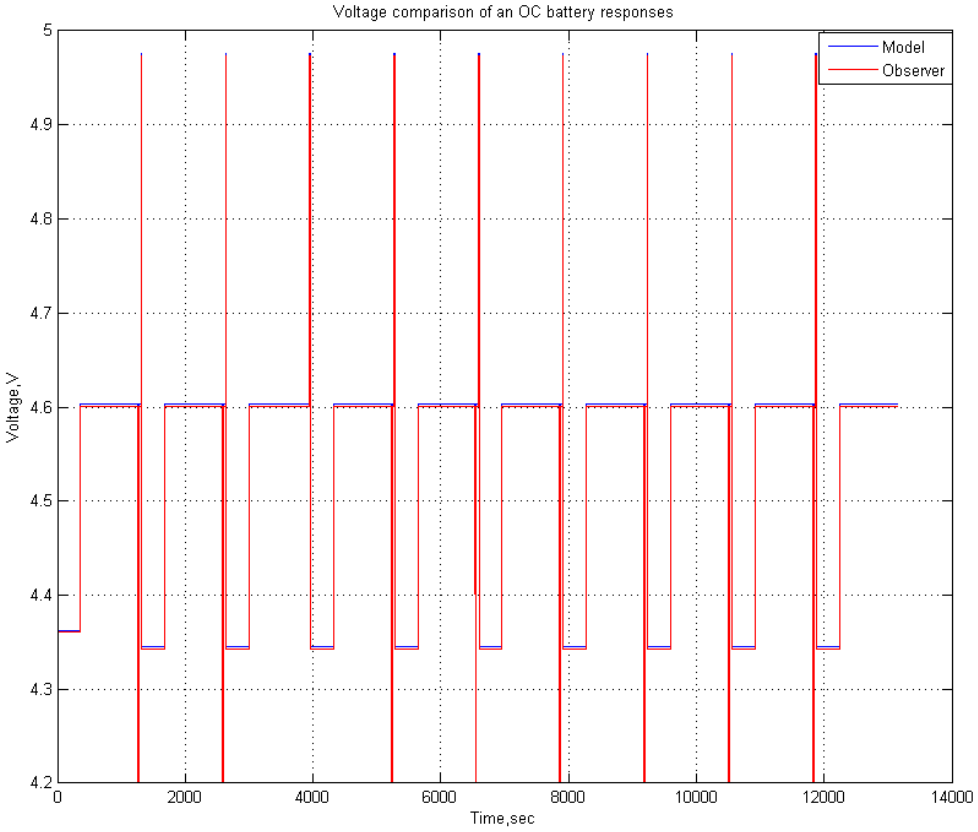

Figure 8.5. Identified 25% OC battery model and observer response for HPPC cycle simulated current

8.3 Differences Between the Identified Model and Observer Responses

The voltage response differences or the residuals are defined as, Voltage residual = Individual model voltage response - the individual battery observer voltage response. The mean value of the differences or residuals is almost zero.

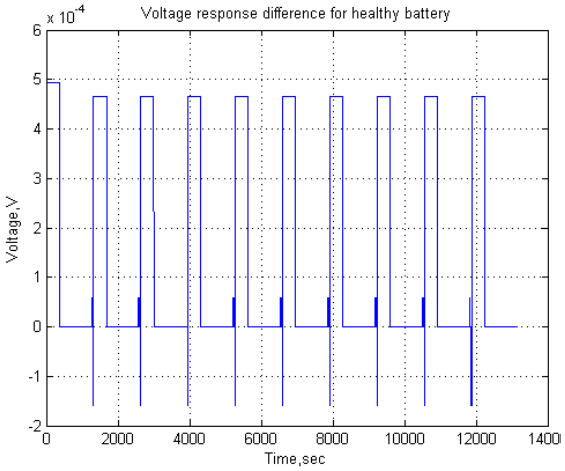

Figure 8.6. Voltage residuals for Healthy battery

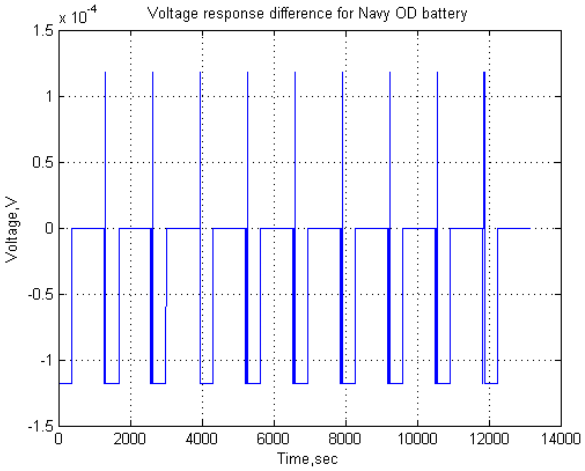

Figure 8.7. Voltage residuals for Navy OD battery

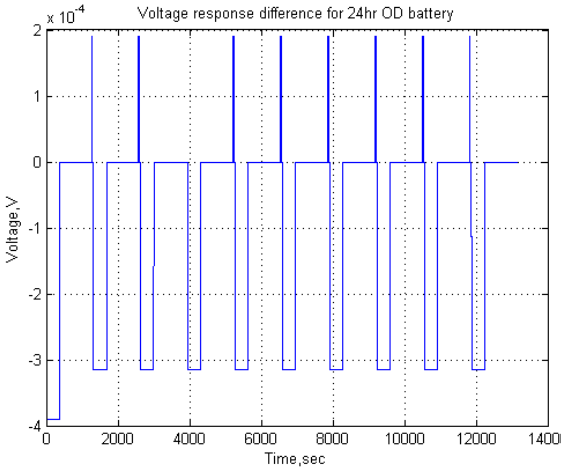

Figure 8.8. Voltage residuals for 24-hr OD battery

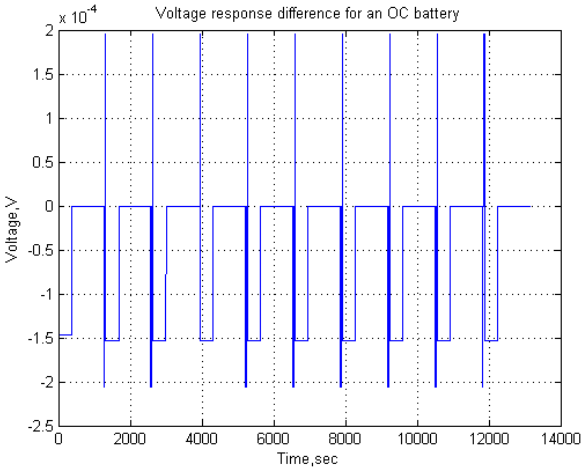

Figure 8.9. Voltage residuals for OC battery

8.4 Plant Model Build-up for Fault Diagnosis

To have the plant model, the following scenario is created. HPPC cycle was for 13140 sec. Within this total length of time, first 2628 sec is for Healthy battery model, next 1314 sec is from Navy OD battery model, next 2628 sec is from 24-hr OD battery, next 1314 sec is again from Healthy battery, next 2628 sec is from OC battery and last 2628 sec is again coming from Healthy operation of the battery. Following these order of battery operation, the built battery plant voltage profile is provided in Figure 8.10.

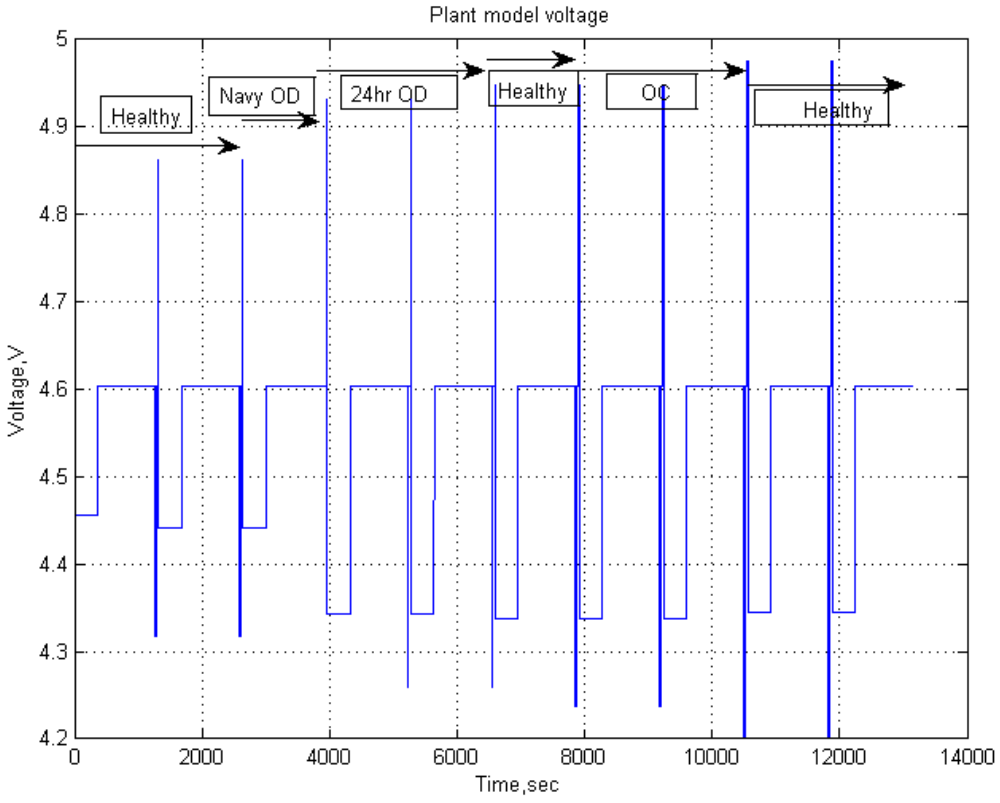

Figure 8.10. Reference plant model voltage response

8.5 Fault Diagnosis Using the Identified Battery Models

PDAE observer responses for all of the battery operating conditions as mentioned previously are deducted from the plant voltage response and the residual are generated for particular battery model. The voltage residuals are provided in Figure 8.11.

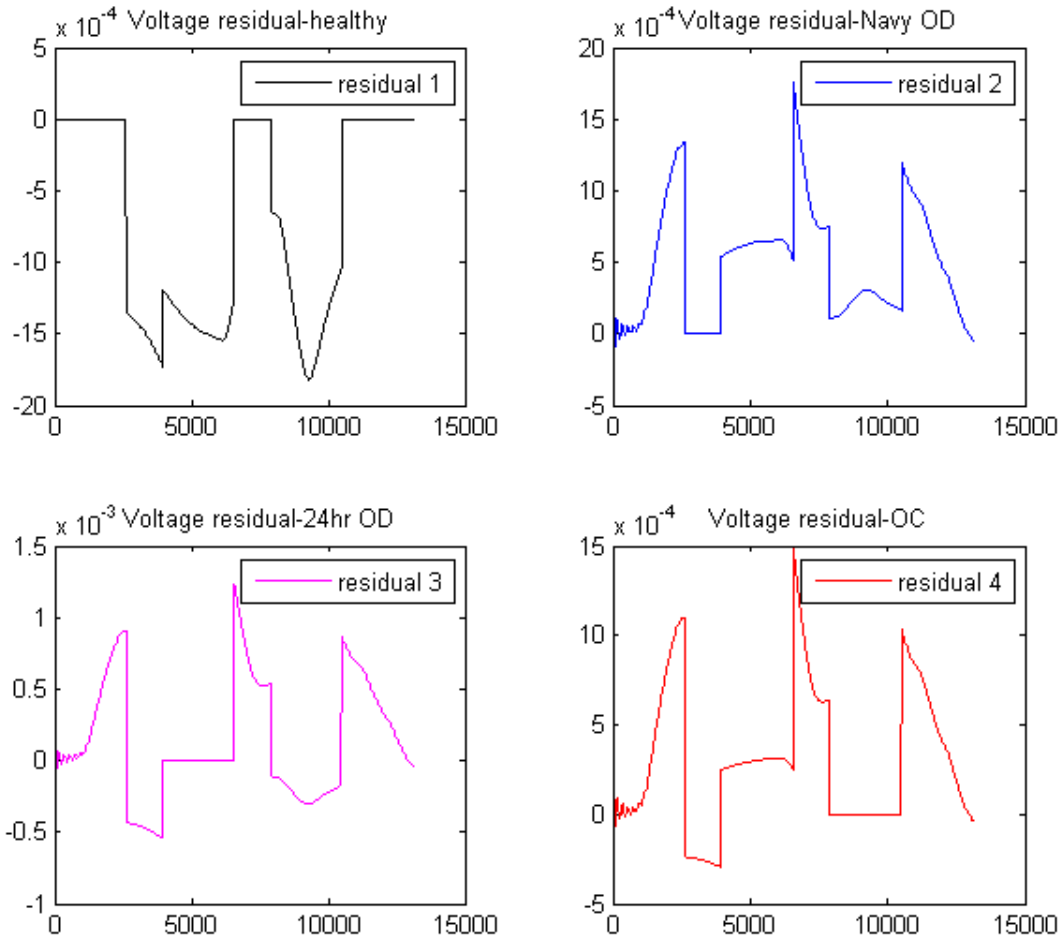

Figure 8.11. Voltage residuals for different operating conditions

Using the system identification toolbox as previously, the state covariance matrices are generated for different battery operating conditions. Using these state covariance

matrices and the voltage residuals, the conditional probability densities are generated for different values of measurement noise covariance matrix, R. If the voltage residual present in this fault diagnosis scheme is analyzed, it is clear that, the maximum value of system residual or the noise signal is in the range of 10^{-4}. Therefore, the measurement noise covariance matrix should be lower than the maximum system noise signal. Conditional probabilities were obtained using different measurement covariances, which is obviously lower than the maximum system noise.

For $R = 1 \times 10^{-5}$, the obtained probability distribution is provided in Figure 8.12. The obtained probability distribution is not exactly what MMAE should have

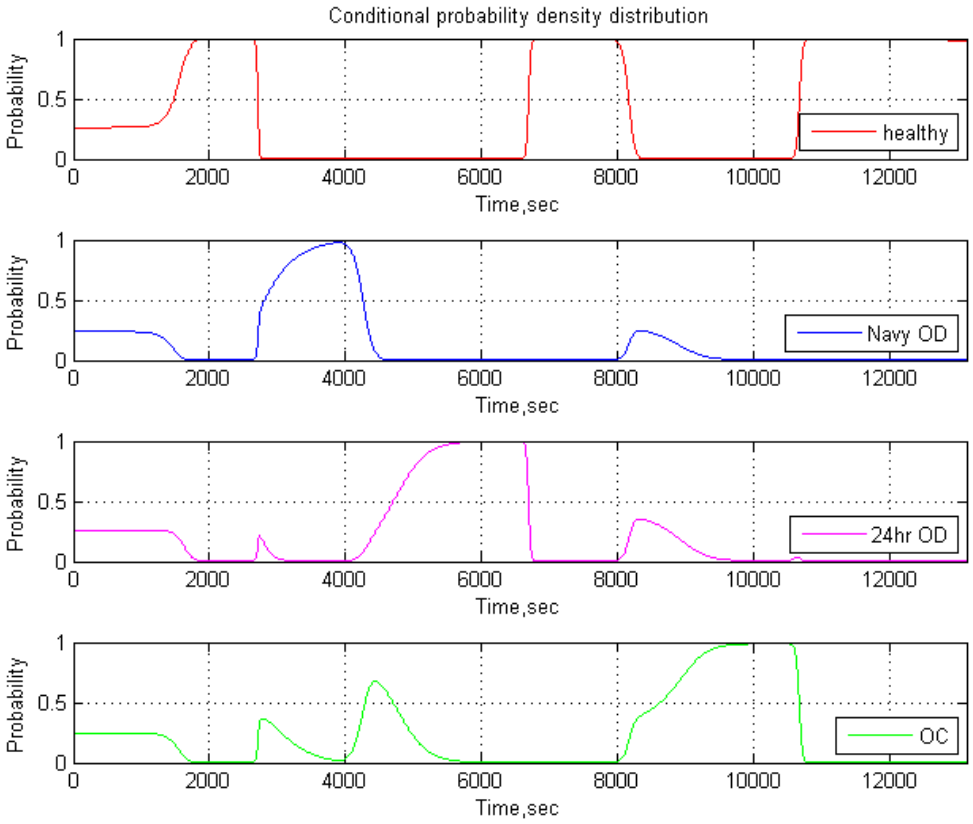

Figure 8.12. Probability distribution for different operating conditions for $R = 1 \times 10^{-5}$

detected. Therefore, the value of R was changed and the probability for different value of the measurement noise covariance matrix was plotted.

For $R = 1 \times 10^{-6}$, the obtained probability distribution is provided in Figure 8.13.

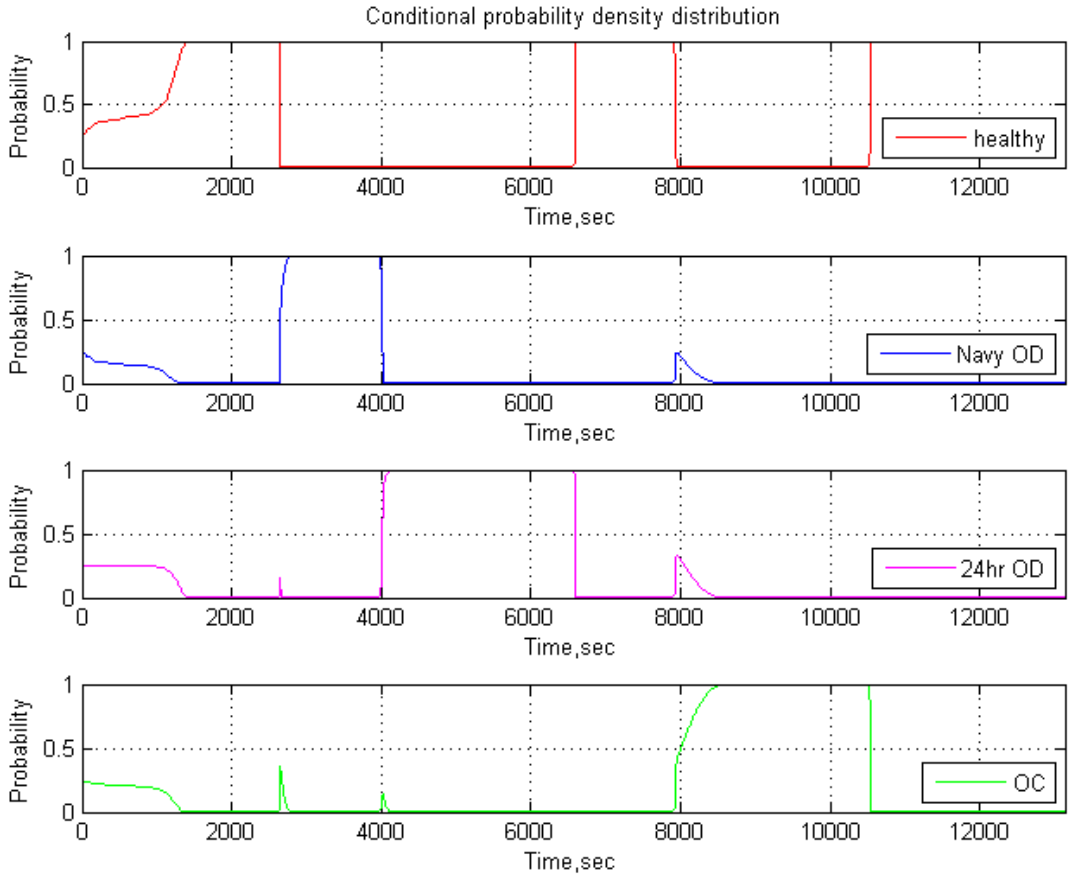

Figure 8.13. Probability distribution for different operating conditions for $R = 1 \times 10^{-6}$

This distribution is better than the previous one but not accurate enough for fault diagnosis.

For $R = 1 \times 10^{-7}$, the obtained probability distribution is provided in Figure 8.14.

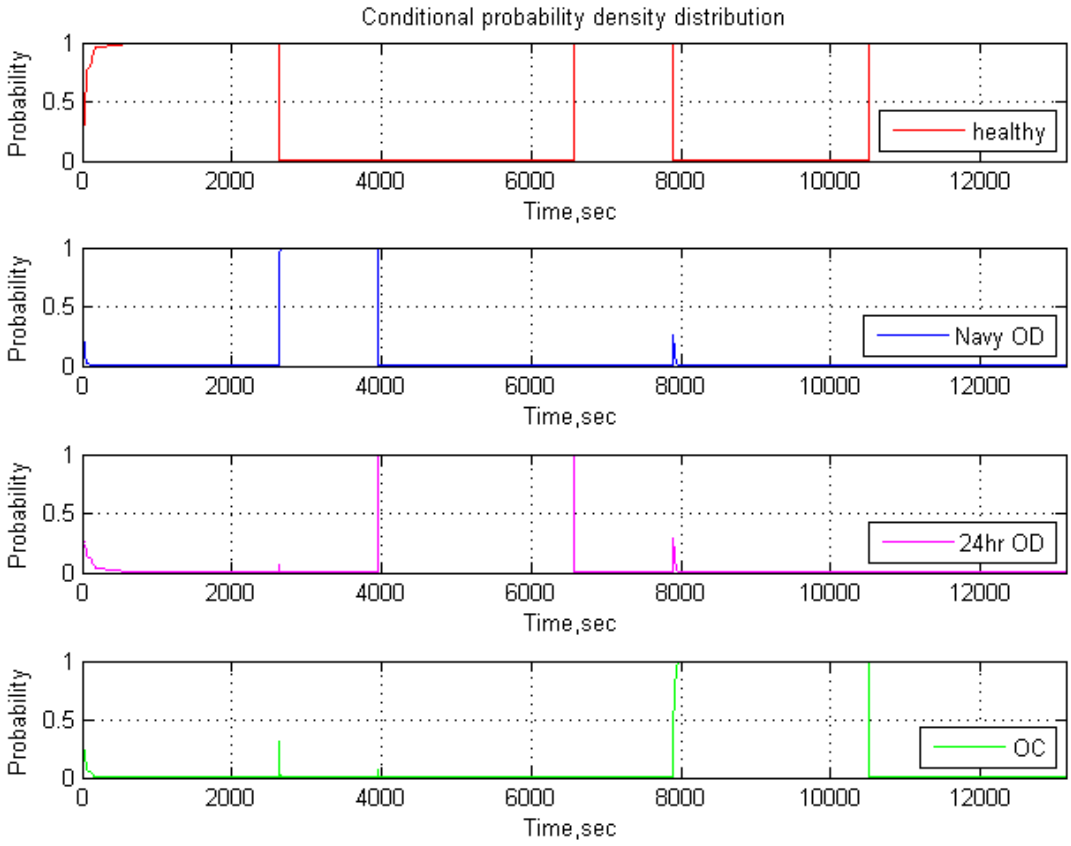

Figure 8.14. Probability distribution for different operating conditions for $R = 1 \times 10^{-7}$

Still, this is not perfect one, so the value of R was changed to 1×10^{-8}, and the probability distribution is obtained as provided in Figure 8.15.

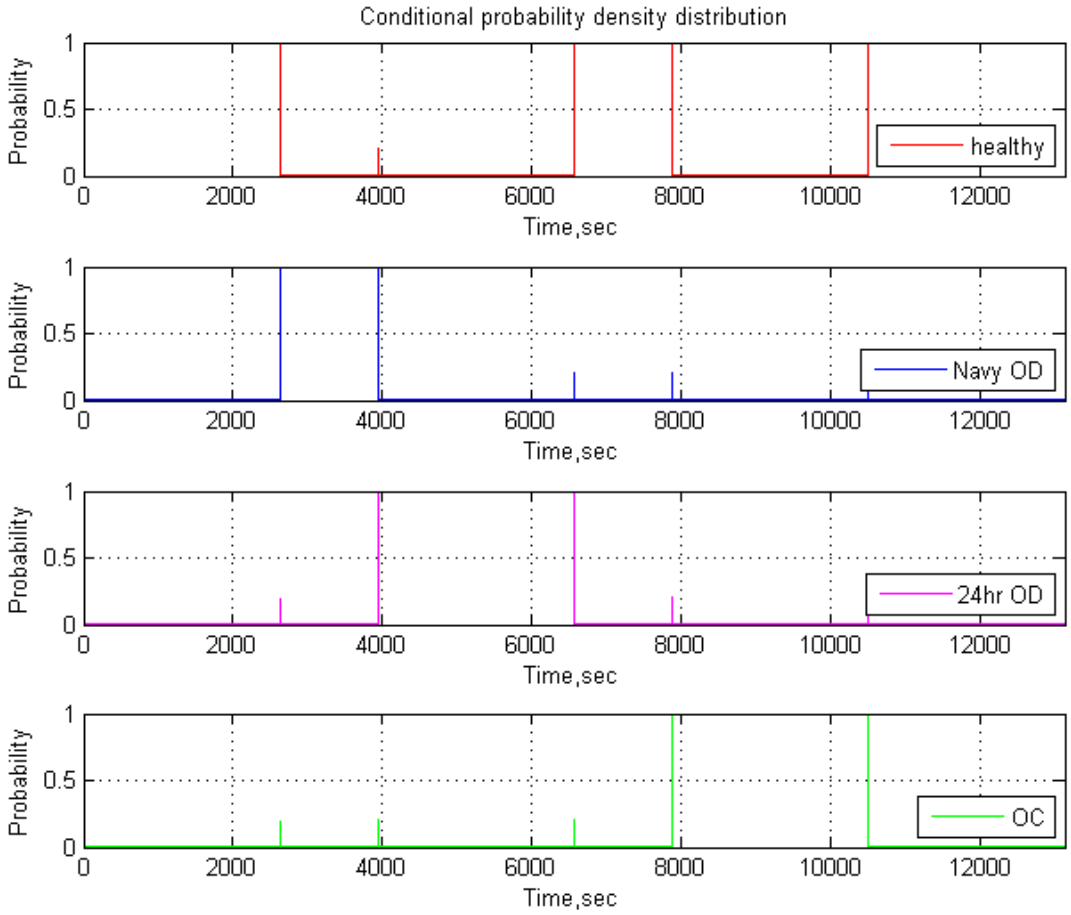

Figure 8.15. Probability distribution for different operating conditions for $R = 1 \times 10^{-8}$

If the last probability distribution is observed, it is clear that, the scenarios of battery operations which was created, was accurately detected with well accuracy. And as the considered models were identified by PSO algorithm, this detection of operating conditions or this fault diagnosis is more reliable and realistic.

9. CONCLUSION AND FUTURE WORKS

9.1 Conclusion

Various battery operating conditions were diagnosed using multiple model adaptive estimation methodology that used the electrochemical model of Li-Ion battery. First, MMAE was successfully designed for UDDS cycle simulated current profile as an input to the electrochemical battery model. Simulation results showed that the proposed methodology was able to successfully identify four different operating conditions, namely, Healthy, aged, over-discharged and over-charged condition. That provided the foundation for next works of this thesis endeavor. A direct optimization methodology, namely particle swarm optimization, was developed for electrochemical model parameter identification. Four significant parameters were considered for identification using PSO. This was successfully completed with good accuracy for a number of operating conditions of the battery, namely, Healthy battery, Navy over-discharged battery, 24-hr over discharged battery and an over-charged battery. To implement the parameter identification process, experiments were carried out on a 3.7 V Panasonic NCR18650B Lithium-Ion battery using a versatile battery tester from CADEX Inc. Electrochemical model of the battery was validated for different sets of test data rather than using the initial test data. Model validations were performed with reasonable accuracy. Temperature measurements throughout the experiments validated the assumption of constant temperature in battery modeling. Finally, all the identified models were used in another set of MMAE based fault diagnosis. This time, HPPC cycle simulated current data was the input to the battery models and PDAE observers. The resulting conditional probability revealed that, the battery conditions were correctly identified for the PSO identified parameter-based models.

The proposed fault diagnosis methodology can have significant impact on the battery management system (BMS) due to its accuracy of fault diagnosis.

9.2 Future Works

In this work, it was assumed that, the temperature distribution was constant throughout the operations. This may not be the case for all operating conditions. The present work can be extended with the assumption of variable temperature distribution in modeling. Also, the electrochemical model was 1-D, where the variation of dynamics in Y and Z directions was not considered. The 1-D model can be updated by adopting the variation in dynamics in other directions. Another potential future work can be the integration of the proposed fault diagnosis technique with the battery management system in real time applications. Moreover, all other battery parameters can be taken as the target parameters to identify using particle swarm optimization algorithm, which will provide more confidence in battery model identification. Mathematical analysis of the PDAE observer integration with MMAE based fault diagnosis can be another great prospective area to work with. In addition to the above, temperature residuals can be considered in fault diagnosis of Li-Ion battery.

REFERENCES

REFERENCES

[1] Jingliang Zhang and Jay Lee. A review on prognostics and health monitoring of li-ion battery. *Journal of Power Sources*, 196(15):6007–6014, 2011.

[2] Kai Goebel, Bhaskar Saha, Abhinav Saxena, Jose R Celaya, and Jon P Christophersen. Prognostics in battery health management. *IEEE instrumentation & measurement magazine*, 11(4):33, 2008.

[3] Nalin A Chaturvedi, Reinhardt Klein, Jake Christensen, Jasim Ahmed, and Aleksandar Kojic. Modeling, estimation, and control challenges for lithium-ion batteries. In *American Control Conference (ACC), 2010*, pages 1997–2002. IEEE, 2010.

[4] It direction. `http://www.itdirection.net/images/lthcll-may-13.png`. Last accessed May 2015.

[5] Domenico Di Domenico, Giovanni Fiengo, and Anna Stefanopoulou. Lithium-ion battery state of charge estimation with a kalman filter based on a electrochemical model. In *Control Applications, 2008. CCA 2008. International Conference on*, pages 702–707. Ieee, 2008.

[6] Osvaldo Barbarisi, Francesco Vasca, and Luigi Glielmo. State of charge kalman filter estimator for automotive batteries. *Control Engineering Practice*, 14(3):267–275, 2006.

[7] JA Prins-Jansen, Joseph D Fehribach, Kas Hemmes, and JHW De Wit. A three-phase homogeneous model for porous electrodes in molten-carbonate fuel cells. *Journal of The Electrochemical Society*, 143(5):1617–1628, 1996.

[8] Kandler Smith and Chao-Yang Wang. Solid-state diffusion limitations on pulse operation of a lithium ion cell for hybrid electric vehicles. *Journal of Power Sources*, 161(1):628–639, 2006.

[9] Mark W Verbrugge and Brian J Koch. Electrochemical analysis of lithiated graphite anodes. *Journal of The Electrochemical Society*, 150(3):A374–A384, 2003.

[10] Nova battery systems. `http://www.novabatterysystems.com/lithium-ion.php`. Last accessed July 2015.

[11] Thomas Stuart, Fang Fang, Xiaopeng Wang, Cyrus Ashtiani, and Ahmad Pesaran. A modular battery management system for hevs. Technical report, SAE Technical Paper, 2002.

[12] Yuang-Shung Lee and Ming-Wang Cheng. Intelligent control battery equalization for series connected lithium-ion battery strings. *Industrial Electronics, IEEE Transactions on*, 52(5):1297–1307, 2005.

[13] Mark W Verbrugge and Ping Liu. Electrochemical characterization of high-power lithium ion batteries using triangular voltage and current excitation sources. *Journal of Power Sources*, 174(1):2–8, 2007.

[14] John Newman and William Tiedemann. Porous-electrode theory with battery applications. *AIChE Journal*, 21(1):25–41, 1975.

[15] Thomas F Fuller, Marc Doyle, and John Newman. Simulation and optimization of the dual lithium ion insertion cell. *Journal of the Electrochemical Society*, 141(1):1–10, 1994.

[16] Karen E Thomas, John Newman, and Robert M Darling. Mathematical modeling of lithium batteries. In *Advances in lithium-ion batteries*, pages 345–392. Springer, 2002.

[17] Irene J Ong and John Newman. Double-layer capacitance in a dual lithium ion insertion cell. *Journal of The Electrochemical Society*, 146(12):4360–4365, 1999.

[18] John Newman and Karen E Thomas-Alyea. *Electrochemical systems*. John Wiley & Sons, 2012.

[19] Marc Doyle, Thomas F Fuller, and John Newman. Modeling of galvanostatic charge and discharge of the lithium/polymer/insertion cell. *Journal of the Electrochemical Society*, 140(6):1526–1533, 1993.

[20] Reinhardt Klein, Nalin A Chaturvedi, Jake Christensen, Jasim Ahmed, Rolf Findeisen, and Aleksandar Kojic. Electrochemical model based observer design for a lithium-ion battery. *Control Systems Technology, IEEE Transactions on*, 21(2):289–301, 2013.

[21] Amardeep Singh, Afshin Izadian, and Sohel Anwar. Fault diagnosis of li-ion batteries using multiple-model adaptive estimation. In *Industrial Electronics Society, IECON 2013-39th Annual Conference*, pages 3524–3529. IEEE, 2013.

[22] Jie Liu, Abhinav Saxena, Kai Goebel, Bhaskar Saha, and Wilson Wang. An adaptive recurrent neural network for remaining useful life prediction of lithium-ion batteries. Technical report, DTIC Document, 2010.

[23] Wen Chen, Wei-Tian Chen, Mehrdad Saif, Meng-Feng Li, and Hai Wu. Simultaneous fault isolation and estimation of lithium-ion batteries via synthesized design of luenberger and learning observers. *IEEE Transactions on Control Systems Technology*, 22(1):290–298, 2014.

[24] Adnan Nuhic, Tarik Terzimehic, Thomas Soczka-Guth, Michael Buchholz, and Klaus Dietmayer. Health diagnosis and remaining useful life prognostics of lithium-ion batteries using data-driven methods. *Journal of Power Sources*, 239:680–688, 2013.

[25] Dong Wang, Qiang Miao, and Michael Pecht. Prognostics of lithium-ion batteries based on relevance vectors and a conditional three-parameter capacity degradation model. *Journal of Power Sources*, 239:253–264, 2013.

[26] James D Kozlowski. Electrochemical cell prognostics using online impedance measurements and model-based data fusion techniques. In *Aerospace Conference, 2003. Proceedings*, volume 7, pages 3257–3270. IEEE, 2003.

[27] Steven X Ding. *Model-based fault diagnosis techniques: design schemes, algorithms, and tools*. Springer Science & Business Media, 2008.

[28] Riccardo Poli, James Kennedy, and Tim Blackwell. Particle swarm optimization. *Swarm intelligence*, 1(1):33–57, 2007.

[29] Maurice Clerc and James Kennedy. The particle swarm-explosion, stability, and convergence in a multidimensional complex space. *Evolutionary Computation, IEEE Transactions on*, 6(1):58–73, 2002.

[30] James Kennedy. Particle swarm optimization. In *Encyclopedia of Machine Learning*, pages 760–766. Springer, 2010.

[31] Rizwan Ahmed, Mohammed El Sayed, Ienkaran Arasaratnam, Jimi Tjong, and Saeid Habibi. Reduced-order electrochemical model parameters identification and soc estimation for healthy and aged li-ion batteries part i: Parameterization model development for healthy batteries. *Emerging and Selected Topics in Power Electronics, IEEE Journal of*, 2(3):659–677, 2014.

[32] Carmelo Speltino, DD Domenico, Giovanni Fiengo, and AG Stefanopoulou. Experimental identification and validation of an electrochemical model of a lithium-ion battery. In *Proceedings of the American Control Conference*, 2009.

[33] Joel C Forman, Scott J Moura, Jeffrey L Stein, and Hosam K Fathy. Genetic identification and fisher identifiability analysis of the doyle–fuller–newman model from experimental cycling of a lifepo 4 cell. *Journal of Power Sources*, 210:263–275, 2012.

[34] Joel Forman, Scott Moura, Jeffrey Stein, and Hosam Fathy. Genetic parameter identification of the doyle-fuller-newman model from experimental cycling of a lifepo 4 battery. In *American Control Conference (ACC), 2011*, pages 362–369. IEEE, 2011.

[35] Amardeep Singh, Afshin Izadian, and Sohel Anwar. Model based condition monitoring in lithium-ion batteries. *Journal of Power Sources*, 268:459–468, 2014.

[36] DOT NAVY. Technical manual for batteries. *Navy Lithium Safety Program Responsibilities And Procedures*, 2004.

[37] Nalin A Chaturvedi, Reinhardt Klein, Jake Christensen, Jasim Ahmed, and Aleksandar Kojic. Algorithms for advanced battery-management systems. *Control Systems, IEEE*, 30(3):49–68, 2010.

[38] Allen J Bard and Larry R Faulkner. *Electrochemical methods: fundamentals and applications*, volume 2. Wiley New York, 1980.

[39] Paul Albertus, Jake Christensen, and John Newman. Experiments on and modeling of positive electrodes with multiple active materials for lithium-ion batteries. *Journal of the Electrochemical Society*, 156(7):A606–A618, 2009.

[40] WB Gu and CY Wang. Thermal-electrochemical modeling of battery systems. *Journal of The Electrochemical Society*, 147(8):2910–2922, 2000.

[41] Venkat R Subramanian, Vinten D Diwakar, and Deepak Tapriyal. Efficient macro-micro scale coupled modeling of batteries. *Journal of The Electrochemical Society*, 152(10):A2002–A2008, 2005.

[42] Venkat R Subramanian, Vijayasekaran Boovaragavan, Venkatasailanathan Ramadesigan, and Mounika Arabandi. Mathematical model reformulation for lithium-ion battery simulations: Galvanostatic boundary conditions. *Journal of The Electrochemical Society*, 156(4):A260–A271, 2009.

[43] Thanh-Son Dao, Chandrika P Vyasarayani, and John McPhee. Simplification and order reduction of lithium-ion battery model based on porous-electrode theory. *Journal of Power Sources*, 198:329–337, 2012.

[44] Timothy E Menke and Peter S Maybeck. Sensor/actuator failure detection in the vista f-16 by multiple model adaptive estimation. *Aerospace and Electronic Systems, IEEE Transactions on*, 31(4):1218–1229, 1995.

[45] Peter S Maybeck. Multiple model adaptive algorithms for detecting and compensating sensor and actuator/surface failures in aircraft flight control systems. *International Journal of Robust and Nonlinear Control*, 9(14):1051–1070, 1999.

[46] Peter S Maybeck and Richard D Stevens. Reconfigurable flight control via multiple model adaptive control methods. *Aerospace and Electronic Systems, IEEE Transactions on*, 27(3):470–480, 1991.

[47] Timothy E Menke and Peter S Maybeck. Multiple model adaptive estimation applied to the vista f-16 flight control system with actuator and sensor failures. In *Aerospace and Electronics Conference, 1992. NAECON 1992., Proceedings of 1992 National*, pages 441–448. IEEE, 1992.

[48] Michael Athans, David Castanon, K-P Dunn, C Greene, Wing Lee, N Sandell Jr, and Alan S Willsky. The stochastic control of the f-8c aircraft using a multiple model adaptive control (mmac) method–part i: Equilibrium flight. *Automatic Control, IEEE Transactions on*, 22(5):768–780, 1977.

[49] Afshin Izadian. Self-tuning fault diagnosis of mems. *Mechatronics*, 23(8):1094–1099, 2013.

[50] Afshin Izadian, Pardis Khayyer, and Parviz Famouri. Fault diagnosis of time-varying parameter systems with application in mems lcrs. *Industrial Electronics, IEEE Transactions on*, 56(4):973–978, 2009.

[51] Afshin Izadian and Parviz Famouri. Fault diagnosis of mems lateral comb resonators using multiple-model adaptive estimators. *Control Systems Technology, IEEE Transactions on*, 18(5):1233–1240, 2010.

[52] Peter D Hanlon and Peter S Maybeck. Multiple-model adaptive estimation using a residual correlation kalman filter bank. *Aerospace and Electronic Systems, IEEE Transactions on*, 36(2):393–406, 2000.

[53] P Eide and P Maybeck. Implementation and demonstration of a multiple model adaptive estimation failure detection system for the f-16. In *Decision and Control, 1995., Proceedings of the 34th Conference on*, volume 2, pages 1873–1878. IEEE, 1995.

[54] Peter Eide and Maybeck. An mmae failure detection system for the f-16. *Aerospace and Electronic Systems, IEEE Transactions on*, 32(3):1125–1136, 1996.

[55] Peter S Maybeck and Peter D Hanlon. Performance enhancement of a multiple model adaptive estimator. *Aerospace and Electronic Systems, IEEE Transactions on*, 31(4):1240–1254, 1995.

[56] Ronald E Kruse and Thomas A Huls. Development of the federal urban driving schedule. Technical report, SAE Technical Paper, 1973.

[57] Protodrive,rapid protyping platfrom for electric vehicle powertrain. `http://mlab.seas.upenn.edu/protodrive/index.html`. Last accessed June 2015.

[58] Namwook Kim, Aymeric Rousseau, and Eric Rask. Autonomie model validation with test data for 2010 toyota prius. Technical report, SAE Technical Paper, 2012.

[59] Vinay KS Muddappa and Sohel Anwar. Electrochemical model based fault diagnosis of li-ion battery using fuzzy logic. In *ASME 2014 International Mechanical Engineering Congress and Exposition*, pages V04BT04A048–V04BT04A048. American Society of Mechanical Engineers, 2014.

[60] Particle swarm optimization. `http://www.swarmintelligence.org/index.php`. Last accessed May 2015.

[61] NM Kwok, QP Ha, TH Nguyen, Jianchun Li, and Bijan Samali. A novel hysteretic model for magnetorheological fluid dampers and parameter identification using particle swarm optimization. *Sensors and Actuators A: Physical*, 132(2):441–451, 2006.

[62] Jakob Vesterstrom and Rene Thomsen. A comparative study of differential evolution, particle swarm optimization, and evolutionary algorithms on numerical benchmark problems. In *Evolutionary Computation, 2004. CEC2004. Congress on*, volume 2, pages 1980–1987. IEEE, 2004.

[63] Qie He, Ling Wang, and Bo Liu. Parameter estimation for chaotic systems by particle swarm optimization. *Chaos, Solitons & Fractals*, 34(2):654–661, 2007.

[64] Hamidreza Modares, Alireza Alfi, and Mohammad-Mehdi Fateh. Parameter identification of chaotic dynamic systems through an improved particle swarm optimization. *Expert Systems with Applications*, 37(5):3714–3720, 2010.

[65] Chao-Ming Huang, Chi-Jen Huang, and Ming-Li Wang. A particle swarm optimization to identifying the armax model for short-term load forecasting. *Power Systems, IEEE Transactions on*, 20(2):1126–1133, 2005.

[66] Russell C Eberhart and Yuhui Shi. Particle swarm optimization: developments, applications and resources. In *Evolutionary Computation, 2001. Proceedings of the 2001 Congress on*, volume 1, pages 81–86. IEEE, 2001.

[67] Konstantinos E Parsopoulos and Michael N. Vrahatis. Recent approaches to global optimization problems through particle swarm optimization. *Natural computing*, 1(2-3):235–306, 2002.

[68] Russ C Eberhart and James Kennedy. A new optimizer using particle swarm theory. In *Proceedings of the sixth international symposium on micro machine and human science*, volume 1, pages 39–43. New York, NY, 1995.

[69] Harpreetsingh Banvait, Xiao Lin, Sohel Anwar, and Yaobin Chen. Plug-in hybrid electric vehicle energy management system using particle swarm optimization. *World Electric Vehicle Association Journal*, 3, 2009.

[70] Gary Hunt and C Motloch. Freedom car battery test manual for power-assist hybrid electric vehicles. *INEEL, Idaho Falls*, 2003.

APPENDICES

A. DETAILS OF DIFFERENT EXPERIMENTS ON BATTERY

For references of the experimental works, the details regarding the experimental methodology using CADEX battery tester is provided here in graphical manner.

A.1 Experiments on Halthy Battery

To run a test on the battery, depending on the battery specifications, first step is to define a function called C-code. The C-code for the Healthy battery operation is provided in Figure A.1.

C-Code Name	panasonic_2	
Chemistry	Li	
Number of cells	1	Cell
Rating	3.400	Ah
Charge rate	3.400	A
Discharge rate	3.400	A
Low temperature limit	0	degC
High temperature limit	45	degC
Delta T (dT)	1	degC/min
Maximum charge voltage	4.490	V
End of discharge	1.001	V
Standby voltage	4.050	V
Charge termination point	0.170	A
Rapid charge voltage	3.000	V
Target capacity	80	percent(%)
Perform automatic ohmtest	No	
Charge timeout (0 = off)	150	C-minute
Discharge timeout (0 = off)	150	C-minute
milli-ohms pass/fail point	150	mOhms
Min. safe operating voltage	1.000	V
Max. safe operating voltage	4.500	V
Max. safe operating charge current	6.800	A
Max. safe operating discharge current	6.800	A
Max. safe operating temperature	60	degC

Figure A.1. Defined C-code for Healthy battery experiments

After defining the C-code, the operating steps and their respective step details, namely, the sequence of operation and the rate of respective steps (charge and discharge) need to be declared. The defied custom program for Healthy battery is provided for both discharge and charge. The custom program for Healthy battery discharge is provided in Figure A.2.

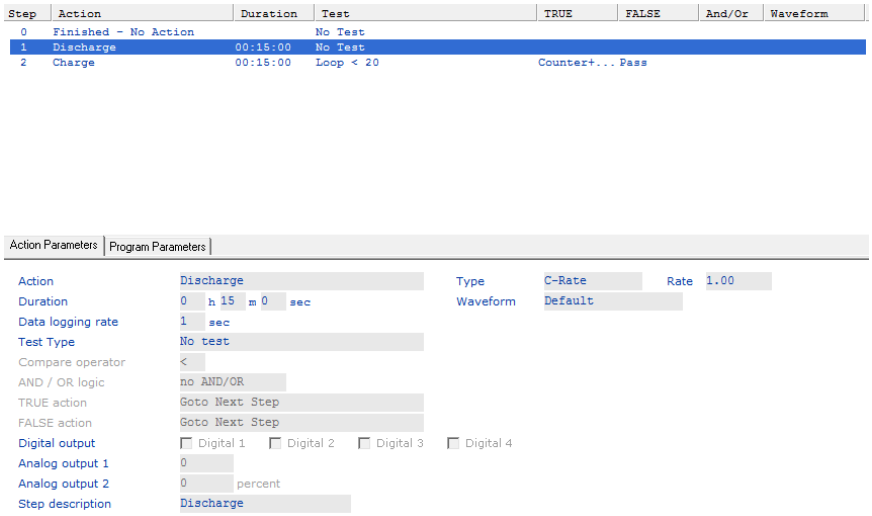

Figure A.2. Custom program for Healthy battery discharge

The custom program for Healthy battery charging step is provided in Figure A.3.

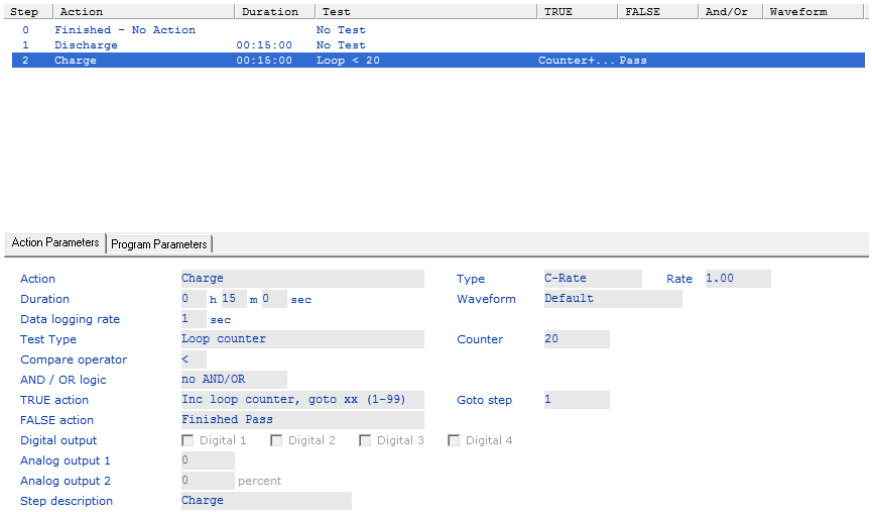

Figure A.3. Custom program for Healthy battery charge

The results of the experiments after combining the C-code and the custom programs Healthy battery showing voltage, current and temperature etc. is provided in Figure A.4.

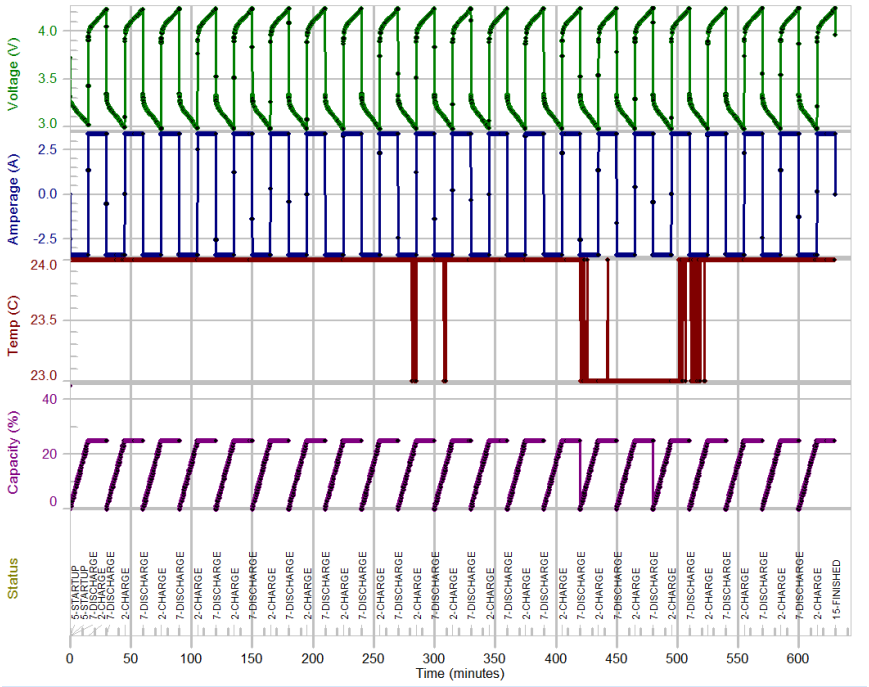

Figure A.4. Result window for Healthy battery experiments

A.2 Experiments on Navy-OD Battery

Similar plots for the experiments on Navy OD battery is provided in this section.

C-Code Name	panasonic_1	
Chemistry	Li	
Number of cells	1	Cell
Rating	3.400	Ah
Charge rate	3.400	A
Discharge rate	3.400	A
Low temperature limit	0	degC
High temperature limit	45	degC
Delta T (dT)	1	degC/min
Maximum charge voltage	4.490	V
End of discharge	1.001	V
Standby voltage	4.050	V
Charge termination point	0.170	A
Rapid charge voltage	3.000	V
Target capacity	80	percent(%)
Perform automatic ohmtest	No	
Charge timeout (0 = off)	150	C-minute
Discharge timeout (0 = off)	150	C-minute
milli-ohms pass/fail point	150	mOhms
Min. safe operating voltage	1.000	V
Max. safe operating voltage	4.500	V
Max. safe operating charge current	6.800	A
Max. safe operating discharge current	6.800	A
Max. safe operating temperature	60	degC

Figure A.5. Defined C-code for Navy OD experiments

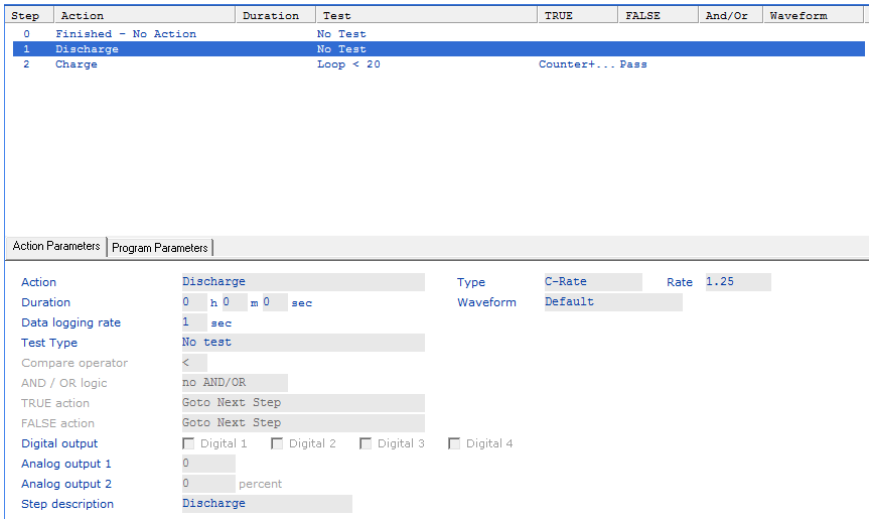

Figure A.6. Custom program for Navy OD discharge

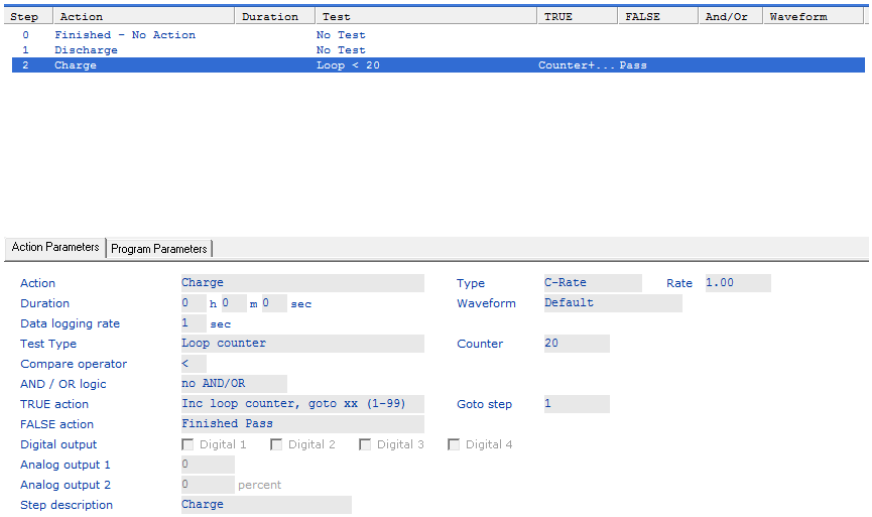

Figure A.7. Custom program for Navy OD battery charge

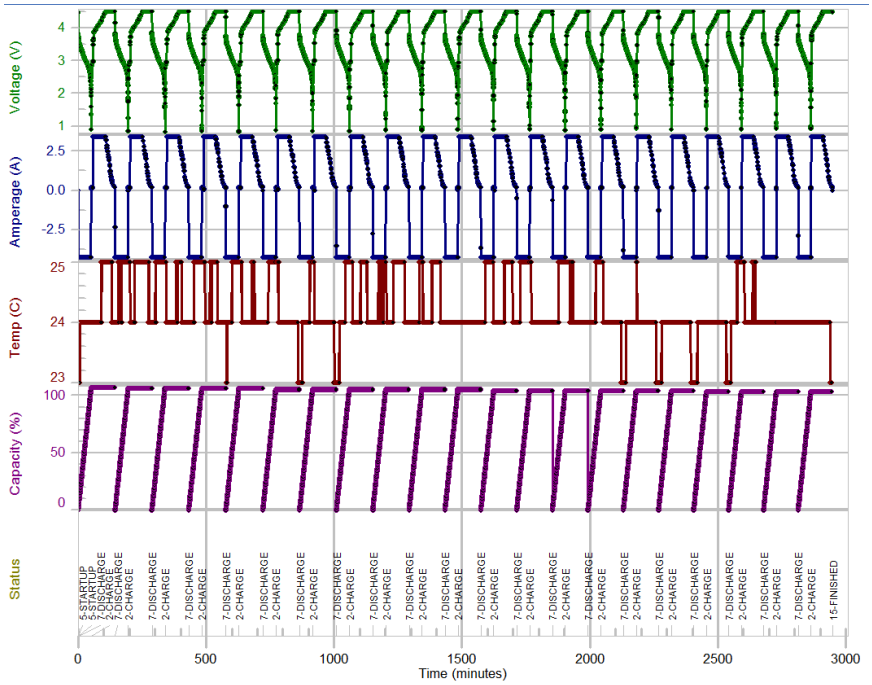

Figure A.8. Result window for Navy OD battery experiments

A.3 Experiments on 24-hr OD Battery

Moreover, similar plots for the experiments on 24-hr OD battery is provided in this section.

C-Code Name	panasonic_6	
Chemistry	Li	
Number of cells	1	Cell
Rating	3.400	Ah
Charge rate	3.400	A
Discharge rate	3.400	A
Low temperature limit	0	degC
High temperature limit	45	degC
Delta T (dT)	1	degC/min
Maximum charge voltage	4.490	V
End of discharge	1.001	V
Standby voltage	4.050	V
Charge termination point	0.170	A
Rapid charge voltage	3.000	V
Target capacity	80	percent(%)
Perform automatic ohmtest	No	
Charge timeout (0 = off)	150	C-minute
Discharge timeout (0 = off)	150	C-minute
milli-ohms pass/fail point	150	mOhms
Min. safe operating voltage	1.000	V
Max. safe operating voltage	4.500	V
Max. safe operating charge current	6.800	A
Max. safe operating discharge current	6.800	A
Max. safe operating temperature	60	degC

Figure A.9. Defined C-code for 24-hr OD battery experiments

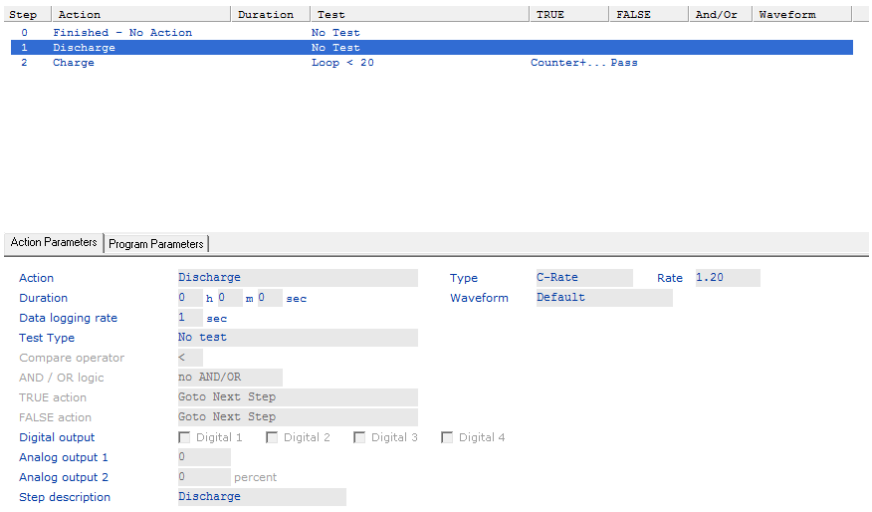

Figure A.10. Custom program for 24-hr OD battery discharge

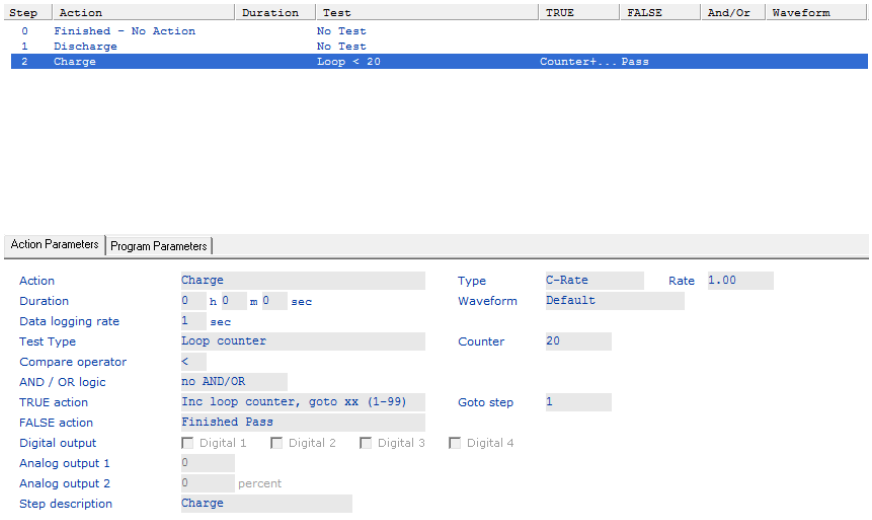

Figure A.11. Custom program for 24-hr OD battery charge

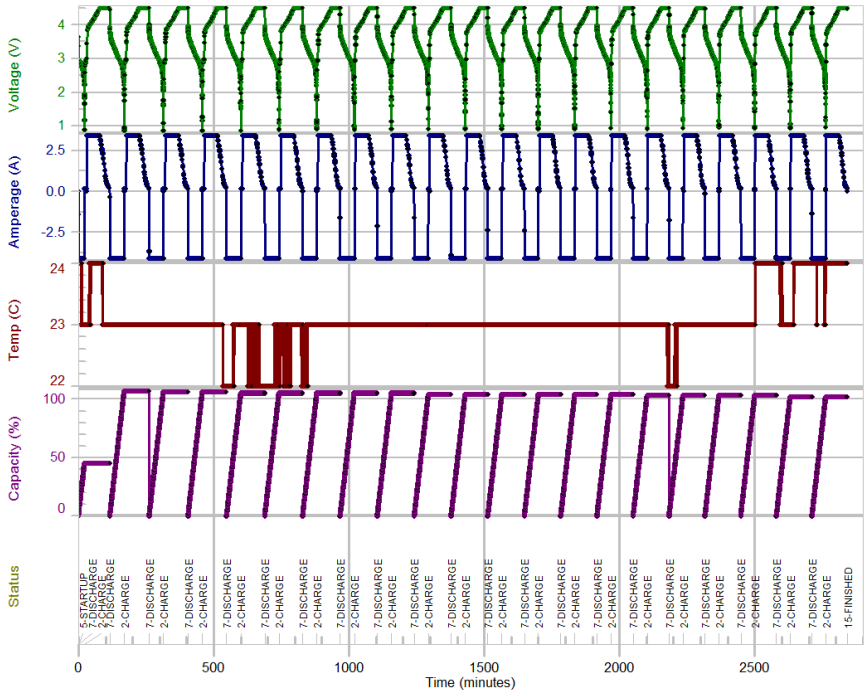

Figure A.12. Result window for 24-hr OD battery experiments

A.4 Experiments on OC Battery

Finally, similar plots for the experiments on OC battery is provided in this section.

C-Code Name	panasonic_8	
Chemistry	Li	
Number of cells	1	Cell
Rating	3.400	Ah
Charge rate	3.400	A
Discharge rate	3.400	A
Low temperature limit	0	degC
High temperature limit	45	degC
Delta T (dT)	1	degC/min
Maximum charge voltage	4.400	V
End of discharge	1.001	V
Standby voltage	4.050	V
Charge termination point	0.170	A
Rapid charge voltage	3.000	V
Target capacity	80	percent(%)
Perform automatic ohmtest	No	
Charge timeout (0 = off)	150	C-minute
Discharge timeout (0 = off)	150	C-minute
milli-ohms pass/fail point	150	mOhms
Min. safe operating voltage	1.000	V
Max. safe operating voltage	4.500	V
Max. safe operating charge current	6.800	A
Max. safe operating discharge current	6.800	A
Max. safe operating temperature	60	degC

Figure A.13. Defined C-code for OC battery experiments

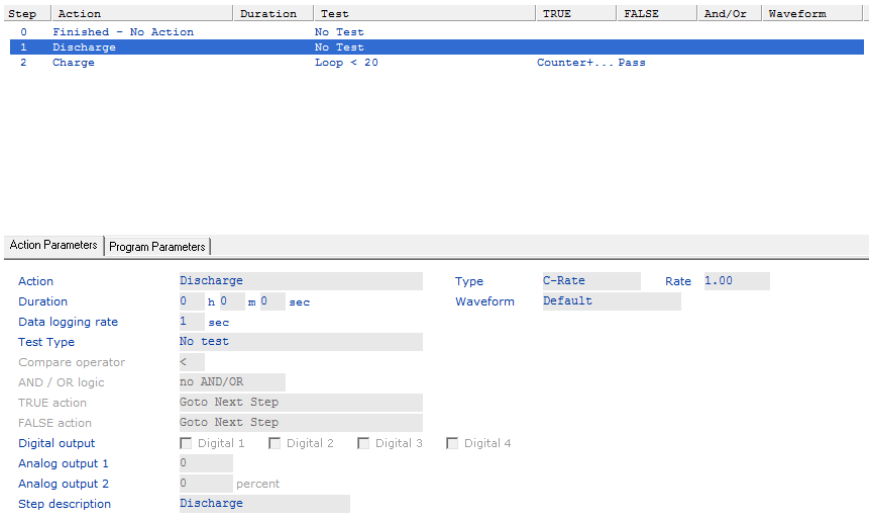

Figure A.14. Custom program for OC battery discharge

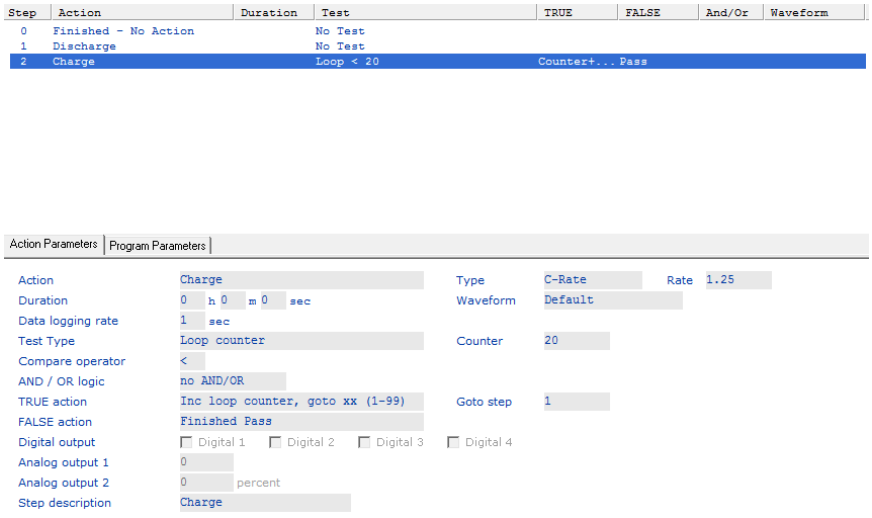

Figure A.15. Custom program for OC battery charge

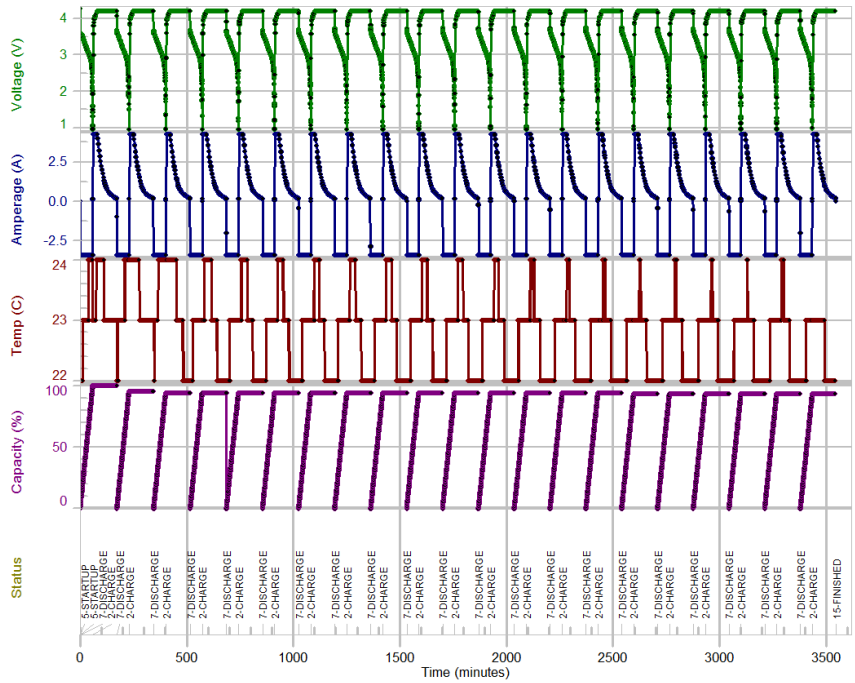

Figure A.16. Result window for OC battery experiments

B. OVERALL IDENTIFIED PARAMETERS USING PSO

Although the parameter identification works using particle swarm optimization algorithm presented at Chapter 6 was based on the last parts (discharge and charge) of the overall experiments of 20 cycles, four target parameters were identified for every single sequence of operation. In this part of the thesis works, these identified parameters are provided in tabular form, which can give a better comprehensive idea about the proposed technique of parameter identification and these results might be helpful for future works in this area of Li-Ion battery research.

B.1 Overall Identified Parameters for Experiments on Healthy Battery

Table B.1. Identified Parameters for Healthy battery overall discharge operations only

Parameter→	Ds_P	k_P	Ds_N	k_N
Discharge-1	5.068×10^{-16}	1.5099×10^{-15}	2.2158×10^{-14}	3.1874×10^{-15}
Discharge-2	3.09×10^{-16}	1.1633×10^{-14}	3.7537×10^{-14}	4.7034×10^{-15}
Discharge-3	4.7938×10^{-16}	1.3235×10^{-14}	1.4592×10^{-14}	3.3326×10^{-16}
Discharge-4	8.7754×10^{-16}	1.2878×10^{-14}	3.5238×10^{-15}	8.2089×10^{-16}
Discharge-5	4.0972×10^{-16}	1.2645×10^{-14}	9.1447×10^{-15}	2.6208×10^{-15}
Discharge-6	3.3951×10^{-16}	1.337×10^{-14}	2.0548×10^{-14}	2.7683×10^{-15}
Discharge-7	6.3677×10^{-16}	1.3599×10^{-14}	1.0901×10^{-14}	8.9762×10^{-16}
Discharge-8	1.5675×10^{-15}	1.2138×10^{-14}	1.1072×10^{-15}	9.1139×10^{-16}
Discharge-9	4.7139×10^{-16}	1.2561×10^{-14}	1.737×10^{-14}	2.0325×10^{-15}
Discharge-10	9.9669×10^{-16}	1.3484×10^{-14}	4.5005×10^{-15}	2.3358×10^{-15}
Discharge-11	5.475×10^{-16}	1.3905×10^{-14}	6.8182×10^{-15}	1.7206×10^{-15}
Discharge-12	2.0772×10^{-16}	1.5069×10^{-14}	1.6559×10^{-15}	1.7434×10^{-15}
Discharge-13	4.3511×10^{-17}	1.3006×10^{-14}	7.2771×10^{-16}	4.2864×10^{-16}
Discharge-14	4.0707×10^{-16}	1.3115×10^{-14}	7.5833×10^{-15}	2.4966×10^{-15}
Discharge-15	3.3414×10^{-16}	1.3636×10^{-14}	1.483×10^{-15}	5.0135×10^{-16}
Discharge-16	3.0545×10^{-16}	1.3873×10^{-14}	1.0215×10^{-14}	6.7886×10^{-15}
Discharge-17	4.567×10^{-16}	1.4448×10^{-14}	1.4743×10^{-14}	1.2515×10^{-15}
Discharge-18	1.475×10^{-16}	1.3209×10^{-14}	1.0086×10^{-14}	3.9276×10^{-15}
Discharge-19	4.4617×10^{-16}	1.2902×10^{-14}	1.0351×10^{-14}	1.1045×10^{-15}
Discharge-20	4.03×10^{-16}	6.0556×10^{-14}	4.32×10^{-14}	3.5484×10^{-15}

Table B.2. Identified Parameters for Healthy battery overall charge operations only

Parameter→	Ds_P	k_P	Ds_N	k_N
Charge-1	1.7458×10^{-15}	6.4392×10^{-14}	5.2755×10^{-14}	9.7765×10^{-15}
Charge-2	1.6094×10^{-15}	6.1088×10^{-14}	2.9822×10^{-14}	1.0871×10^{-14}
Charge-3	1.9904×10^{-15}	9.7494×10^{-14}	1.1304×10^{-14}	1.0583×10^{-14}
Charge-4	2.5663×10^{-15}	5.9313×10^{-14}	6.2859×10^{-14}	2.211×10^{-15}
Charge-5	1.8753×10^{-15}	8.2967×10^{-14}	2.3778×10^{-14}	2.4636×10^{-15}
Charge-6	5.589×10^{-16}	5.7573×10^{-14}	3.2486×10^{-14}	6.362×10^{-15}
Charge-7	1.38×10^{-15}	8.3722×10^{-14}	3.4494×10^{-14}	4.7176×10^{-15}
Charge-8	9.9876×10^{-16}	6.5404×10^{-14}	8.9354×10^{-15}	9.4332×10^{-15}
Charge-9	7.3487×10^{-16}	6.1882×10^{-14}	1.9374×10^{-14}	6.3741×10^{-15}
Charge-10	1.3446×10^{-15}	5.695×10^{-14}	3.2146×10^{-14}	1.925×10^{-16}
Charge-11	1.107×10^{-15}	5.7407×10^{-14}	8.8342×10^{-15}	1.1744×10^{-14}
Charge-12	1.0393×10^{-16}	7.7282×10^{-14}	1.897×10^{-15}	1.9061×10^{-15}
Charge-13	1.5249×10^{-15}	7.1806×10^{-14}	2.8375×10^{-14}	3.8407×10^{-15}
Charge-14	7.2995×10^{-16}	6.5732×10^{-14}	4.6362×10^{-14}	9.387×10^{-15}
Charge-15	7.4974×10^{-16}	4.9376×10^{-14}	5.1328×10^{-14}	1.1701×10^{-14}
Charge-16	8.5518×10^{-16}	7.3861×10^{-14}	1.0017×10^{-14}	4.1246×10^{-15}
Charge-17	2.3808×10^{-15}	4.3418×10^{-14}	3.5982×10^{-14}	9.6652×10^{-15}
Charge-18	8.6069×10^{-16}	6.0218×10^{-14}	2.0327×10^{-14}	6.9401×10^{-15}
Charge-19	1.8523×10^{-15}	4.9156×10^{-14}	3.5722×10^{-14}	7.4707×10^{-15}
Charge-20	1.75×10^{-15}	7.73589×10^{-14}	4.61743×10^{-15}	1.05318×10^{-14}

B.2 Overall Identified Parameters for Experiments on Navy-OD Battery

Table B.3. Identified Parameters for Navy-OD battery overall discharge operations only

Parameter→	Ds_P	k_P	Ds_N	k_N
Discharge-1	1.3839×10^{-15}	1.1678×10^{-14}	9.8609×10^{-15}	3.3702×10^{-16}
Discharge-2	5.3913×10^{-16}	1.6845×10^{-14}	9.2637×10^{-15}	3.8546×10^{-15}
Discharge-3	5.4951×10^{-16}	1.3741×10^{-14}	2.0048×10^{-15}	3.1009×10^{-15}
Discharge-4	4.6127×10^{-16}	1.017×10^{-14}	5.4924×10^{-15}	9.0324×10^{-16}
Discharge-5	2.1777×10^{-16}	3.93×10^{-14}	2.5285×10^{-14}	3.8347×10^{-16}
Discharge-6	1.418×10^{-16}	3.8427×10^{-14}	1.9286×10^{-14}	5.4634×10^{-15}
Discharge-7	3.2792×10^{-16}	3.1065×10^{-14}	2.0664×10^{-14}	1.973×10^{-15}
Discharge-8	4.1475×10^{-16}	3.0801×10^{-14}	1.3698×10^{-14}	7.2409×10^{-16}
Discharge-9	5.7524×10^{-16}	4.5321×10^{-14}	4.6261×10^{-15}	2.5178×10^{-16}
Discharge-10	2.661×10^{-16}	3.5827×10^{-14}	1.3584×10^{-14}	3.3358×10^{-16}
Discharge-11	2.9111×10^{-16}	4.5107×10^{-14}	8.9852×10^{-15}	2.2553×10^{-15}
Discharge-12	6.5434×10^{-16}	5.8587×10^{-14}	1.3638×10^{-14}	6.8052×10^{-16}
Discharge-13	5.1403×10^{-16}	3.3332×10^{-14}	1.6825×10^{-14}	1.6092×10^{-15}
Discharge-14	3.7749×10^{-16}	4.1476×10^{-14}	1.4179×10^{-14}	3.8085×10^{-15}
Discharge-15	5.3117×10^{-16}	4.0574×10^{-14}	2.4536×10^{-15}	2.1379×10^{-15}
Discharge-16	5.5112×10^{-16}	4.6301×10^{-14}	1.2483×10^{-14}	2.883×10^{-15}
Discharge-17	9.3196×10^{-16}	4.862×10^{-14}	2.1711×10^{-16}	5.9389×10^{-17}
Discharge-18	5.8813×10^{-16}	4.2352×10^{-14}	2.0615×10^{-15}	2.7761×10^{-15}
Discharge-19	5.0652×10^{-16}	4.1221×10^{-14}	1.9433×10^{-14}	7.6539×10^{-16}
Discharge-20	6.55×10^{-16}	7.3194×10^{-13}	3.35×10^{-15}	1.129×10^{-15}

Table B.4. Identified Parameters for Navy-OD battery overall charge operations only

Parameter→	Ds_P	k_P	Ds_N	k_N
Charge-1	8.3185×10^{-16}	6.2414×10^{-14}	9.6919×10^{-15}	2.9736×10^{-15}
Charge-2	8.8983×10^{-16}	6.9636×10^{-14}	2.1385×10^{-14}	6.0174×10^{-15}
Charge-3	1.9245×10^{-16}	7.161×10^{-14}	1.5873×10^{-14}	5.4272×10^{-15}
Charge-4	2.1629×10^{-15}	9.4049×10^{-14}	5.0066×10^{-14}	1.2666×10^{-15}
Charge-5	5.3024×10^{-16}	6.0269×10^{-14}	2.137×10^{-14}	2.7408×10^{-15}
Charge-6	1.4999×10^{-15}	9.9209×10^{-14}	1.2409×10^{-14}	8.2224×10^{-15}
Charge-7	1.1434×10^{-15}	6.1796×10^{-14}	7.0899×10^{-15}	5.8282×10^{-15}
Charge-8	1.8538×10^{-15}	8.3978×10^{-14}	3.3779×10^{-14}	6.4244×10^{-15}
Charge-9	9.6847×10^{-16}	5.6472×10^{-14}	9.01×10^{-16}	6.2152×10^{-15}
Charge-10	4.7708×10^{-16}	3.5183×10^{-14}	2.126×10^{-14}	3.2781×10^{-15}
Charge-11	2.8955×10^{-15}	5.2067×10^{-14}	4.1271×10^{-15}	7.478×10^{-15}
Charge-12	2.1685×10^{-15}	2.0712×10^{-14}	2.6981×10^{-14}	8.0202×10^{-15}
Charge-13	2.3855×10^{-15}	4.727×10^{-14}	6.4567×10^{-15}	5.9403×10^{-15}
Charge-14	3.7238×10^{-16}	6.465×10^{-14}	2.4397×10^{-14}	3.0284×10^{-15}
Charge-15	2.0551×10^{-16}	1.5279×10^{-14}	1.303×10^{-14}	1.5295×10^{-15}
Charge-16	1.7342×10^{-15}	3.7894×10^{-14}	2.487×10^{-14}	8.1925×10^{-15}
Charge-17	1.0986×10^{-16}	8.8587×10^{-14}	2.8155×10^{-14}	3.8×10^{-15}
Charge-18	2.0983×10^{-15}	5.8279×10^{-14}	1.0371×10^{-14}	1.2534×10^{-14}
Charge-19	8.0145×10^{-16}	8.7052×10^{-14}	2.1425×10^{-15}	2.2624×10^{-15}
Charge-20	2.08×10^{-15}	5.4301×10^{-14}	9.35×10^{-16}	8.4599×10^{-15}

B.3 Overall Identified Parameters for Experiments on 24-hr OD Battery

Table B.5. Identified Parameters for 24-hr OD battery overall discharge operations only

Parameter→	Ds_P	k_P	Ds_N	k_N
Discharge-1	1.3641×10^{-15}	7.1516×10^{-14}	1.1438×10^{-14}	1.2581×10^{-15}
Discharge-2	9.4944×10^{-16}	9.1704×10^{-14}	1.2729×10^{-14}	1.1961×10^{-15}
Discharge-3	8.5828×10^{-16}	6.8718×10^{-14}	9.5388×10^{-15}	1.7374×10^{-15}
Discharge-4	1.0275×10^{-15}	7.2731×10^{-14}	7.0636×10^{-15}	1.5572×10^{-15}
Discharge-5	6.8239×10^{-16}	8.4943×10^{-14}	7.7931×10^{-15}	1.2682×10^{-15}
Discharge-6	1.4701×10^{-15}	8.9377×10^{-14}	1.2856×10^{-14}	1.6084×10^{-15}
Discharge-7	8.4052×10^{-16}	9.104×10^{-14}	1.3262×10^{-14}	1.1452×10^{-15}
Discharge-8	9.3468×10^{-16}	9.0133×10^{-14}	1.1587×10^{-14}	1.4729×10^{-15}
Discharge-9	6.6563×10^{-16}	1.0624×10^{-13}	1.5532×10^{-14}	9.9683×10^{-16}
Discharge-10	1.1811×10^{-15}	8.071×10^{-14}	1.2348×10^{-14}	7.5182×10^{-16}
Discharge-11	8.8987×10^{-16}	1.1451×10^{-13}	2.8316×10^{-14}	2.1026×10^{-15}
Discharge-12	9.7468×10^{-16}	1.9977×10^{-13}	8.7809×10^{-15}	1.6015×10^{-15}
Discharge-13	5.7137×10^{-16}	1.8837×10^{-13}	2.1768×10^{-14}	2.6394×10^{-15}
Discharge-14	8.588×10^{-16}	1.7682×10^{-13}	9.4359×10^{-15}	8.128×10^{-16}
Discharge-15	1.3594×10^{-15}	1.6855×10^{-13}	2.259×10^{-14}	1.2328×10^{-15}
Discharge-16	1.7676×10^{-15}	8.801×10^{-14}	1.597×10^{-14}	2.1461×10^{-15}
Discharge-17	3.0323×10^{-15}	1.7416×10^{-13}	1.2885×10^{-14}	1.7765×10^{-15}
Discharge-18	8.9286×10^{-16}	1.7796×10^{-13}	1.0922×10^{-14}	1.4666×10^{-15}
Discharge-19	6.5025×10^{-16}	1.5069×10^{-14}	6.9731×10^{-15}	1.7833×10^{-15}
Discharge-20	4.10×10^{-16}	2.1611×10^{-13}	3.6899×10^{-15}	1.0775×10^{-15}

Table B.6. Identified Parameters for 24-hr OD battery overall charge operations only

Parameter→	Ds_P	k_P	Ds_N	k_N
Charge-1	9.6183×10^{-16}	6.4015×10^{-14}	1.465×10^{-14}	7.0137×10^{-15}
Charge-2	1.6071×10^{-15}	8.8533×10^{-14}	1.684×10^{-14}	2.183×10^{-15}
Charge-3	9.657×10^{-16}	7.7912×10^{-14}	1.1126×10^{-14}	6.7975×10^{-15}
Charge-4	4.6922×10^{-16}	4.3413×10^{-14}	2.8483×10^{-14}	5.7736×10^{-15}
Charge-5	1.3287×10^{-15}	7.3049×10^{-14}	1.5408×10^{-14}	2.8278×10^{-15}
Charge-6	1.8981×10^{-15}	8.9299×10^{-14}	8.1269×10^{-15}	7.3966×10^{-15}
Charge-7	5.2839×10^{-16}	2.9757×10^{-14}	2.6948×10^{-14}	5.5065×10^{-16}
Charge-8	2.0157×10^{-15}	7.3598×10^{-14}	1.3369×10^{-14}	9.3578×10^{-15}
Charge-9	9.3336×10^{-16}	8.5108×10^{-14}	2.225×10^{-14}	2.8022×10^{-15}
Charge-10	9.7341×10^{-16}	6.6843×10^{-14}	4.5378×10^{-15}	1.0583×10^{-14}
Charge-11	2.0673×10^{-15}	6.2894×10^{-14}	1.7334×10^{-14}	7.7703×10^{-16}
Charge-12	9.8538×10^{-16}	4.468×10^{-14}	2.0863×10^{-14}	6.5176×10^{-15}
Charge-13	1.8238×10^{-15}	3.9131×10^{-14}	3.5075×10^{-14}	1.2252×10^{-15}
Charge-14	1.4689×10^{-15}	5.5749×10^{-14}	2.7727×10^{-14}	7.4505×10^{-15}
Charge-15	5.3553×10^{-16}	5.3997×10^{-14}	1.548×10^{-14}	7.6122×10^{-15}
Charge-16	5.7501×10^{-16}	6.5276×10^{-14}	2.571×10^{-14}	3.402×10^{-15}
Charge-17	2.3985×10^{-15}	5.0238×10^{-14}	2.6225×10^{-14}	9.1083×10^{-15}
Charge-18	6.9537×10^{-16}	7.3659×10^{-14}	1.6162×10^{-14}	2.3761×10^{-15}
Charge-19	7.9637×10^{-16}	9.0571×10^{-14}	3.1154×10^{-14}	1.019×10^{-14}
Charge-20	1.8848×10^{-15}	5.0345×10^{-14}	9.5869×10^{-15}	3.3563×10^{-15}

B.4 Overall Identified Parameters for Experiments on an OC Battery

Table B.7. Identified Parameters for OC battery overall discharge operations only

Parameter→	Ds_P	k_P	Ds_N	k_N
Discharge-1	2.1479×10^{-16}	9.3194×10^{-14}	7.1353×10^{-15}	2.422×10^{-15}
Discharge-2	5.0458×10^{-16}	1.3793×10^{-13}	1.9084×10^{-15}	2.6448×10^{-16}
Discharge-3	7.9799×10^{-16}	1.6309×10^{-14}	6.0309×10^{-16}	7.8994×10^{-15}
Discharge-4	6.8691×10^{-16}	1.4398×10^{-14}	6.9432×10^{-16}	1.451×10^{-15}
Discharge-5	1.22624×10^{-16}	1.5189×10^{-14}	8.4484×10^{-15}	3.4025×10^{-15}
Discharge-6	8.9039×10^{-16}	1.2636×10^{-13}	1.1021×10^{-15}	1.3438×10^{-16}
Discharge-7	7.3174×10^{-16}	1.7632×10^{-13}	9.1888×10^{-15}	9.9159×10^{-16}
Discharge-8	8.1948×10^{-16}	2.3973×10^{-14}	2.282×10^{-14}	2.9036×10^{-16}
Discharge-9	4.5223×10^{-16}	2.8255×10^{-14}	1.2616×10^{-14}	3.7212×10^{-15}
Discharge-10	3.3434×10^{-16}	3.1055×10^{-13}	1.1358×10^{-14}	3.9127×10^{-16}
Discharge-11	3.5774×10^{-16}	3.3769×10^{-14}	2.4377×10^{-16}	6.0374×10^{-15}
Discharge-12	8.5553×10^{-17}	4.0223×10^{-14}	2.4119×10^{-16}	9.9784×10^{-16}
Discharge-13	1.6308×10^{-16}	3.8003×10^{-13}	1.4623×10^{-14}	2.4149×10^{-15}
Discharge-14	4.382×10^{-16}	4.1243×10^{-14}	3.1239×10^{-15}	4.0671×10^{-15}
Discharge-15	3.291×10^{-16}	3.8081×10^{-14}	3.9996×10^{-15}	4.6473×10^{-15}
Discharge-16	5.5084×10^{-16}	3.8377×10^{-14}	1.7864×10^{-14}	2.6408×10^{-15}
Discharge-17	3.0736×10^{-16}	4.2971×10^{-14}	3.7055×10^{-16}	1.5165×10^{-15}
Discharge-18	7.2642×10^{-17}	1.3458×10^{-13}	1.6051×10^{-14}	2.2223×10^{-15}
Discharge-19	8.169×10^{-16}	4.2695×10^{-14}	1.4232×10^{-14}	2.5666×10^{-15}
Discharge-20	1.29×10^{-16}	3.3685×10^{-13}	9.7622×10^{-15}	1.9175×10^{-15}

Table B.8. Identified Parameters for OC battery overall charge operations only

Parameter→	Ds_P	k_P	Ds_N	k_N
Charge-1	6.2167×10^{-16}	9.1658×10^{-14}	1.0579×10^{-14}	3.2479×10^{-15}
Charge-2	2.4764×10^{-15}	7.0083×10^{-14}	3.0076×10^{-14}	8.7865×10^{-15}
Charge-3	1.3905×10^{-15}	4.6936×10^{-14}	2.416×10^{-15}	3.1402×10^{-15}
Charge-4	1.7493×10^{-15}	5.7965×10^{-14}	8.714×10^{-15}	3.404×10^{-15}
Charge-5	3.8262×10^{-16}	5.1545×10^{-14}	5.833×10^{-15}	1.8065×10^{-15}
Charge-6	1.5199×10^{-15}	9.2365×10^{-14}	1.3317×10^{-14}	9.1295×10^{-15}
Charge-7	1.2957×10^{-15}	7.1602×10^{-14}	2.1071×10^{-14}	7.6773×10^{-16}
Charge-8	7.0318×10^{-16}	6.5964×10^{-14}	3.196×10^{-14}	3.5026×10^{-15}
Charge-9	3.2958×10^{-15}	3.6137×10^{-14}	3.1027×10^{-14}	8.0549×10^{-16}
Charge-10	7.3042×10^{-16}	9.9035×10^{-14}	4.3673×10^{-15}	7.0384×10^{-15}
Charge-11	1.6011×10^{-15}	7.421×10^{-14}	3.1651×10^{-14}	8.7629×10^{-15}
Charge-12	1.9203×10^{-15}	1.0633×10^{-13}	1.7819×10^{-14}	1.0701×10^{-14}
Charge-13	1.7181×10^{-15}	6.1435×10^{-14}	3.6137×10^{-14}	8.1202×10^{-15}
Charge-14	7.1731×10^{-16}	5.892×10^{-14}	1.8727×10^{-14}	5.2105×10^{-15}
Charge-15	6.4365×10^{-16}	7.4556×10^{-14}	2.9287×10^{-14}	7.7945×10^{-15}
Charge-16	1.247×10^{-15}	5.6433×10^{-14}	1.1767×10^{-15}	5.064×10^{-15}
Charge-17	1.1162×10^{-15}	7.3772×10^{-14}	2.7835×10^{-14}	1.2958×10^{-15}
Charge-18	1.3636×10^{-15}	4.939×10^{-14}	4.8185×10^{-15}	2.8314×10^{-15}
Charge-19	2.3307×10^{-16}	7.835×10^{-14}	1.0177×10^{-15}	6.5076×10^{-15}
Charge-20	2.0986×10^{-15}	3.3064×10^{-14}	1.9827×10^{-14}	2.4734×10^{-15}